A Bigger Splat:

Rock fall impact processes in wet sediment - an example from Clachtoll, NW Scotland

Zachary Killingback

Department of Earth Sciences

Durham University

2019

This thesis was submitted to the University of Durham in full fulfilment of the requirements for the degree of Master of Science by Research.

Abstract

At Clachtoll, in NW Scotland, an enigmatic outcrop of Lewisian gneiss is observed. This zone, ~60 m by 100 m in aerial view, contains abundant fractures filled with clastic material from the immediately adjacent and stratigraphically overlying Stoer Group. This zone also displays foliation that is misoriented by 90 degrees, relative to that in the surrounding basement. Fractures on top of this outcrop contain sedimentary structures, such as laminations, indicative of passive infilling, whilst fractures at the base and on the lateral flanks show characteristics more indicative of forceful injection.

This study proposes that the aforementioned zone represents a hitherto unrecognised fallen block, termed the Clachtoll Megablock, lying on the regional scale nonconformity between the Lewisian gneiss and the Mesoproterozoic sedimentary rocks of the Stoer Group (ca. 1.2 Ga). It is proposed that vertical emplacement of a falling block onto unconsolidated and fluid laden sediment, could cause rapid over-pressuring and liquefaction of said sediment, leading to hydrofracture and sediment slurry injection into the impacting block. Fractures on the top of the block would then be passively infilled under gravity. Simple numerical modelling yields a fall height of 6 m as being sufficient for rapid liquid over-pressuring to overcome the tensile strength of the gneiss.

Several models of emplacement were considered in an attempt to reconcile all of the features observed in the block. Features, including WNW-ESE oriented tensile fractures in the back of the block, and a small thrust associated with brittle folding in the front of the block, indicate an incomplete syn-emplacement disaggregation of the Clachtoll Megablock, consistent with gravity-driven transport from the NNE. Emplacement must have involved an element of sliding, and the misorientation of foliation inside vs. outside of the block can only be explained by rotation of the block.

Evidence of soft sediment deformation in the basal part of the Stoer Group, along with knowledge of the active rift setting of the event suggest that emplacement of the Clachtoll Megablock was triggered by an earthquake ca. 1.2 Ga. Weathering processes, such as freeze-thaw, in an arid environment likely contributed to this.

Contents

List of figures

List of tables

Declaration and statement of copyright

I declare that this thesis which is presented for the degree of Master of Science by Research at Durham University is a result of my own original research, except where acknowledgement is made in the text. This thesis has not been previously submitted to the University of Durham or any other institution.

Zachary Killingback

June 2019

Copyright

Acknowledgements

My utmost thanks go to my primary supervisor, Bob Holdsworth, for creating this project for me, for his support and guidance, his extreme patience, for reigning in my wilder ideas, and for digging me out of the details I have a habit of getting bogged down in. I am also grateful to Eddie Dempsey for facilitating my trip to northwest Scotland to do fieldwork, and then for his continued support and encouragement, and also to Stefan Nielsen for all of his help with the mathematical parts of my research.

I am also eternally grateful to Janice in the department, my mentor Jenny, and to Phil and Charlotte in college for their valiant attempts to keep me sane for the last few years. It might not always have worked, but I wouldn't have survived without them.

I must also mention my gratitude to the Charles Waites Scholarship which funded my research.

Thanks also go to my friends (in and outside of the department) for their support and welcome (most of the time) distractions.

Finally, and most importantly, my thanks go to my mum for not giving up on me, and for all of the texts reminding me to make a cup of tea!

CHAPTER 1
Introduction

1.1. Location and regional context

An enigmatic outcrop of Lewisian gneiss is observed on the coast at Clachtoll, 7km northwest of Lochinver, in the northwest Highlands of Scotland (Fig. 1.1.1.). Here, an area of basement rocks measuring approximately 60 m by 100 m, contains abundant fractures filled with clastic material from the immediately adjacent Stoer Group. The block also displays foliation which is misoriented relative to that in the surrounding gneiss. As will be shown in this thesis, fractures on top of this outcrop contain sedimentary structures, such as laminations, indicative of passive infilling, whilst fractures at the base and on the lateral flanks show characteristics more indicative of forceful injection. Henceforth, this area of misoriented and fractured basement gneiss is referred to as the 'Clachtoll Megablock'.

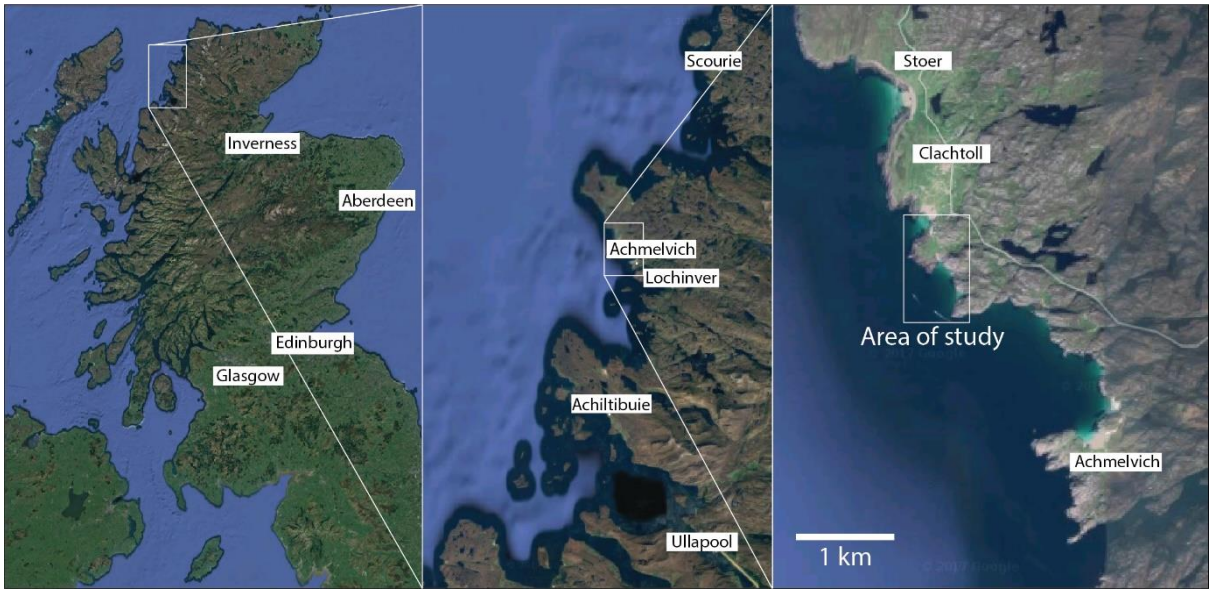

Figure 1.1.1. *Location of field area at Clachtoll, on the base of the Stoer Peninsula in northwest Scotland.*

The Clachtoll Megablock occupies a position on or very close to the unconformable contact between the gneiss and the adjacent Clachtoll Formation of the Stoer Group. The southeast margin of the block is defined by the side of a small valley delineating the location of an

ultramafic dyke in the gneiss. The gneisses comprising the Clachtoll Megablock and the surrounding area belong to the Assynt Terrane of the Lewisian Gneiss Complex. These intermediate (quartz-plagioclase) to mafic (amphibole-biotite), banded gneisses originated as tonalite-trondhjemite-granodiorite (TTG) plutons that most likely intruded the mafic to ultramafic ocean floor rocks of the volcanic arc above a subduction zone at ca. 3.13 – 2.96 Ga (Strachan, Storey & Prave 2012 p.50). At 2.80 – 2.76 Ga they were subjected to high grade metamorphism at granulite facies in the Badcallian event, and later shearing and retrograde metamorphism to amphibolite facies during the Inverian event at ~2.50 Ga (Strachan, Storey & Prave 2012 pp.51–52). The local gneisses display a strong ESE-WNW, steeply dipping foliation, attributed to deformation during the latter event and the formation of the Canisp Shear Zone.

Overlying the Lewisian gneiss is the 1150 ± 50 Ma Stoer Group (Stewart 2002); the lowermost group of the Torridonian supergroup (Fig. 1.1.2). The Torridonian Supergroup comprises Proterozoic, predominantly alluvial, fluvial and lacustrine deposits (mainly sandstones, siltstones, mudstones), forming the Stoer Group, Sleat Group and Torridon Group. Nowhere is the Sleat Group found in contact with the underlying Stoer Group (Stewart 2002). These lithologies are separated from the Archaean gneisses of the Lewisian complex by a significant, regional scale nonconformity, with local relief of up to 300m (Stewart 1990). The shallowly west dipping Stoer group formed during Mesoproterozoic rifting of the Laurentian margin as Baltica pulled away from East Greenland (Strachan, Holdsworth & Prave 2012 p.62). From base to top, the Group itself is comprised of the Clachtoll Formation, the Bay of Stoer Formation (including the infamous Stac Fada member), and the Meall Dearg Formation (Stewart 1990) (Fig. 1.1.3). Clastic, fluvial and alluvial, braided river deposits are occasionally overlain by thin evaporitic units formed in ephemeral lakes (Stewart 1990). The Clachtoll Formation at the base of the Stoer Group is formed entirely from material derived from the local gneiss (Stewart 1990) van de Kamp & Leake 1997). Its lowermost units represent alluvial fans, which grade upwards into fluvial and lacustrine deposits. Muddy layers with desiccation cracks indicate the ephemeral nature of the lakes (Stewart 2002). The Bay of Stoer and Meall Dearg Formations are characterised by cross bedded sands which are significantly more mature than those in the Clachtoll formation (Stewart 1990). The Bay of Stoer and Meall Dearg Formations are also less mafic in their composition than the Clachtoll Formation. Hence, the Clachtoll Formation sandstones contain more epidote and chlorite, and less quartz, along with being enriched in

Fe, Mg, Ca, Ti, Co, Ni, Sr, and Sn. This is logical given the more mafic basement in the source area of the Clachtoll Formation (van de Kamp & Leake 1997). Stewart (1990) used the wetting and drying textures observable in massive sandstones and siltstones, along with a lack of Ca depletion to infer a semi-arid palaeoclimate at a latitude of 10-30º, supported by a similar palaeolatitude found by palaeomagnetism (Stewart & Irving 1974). Young (1999) noted that the low Chemical Index of Alteration values obtained for mudstones in the Stoer Group suggest a lack of weathering indicative of an arid environment. In contrast to the seasonal, semi-arid environment interpreted by van de Kamp and Leake (1997) and Stewart (1990), Davison and Hambrey (1996) inferred that the lowermost section of the Clachtoll formation represents a glacial tillite, on the basis of observations including features they interpreted as roche moutonnées and dropstones. Both Stewart (1997) and Young (1999) strongly dispute this interpretation, and as Stewart (2002) points out, there is no evidence for glaciation anywhere in the world at this time, making it even less likely at the tropical latitudes indicated by palaeomagnetic studies. Stewart (1990), van de Kamp and Leake (1997) and Young (1999) all concluded that Stoer Group deposition occurred in a closed NNE oriented rift basin, approximately 80 km wide and more than 200 km long located between the Minch fault and present day Moine thrust (van de Kamp & Leake 1997). During Stoer Group deposition, the NNE-SSW Coigach fault was active as a normal fault, with downthrow to the east. Stoer Group bedding dips approximately 25º west, towards the fault, and likely results – at least in part – from rotational movement on this fault (Stewart 1993).

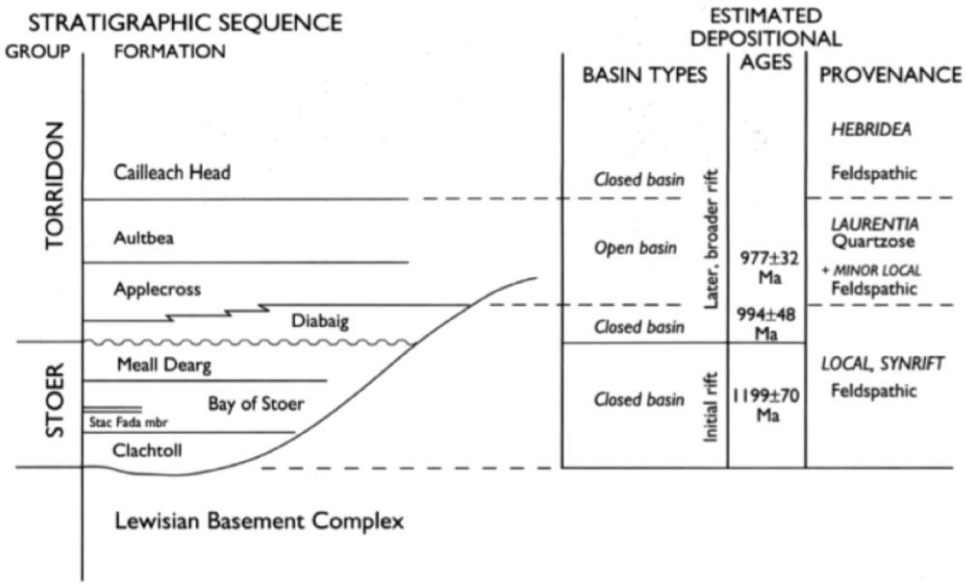

Figure 1.1.2. *Torridonian stratigraphic sequence – note the Sleat Group is missing from the stratigraphy here. Figure taken from van de Kamp and Leake* (1997).

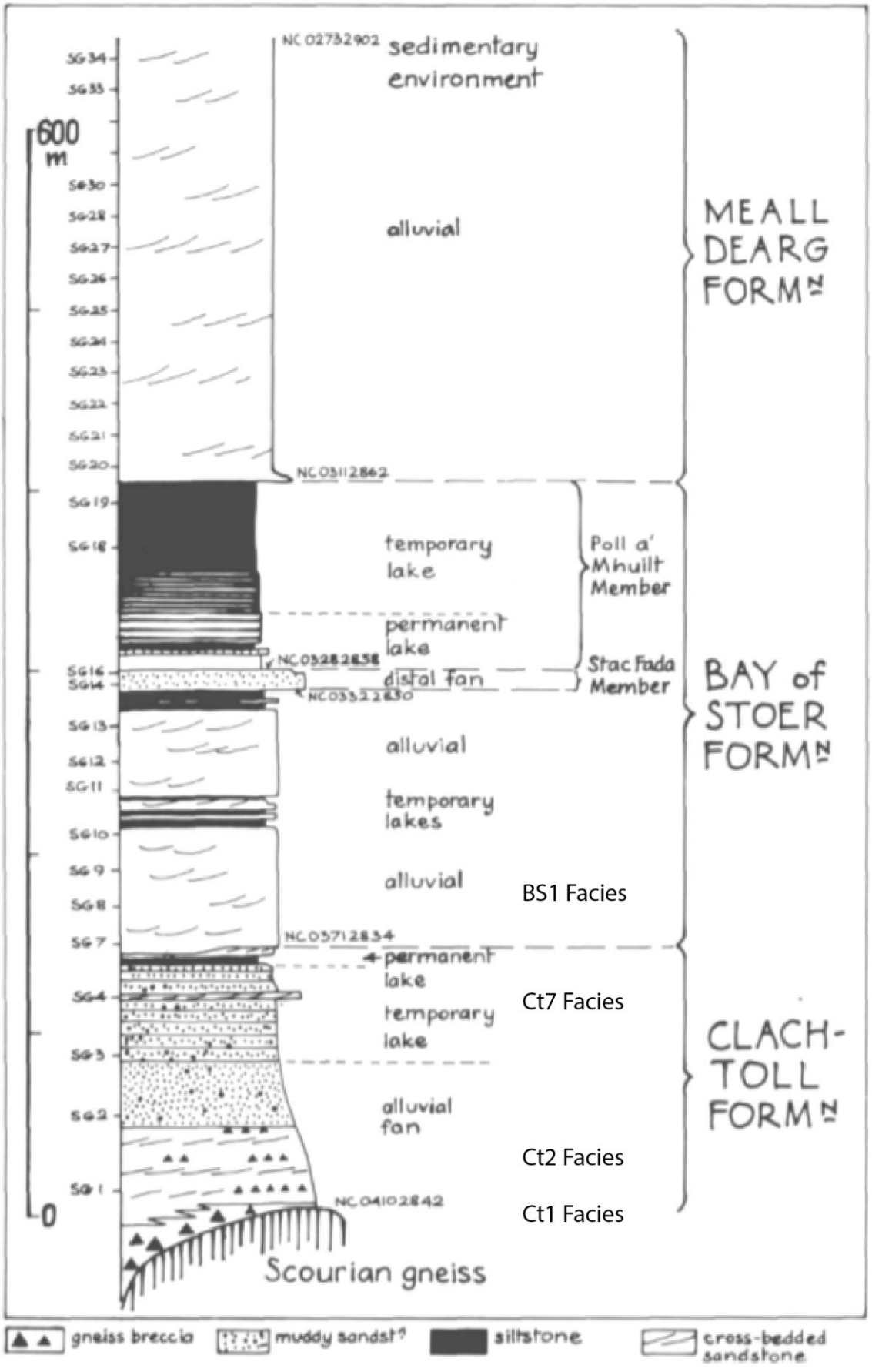

Figure 1.1.3. *Stoer Group Stratigraphy. Figure taken from Stewart* (Stewart 1990).

1.2. Sediment filled fractures

Globally, sediment filled fractures are found in a wide variety of settings. They can broadly be divided into those that have been passively infilled under gravity or those that have been forcefully intruded.

Passively infilled fractures most frequently develop at - or near to - the surface. In sub-aerial conditions, sediment periodically inundates open fractures and cavities (e.g. Richter 1966). This process may also occur sub-aqueously, either over a prolonged period of time, as for sub-aerial fractures, or in a single event, should the fracture network be suddenly breached (e.g. Winterer, Metzler & Sart 1991). Alternatively, passively filled fractures do also develop at depths of up to around 2 kilometres, provided a network of subterranean fractures and voids is held open and connects to the surface (e.g. (Gent, Abe, Urai, *et al.* 2010; Walker, Holdsworth, Imber, *et al.* 2011; Holland, van Gent, Bazalgette, *et al.* 2011).

Forcefully intruded fractures can also occur at the surface, either beneath glaciers, resulting from overpressure of meltwater and unlithified sediments, causing hydrofracture (e.g. (Le Heron & Etienne 2005), or in sub-aqueous conditions, where tectonic events suddenly open fractures, creating a negative pressure gradient and sucking in fluidized sediment (Harms 1965, Jonk, Kelly & Parnell 2004). Otherwise, forcefully intruded fractures typically form in the sub-surface, usually at depths greater than 1.5 km (Jolly & Lonergan 2002), and are most commonly related to overpressuring events. Here, some form of barrier develops, which prevents fluid escape, thus driving up the pore fluid pressure until it overcomes the tensile strength of the rock (e.g. Montenat, Barrier & d'Estevou 1991, Winslow 1983, Phillips & Alsop 2000). Alternatively, the sudden addition of extraneous fluid may drive up pore fluid pressure.

Sediment filled fractures occur in both sedimentary sequences and igneous and metamorphic basements. Forceful intrusion is found to occur more frequently in deep-water marine settings than any other environment, (Jolly & Lonergan 2002). Jolly & Lonergan (2002) also note that most published examples come from tectonically active areas, where high sedimentation rate, and mud-dominated systems, favour the development of high fluid pressures.

Mechanism	*Fracture fill characteristics*	*Sources*
Passive infilling under gravity or groundwater flow	Stratification such as bedding or laminations	(Walker *et al.* 2011)
	Possibly other sedimentary structures such as clast imbrication, ripples, grading, cross-laminations, gravel lenses, scour structures, etc.	(Walker *et al.* 2011)
	Absence of wall rock brecciation	
	Possible wall rock mineralisation	(Richter 1966)
Forceful intrusion or injection	No bedding or other sedimentary structures	
	Complex fracture networks	
	Brecciation of wall rock – jigsaw breccias and autoclastic breccias	(Montenat *et al.* 2007)
	Rafts of host material stoped from the fracture walls	(Dott 1966)
	Fracture wall parallel laminations, sometimes with grading perpendicular to the wall.	(Dott 1966) (Peterson 1968)
	Grading sometimes occurs parallel to fracture margins – fining upwards.	
	Wall parallel banding defined by sharp boundaries formed by differences in grain size and grain alignment.	
	Injection features branching off of larger fractures – analogous to those in pseudotachylytes.	
	Larger, matrix supported clasts, oriented parallel to the fracture walls – analogous to aligned phenocrysts in igneous dykes.	(Peterson 1968)
	Lack of wall rock mineralisation	
	In the case of overpressure, fracture geometries are typically upwards.	
	Occasionally, grooves or flute marks on sides of fracture fill	(Dott 1966) (Peterson 1968)
	Occasionally, scales of mica oriented parallel to fracture walls, which may become crushed in a direction suggesting wall parallel flow of sand grains.	(Diller 1889) (Peterson 1968)

Table 1.2.1. *Diagnostic features of passively filled vs. forcefully intruded sediment filled fractures. For the forceful intrusion criteria, sources cited are in addition to* (Hurst, Scott & Vigorito 2011).

Hurst, Scott and Vigorito (2011) describe in detail, the characteristics of sediment filled fractures resulting from forceful injection, here summarised in Table 1.2.1. These features

result from laminar flow during injection within the central portion of the fractures, and the interaction between the walls of the fracture and the pressurized, fluidized material being intruded. Jigsaw breccias are particularly indicative of hydraulically fractured hosts (Hurst, Scott & Vigorito 2011).

Care must be taken when using the forceful intrusion criteria, as features such as parallelism with the fracture wall of elongated clasts may also occur in fracture fills with a passive emplacement mechanism. For example, if open fractures undergoing filling, further propagate downwards, a negative pressure may suck already deposited sediments downwards, rotating clasts into alignment with the walls (Friese, Vollbrecht, Leiss, *et al.* 2011). These criteria should therefore be used in conjunction with other criteria such as jigsaw breccias and small injections branching off of larger fractures.

1.3. Previous work at Clachtoll

Previous work at Clachtoll has primarily focused on understanding the sedimentology and stratigraphic relationships of the Stoer Group as a whole. Whilst the sediment filled fractures are often noted, only two studies have been conducted that specifically address these fractures at Clachtoll; that of Beacom et al. (1999) and later Dulin et al. (2005). No previous work offers an explanation for the misorientation of foliation within the Clachtoll Megablock relative to the surrounding gneiss; in fact, rarely is this misorientation even acknowledged.

Torridonian age, sediment filled fractures, most often referred to in the literature as clastic or sedimentary dykes, are a relatively common occurrence throughout the basement of the Hebridean terrane (Jonk, Kelly & Parnell 2004). Peach et al. (1907) were the first to refer to these dykes, mentioning examples observed at Gairloch which cut the Lewisian basement. They additionally refer to sandstone dykes at Gairloch, which vertically cut the Torridon Group which here overlies the Lewisian. Dyke examples in both the basement, and the overlying Torridon, trend NNE to ENE. Those found in the basement occur to at least 500 m below the surface (Stewart 1993). Jonk, Kelly and Parnell (2004) later analysed these dykes in more detail and concluded that fracturing and filling occurred simultaneously in a NW-SE directed extensional setting. The dykes are not simple Mode I fractures, however,

having an element of shear. They infer that fractures opened in a NE oriented localized zone of fracturing, setting up a negative pressure gradient, thus sucking in pore fluid from the overlying Torridon, along with unlithified sediment. This, they suggested, was exacerbated by the weight of the overlying material.

At Clachtoll, Stewart (in Barber et al. (1978), describes the following:

"Muddy sandstone injects the underlying gneiss which show extensive in-situ fracturing on the southward facing cliff. This perhaps resulted from high pore-water pressures in the overlying sediment, the result of seismic action"

Here, Stewart appears to be inferring a similar emplacement mechanism as Jonk, Kelly and Parnell (2004) have proposed for the sediment filled fractures found at Gairloch.

In contrast, Davison and Hambrey (1996) have used the sediment filled fractures at Clachtoll as evidence for their interpretation of the basal section of the Clachtoll Formation as having a glacial origin. Their preferred mechanism of emplacement is hydro-fracturing resulting from overpressure of subglacial meltwater combined with a strong basal shear stress acting beneath the glacier.

Not until the work of Beacom, Anderson and Holdsworth (1999) were the sediment filled fractures at Clachtoll analysed in any significant detail. They attribute these fractures (termed clastic veins in their study) to an inferred NE-SW trending oblique sinistral-normal fault zone located on the southwest edge of this study's Clachtoll megablock. Beacom, Anderson and Holdsworth (1999) identify two sets of clastic veins; an early set, passively infilled under gravity as the fractures were held open during WNW-ESE oriented extension, and a later set of forcefully injected, fluidized sand along new fractures. This later phase accounts for the severely brecciated gneiss observed within their Clachtoll Fault zone. The WNW-ESE direction of extension was determined using fault slickenline and slickenfibre data along with tensile fracture opening directions, observed at both Clachtoll and the Gairloch region. Beacom, Anderson and Holdsworth (1999) suggest a depth of emplacement of the clastic veins of around 2 km, but don't say whether this applies to the early or later phase of emplacement, or whether a change in depth occurs between the two. Stewart (2002) cites an emplacement depth of 3-4 km. Also of concern, is the disparity between the locations where

observations and measurements have actually been made in Beacom, Anderson and Holdsworth's (1999) study (as evidenced by the photos in their Figure 5), and the grid references given for said localities, along with the location of features annotated on the map in their Figure 1. They also fail to mention the misorientation of foliation in the area surrounding and immediately north of their fault zone.

Beacom, Anderson and Holdsworth (1999) then go on to compare the kinematic and geometric relationships of the faulting they observe at Clachtoll to that observed in the Gairloch region which is found to be very similar. They therefore conclude that the structures formed during the same faulting episode.

The emplacement of the sediment filled fractures is inferred to be syn-depositional with the Stoer Group due to the ability to trace the fill material of some fractures into the overlying Stoer Group. Dulin et al. (2005) have independently constrained this age using palaeomagnetic analysis, which indicates a Stoer Group age magnetization. They also determined the age of the sediment filled fractures in the Gailoch region and found them to be younger. Rather than forming in the same faulting episode as those at Clachtoll, as concluded by Beacom, Anderson and Holdsworth (1999), they could instead be attributed to a later episode of syndepositional extensional faulting during late Torridon Group deposition (Dulin, Elmore, Engel, *et al.* 2005, Jonk, Kelly & Parnell 2004).

1.4. Project aims and initial hypothesis

This project aims to characterise the different types of clastic fracture fill observed at Clachtoll and offer an explanation for their source and emplacement mechanism. Ultimately, a mechanism is sought after that can also account for the misorientation of the foliation within the block, compared to the surrounding gneiss. Evidence for Beacom, Anderson and Holdsworth's (1999) Clachtoll Fault zone will also be assessed.

The initial hypothesis to be tested is that the region of misoriented basement with sediment filled fractures is a large fallen block. The vertical emplacement of a falling block onto wet sediment could be sufficient to locally fluidize and overpressure the sediment into which it

fell and overcome the tensile strength of the block and induce hydrofracturing. The block would therefore not be physically attached to the surrounding gneiss at all, thus also explaining the change in foliation orientation. Proving this hypothesis would further our understanding of impact processes related to rock fall development and enable us to characterise and identify such processes in the ancient geological record. It would also challenge our understanding of the environments in which hydraulic fracturing can occur. Basement-hosted, sedimentary injectities need not be emplaced at depth and/or be tectonically controlled. Under the right conditions, they could instead represent processes occurring at the surface.

In addition to using field data, the processes involved in this hypothesis will also be investigated using experimental data and simple mathematical modelling.

CHAPTER 2

Field relationships and fracture fill characterisation

2.1. Methodology

Fieldwork:

12 days of fieldwork were undertaken at Clachtoll in late September, early October of 2016. This initially included reconnaissance of the field area to identify key field relationships (Fig. 2.1.1), prior to mapping the lithologies and boundaries throughout the area. Aerial photographs were also examined to identify areas of potential interest prior to the main period of field study. Observations and measurements recorded in the field included lithological descriptions, fracture, fault and foliation orientations, fault and fracture kinematic indicators and spatial relationships of lithological and structural features. In addition to orientation, a more detailed analysis of fractures included length, aperture, interconnectivity and intensity, sediment fill type, sedimentary structures, orientation of lamination of sediments in the fractures and the relationships between clasts in the fractures and with the fracture walls. Finally, hand specimens were collected of the in-situ gneiss along with examples of fracture fills.

Data analysis:

Numerical data were compiled into an Excel spreadsheet to allow easy creation of text-files to be imported into Rick Allmendinger's Stereonet software (version 9 and later version 10). Suites of stereonets were plotted to allow comparison of multiple sets of data.

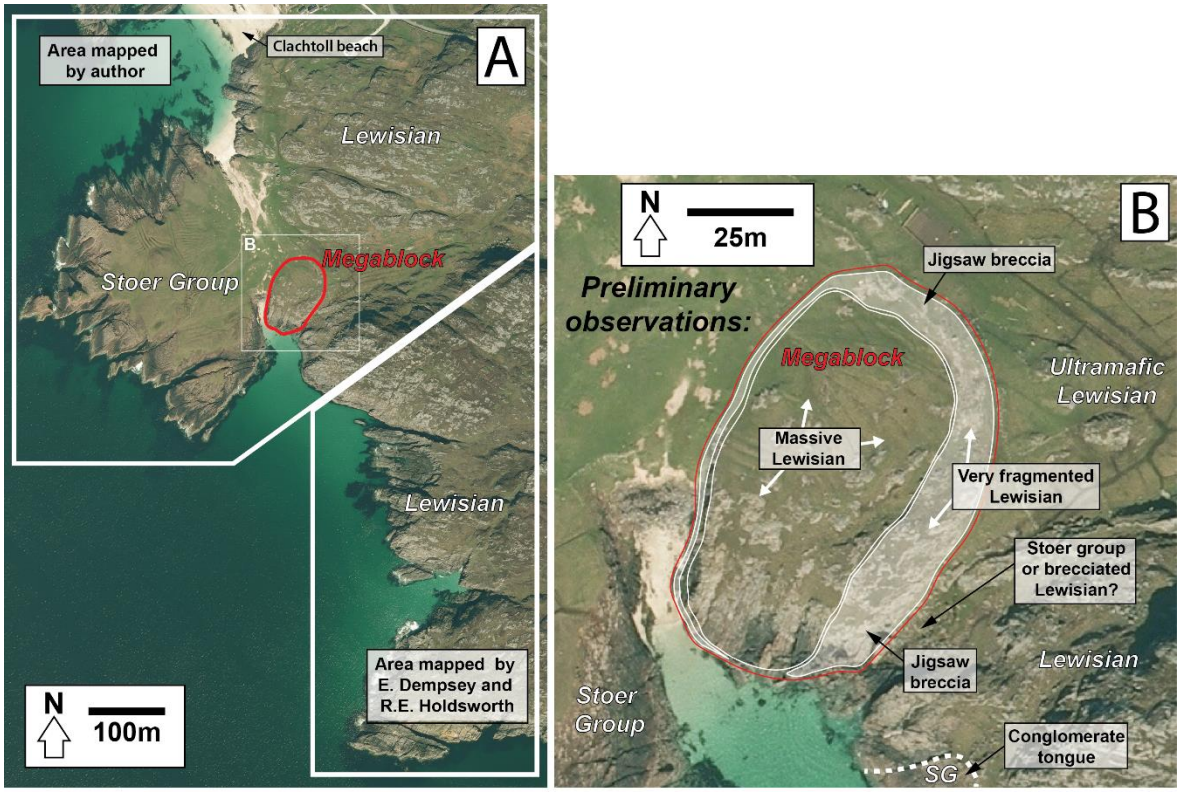

Figure 2.1.1. *The area of study is shown in Figure 2.1.1A, with the northern area having been mapped by the author, and the southern area mapped by E. Dempsey and R.E. Holdsworth. The inset, Figure 2.1.1B denotes the primary area of interest; the Clachtoll megablock.*

2.2. Maps

A geological map was made of an area that extends from Clachtoll beach (NC 0397 2708) down to the promontory of gneiss 1 km to the SSW (NC 0420 2615). The area includes the entirety of the lozenge shaped peninsula of Stoer Group lithologies, and extends eastwards inland of Clachtoll beach for 400 m. The map (Fig. 2.2.1.) shows the larger scale geological setting in which the Clachtoll megablock is situated. The most important feature is the position of the megablock apparently lying close to or on top of the contact between the Stoer Group and subjacent Lewisian gneiss, along with the misorientation of foliation within the megablock when compared to the surrounding gneiss. The map also shows a relatively dense network of two sets of faults within the Stoer Group which appear not to affect the gneiss. These faults are analysed in more detail in section 2.4.

Smaller maps were also made, specifically focusing on the Clachtoll megablock. Figure 2.2.2 shows the strike and dip of the foliation throughout the megablock, whilst Figure 2.2.3 shows the foliation as form lines in both the megablock and the surrounding gneiss. It also shows the approximate positions and orientations of sediment-filled fractures found within the megablock. The extent of the exposure can be seen in the aerial photograph maps showing fieldwork localities in Appendix A.

2.3. The Regional Gneiss

The amphibolite grade gneiss at Clachtoll displays typical gneissic banding across multiple scales. Bands of acid to intermediate gneiss (quartz and plagioclase abundant) alternate with bands of mafic gneiss (amphibole and biotite abundant) at the mm to cm scale (Fig. 2.3.1a) up to the decametre scale. Acid to intermediate bands at the metre to decametre scale are themselves typically composed of smaller alternating bands, where the acid to intermediate bands are more abundant. The opposite is sometimes true of metre to decametre scale mafic bands, however mafic bands at this scale also exist containing very little acid-intermediate material. These may represent very early stage mafic to ultramafic dykes that have since been sheared into parallelism with the surrounding gneiss (Beacom, Anderson & Holdsworth 1999). These are unlikely to be Scourie dykes which formed later and are generally still discordant in much of the Assynt Terrane, which was largely unaffected by Laxfordian deformation (Strachan, Holdsworth & Prave 2012).

This banding within the gneiss defines a strong, steeply dipping, ESE-WNW oriented foliation (Fig. 2.3.1b), characteristic of the gneisses of the Assynt Terrane, and particularly of the Canisp Shear Zone. Clachtoll itself, lies just north of the margin of the Canisp Shear Zone, whilst all of the gneiss south of the Clachtoll Megablock lies within this shear zone.

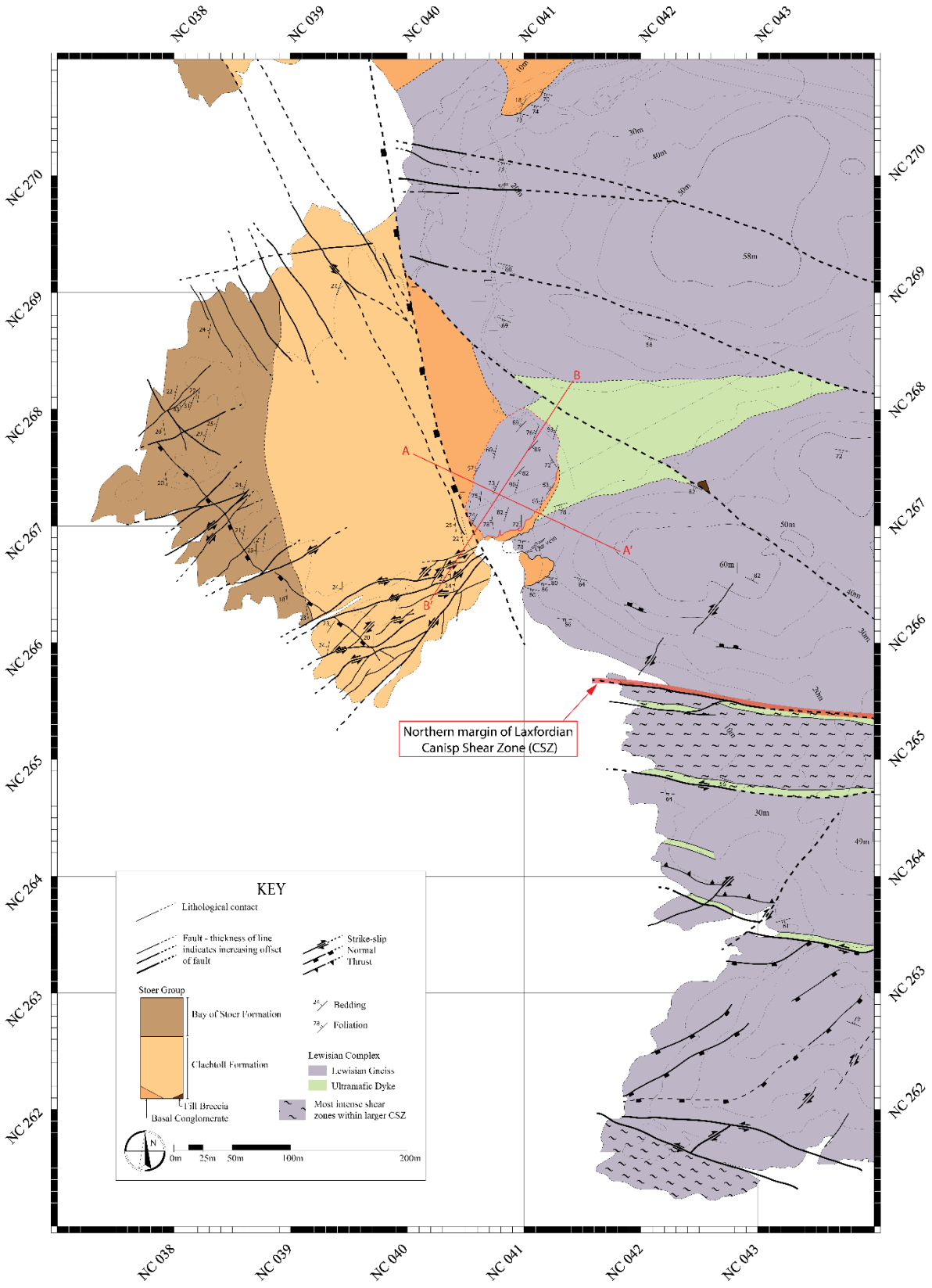

Figure 2.2.1. *Larger context map of geology. Red lines marked A-A' and B-B' denote the lines of section used to construct the cross sections found in figure 2.6.1.3. Location of northern margin of Laxfordian CSZ after* Attfield (1987).

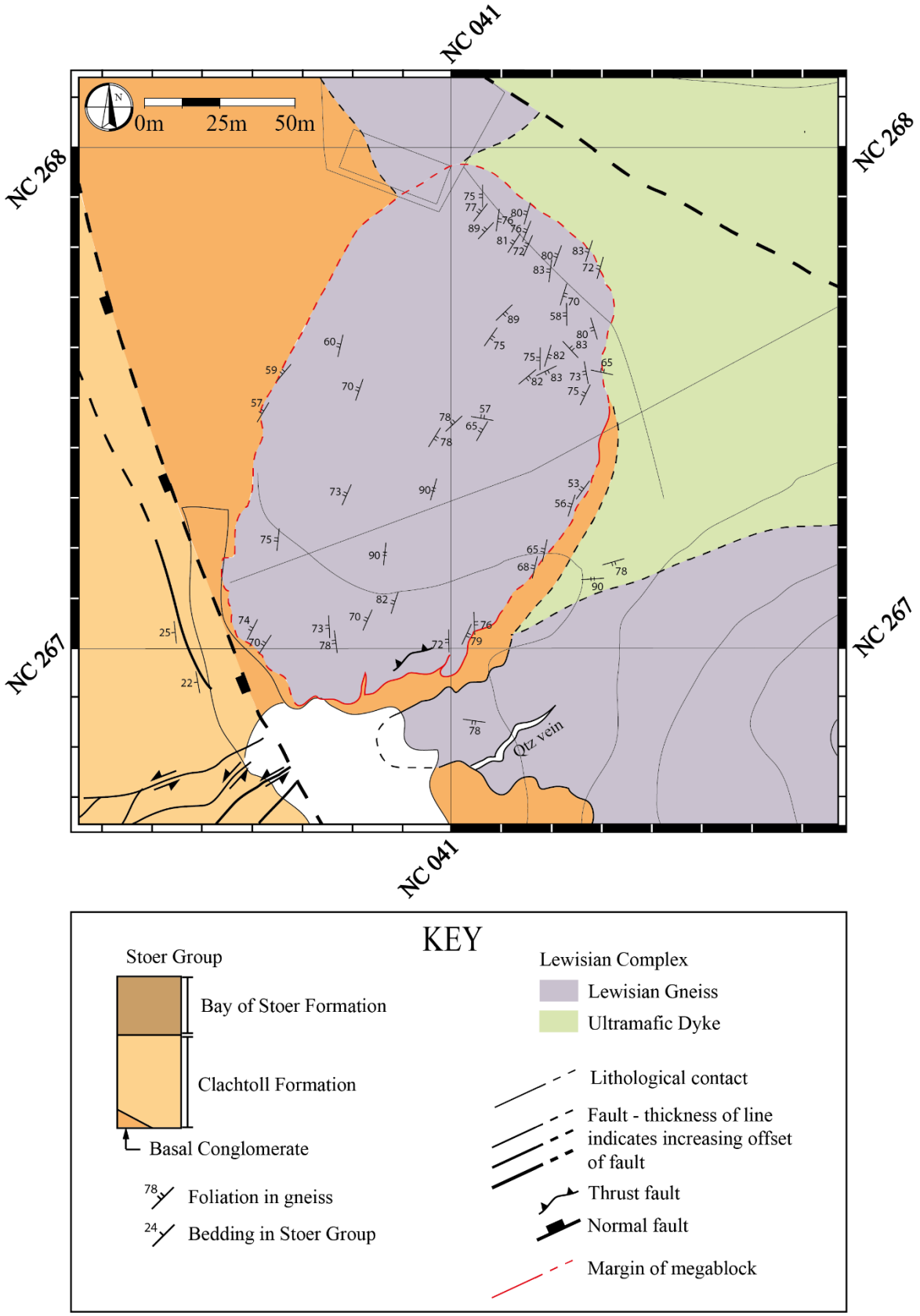

Figure 2.2.2. *Geological map of the Clachtoll Megablock, showing foliation data.*

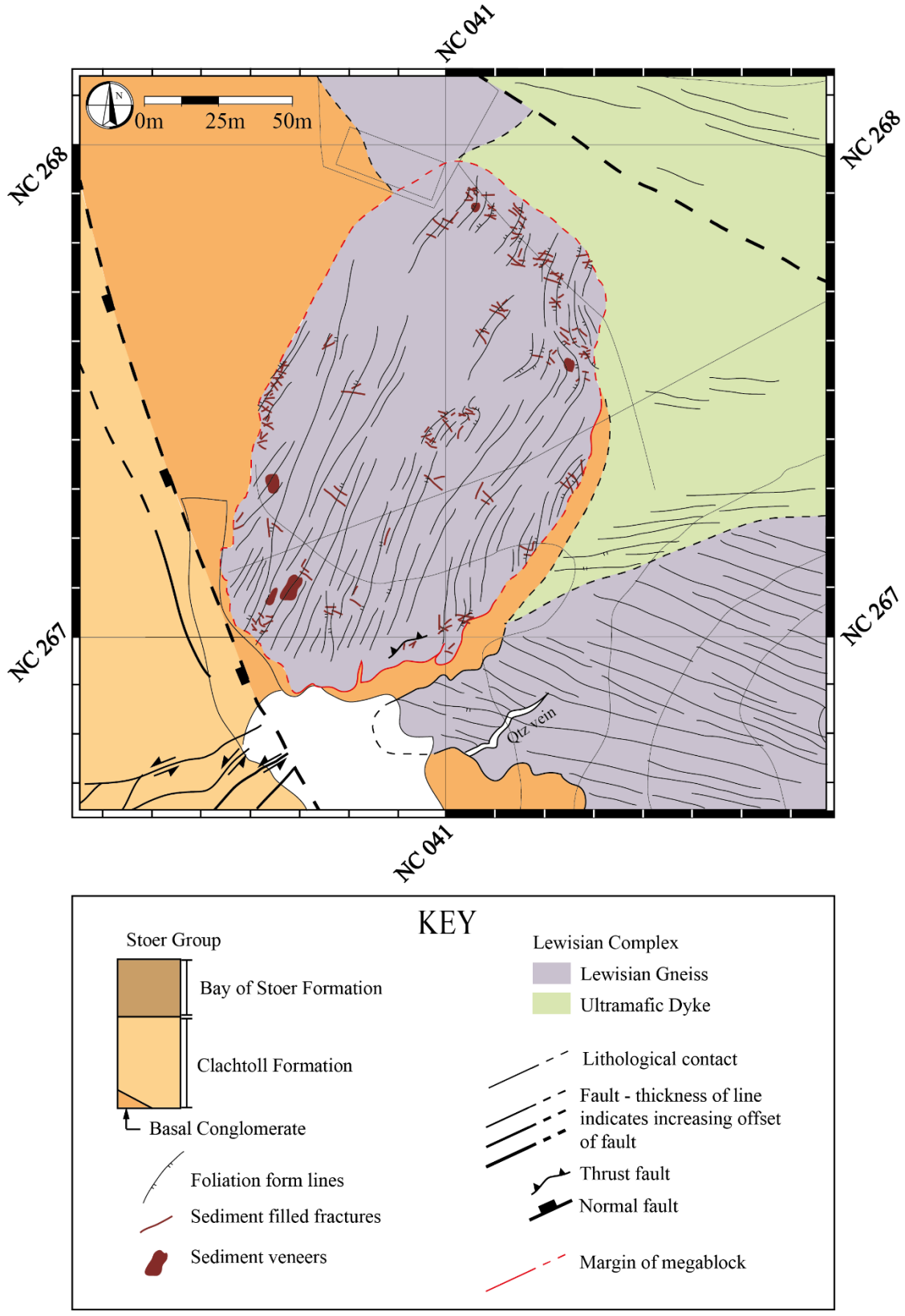

Figure 2.2.3. *Geological map of the Clachtoll Megablock, showing foliation form lines and fractures.*

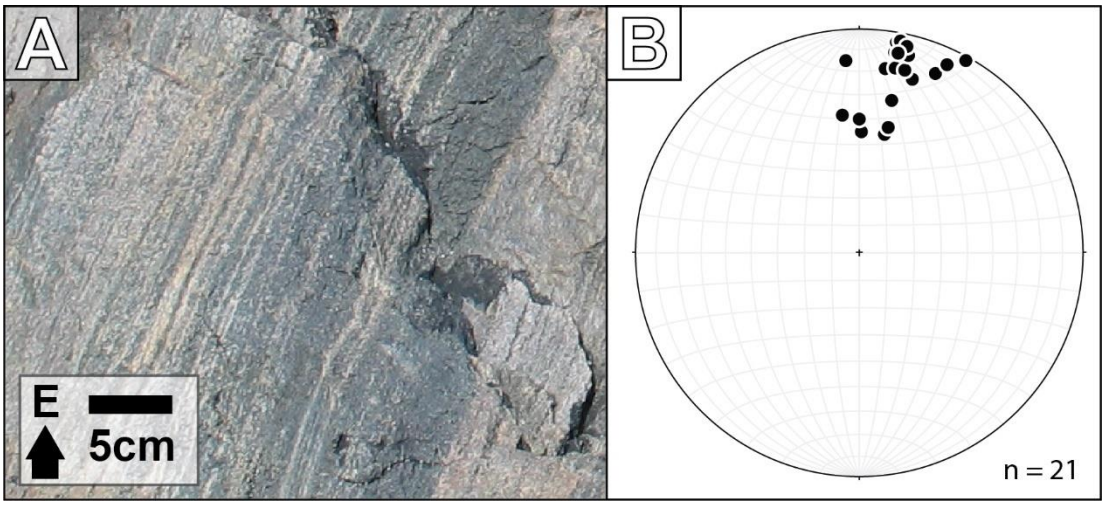

Figure 2.3.1. *(A) Close up of the mm-cm scale gneissic banding characteristic of the Lewisian gneiss in the region. (B) Regional foliation strikes ESE-WNW and dips steeply to the south.*

2.4. The Stoer Group

In the area of study, three distinct lithologies were identified belonging to the Stoer Group. Their spatial relationships, along with the locations of the faults that intersect them, are shown in Figure 2.4.1. The first two lithologies belong to the Clachtoll Formation (Stewart 2002). One is simply referred to as the Clachtoll Formation in this study, though it excludes the lowermost section which forms the second lithology; the basal conglomerate. This conglomerate is equivalent to Stewart's (2002) Ct1 facies. These two lithologies are not seen in contact with one another at Clachtoll and are assumed to be separated here by an inferred normal fault with downthrow to the west (Section 2.5 – tectonic contact). The third lithology is the stratigraphically lowermost section of Stewart's (2002) Bay of Stoer Formation. The three lithologies are likely conformable with one another and all dip 20º to 25º west (Fig. 2.4.4 [1]), as is consistent with Stewart's (2002) observations for the Stoer Group at a regional scale. The only exception is a bedding plane that has been progressively folded to a maximum dip of 43º adjacent to the plane of a small fault at NC 0380 2680.

The basal conglomerate (Fig. 2.4.2a) forms a tongue shaped outcrop, 50 m SSE of the Clachtoll megablock, where it infills a palaeovalley in the gneiss. It is a massive, poorly sorted, clast supported breccio-conglomerate, comprised of clasts of locally derived gneiss and quartz vein material. At its base, the basal conglomerate is composed of rounded

ultramafic to mafic clasts, averaging 20 to 40 cm, with a few clasts reaching 200 cm in size. Above this, the clasts become more angular and acidic in composition. Clast size grades upwards from around 40 cm to 4cm.

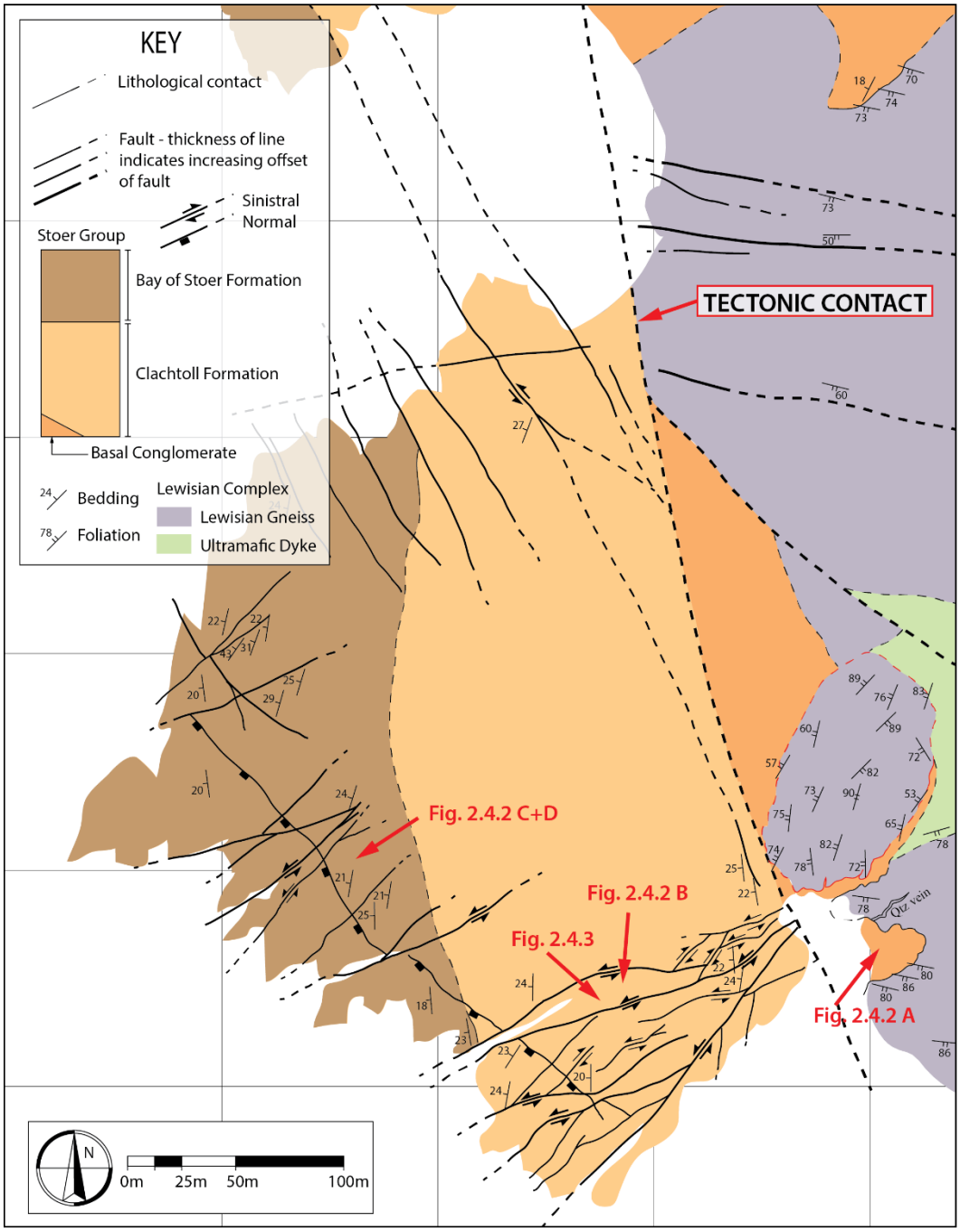

Figure 2.4.1. *Zoomed in map of the geology of the Stoer Group and Stoer-Lewisian contact in the study area. Areas where the contact represents a landscape unconformity with high relief are seen in the top and bottom right of the figure. Red arrows denote the locations of photographs used in Figures 2.4.2. and 2.4.3.*

300 m north of the Clachtoll megablock, the conglomerate outcrops again as isolated patches along the track, as seen in the northernmost part of the map in fig. 2.2.1. Here the conglomerate contains a much higher proportion of sand. Clast supported patches comprising 30% sand matrix and 70 % sub-rounded to sub-angular, acid gneiss clasts, are separated by matrix supported patches comprising 80% sand and 20% clasts. There is some evidence of cm to dm scale bedding throughout the outcrop, but it is not laterally continuous. This bedding truncates against clasts up to 1 m in size. Large parts of this outcrop are equivalent to Stewart's (2002) Ct2 facies (fig. 1.1.3), interpreted to represent small alluvial cones.

The remainder of the Clachtoll Formation in the study area (Fig. 2.4.2b) is comprised of massive beds of dark red, very fine-grained sandstone, 0.5 to 2 m thick. A few grains reach medium grade, but are still less than 0.5 mm. Sub-rounded to angular, white, pink and black clasts comprise less than 5% of the rock by volume. The bedding surfaces have a polygonally cracked appearance, where chips of the material is being weathered away between cracks. This lithology is equivalent to Stewart's (2002) Ct7 facies (fig. 1.1.3), interpreted as ephemeral lake deposits.

The Bay of Stoer Formation at Clachtoll (Fig. 2.4.2c & d) outcrops on the western side of the lozenge shaped peninsula. It intercalates with the uppermost beds of the Clachtoll Formation but is distinguished by its clear bedding, ~10 m to 50 m thick, and its well preserved trough cross bedding. This lithology is Stewart's (2002) BS1 facies (fig. 1.1.3), interpreted as the deposits of braided streams crossing a bajada.

It is the basal conglomerate that lies in the closest proximity to the Clachtoll megablock.

Another defining feature of the Stoer Group at this locality is the two sets of faults that cut through it. A steeply dipping NE-SW oriented set display strike slip kinematics, and orthogonal to this, a NW-SE oriented set (Fig. 2.4.4 [2&3]). The NW-SE oriented set is comprised primarily of steeply dipping faults speculatively inferred to be strike slip (purely from their sub-vertical dip), but a shear sense could not be identified. A few NW-SE oriented faults were identified as more shallowly dipping, normal faults. Almost all the NE-SW oriented strike slip faults have a sinistral sense of movement, with only a couple of faults

displaying a dextral sense of movement. These shear senses are evidenced, rarely by the offset of markers, and always by the presence of Riedel and Anti-Riedel fractures. Strictly speaking, the majority of these are only *apparent* strike slip faults, given the lack of slickenlines or clear offsets. The less frequent dextral faults appear to act as Anti-Riedel fractures between two larger, parallel sinistral faults. Except for the NW-SE normal faults, there is no exposure of any intersection between the NW-SE and NE-SW faults, so cross cutting relationships cannot be observed. There is evidence at a few localities that the NW-SE normal faults have been offset by the NE-SW sinistral faults, making the sinistral faults younger. In general, a lack of markers makes the degree of offset difficult to infer. Figure 2.4.3 shows an example of the appearance of the NE-SW sinistral faults in the area.

A distinction had to be made between the faults observed, and the vast number of fractures associated with them. These features cutting through the Stoer Group were defined as faults if they were comprised of a zone of parallel fractures that was laterally continuous for 10 or more metres. The fractures always abutted against or splayed off of these faults, were discreet planes, and were much shorter in length.

These smaller fractures are also extremely abundant in the Stoer Group in this area. Many of these were obvious in the field as structures synthetic and antithetic to the larger faults. This is further evidenced by plotting the faults and the smaller fractures on a stereonet (Fig. 2.4.4 [2]). Vertical strike slip faults, having a horizontal movement, should produce vertical antithetic and synthetic structures. This is seen to be the case; most of the fractures plot as clusters on or adjacent to the primitive circle, either side of the faults. The remaining fractures appear to plot along a NE-SW oriented, moderate to steeply dipping great circle. These fractures may represent structures that are antithetic and synthetic to the normal faults.

Interestingly, the adjacent Lewisian gneiss appears to be unaffected by the faulting seen in the Stoer Group, despite being older. Other than the basal conglomerate of the Clachtoll formation, the Stoer Group at Clachtoll has been downfaulted along a large inferred normal fault to juxtapose it against older lithologies. Therefore, one possibility is that the faulting within the Stoer Group occurred prior to this juxtaposition. An alternative and possibly preferable explanation is that the faulting occurred after this juxtaposition, and the stress regime resulting in faulting in the Stoer Group, simply didn't overcome the strength of the gneiss or there were no suitably oriented structures to be reactivated. Assuming the stress

regime didn't overcome the strength of the gneiss, it follows that strike displacements were likely small (e.g. cm to mm scale). This is consistent with the lack of obvious offset observed. The small normal fault in the Stoer Group could then be related to the larger scale inferred normal fault.

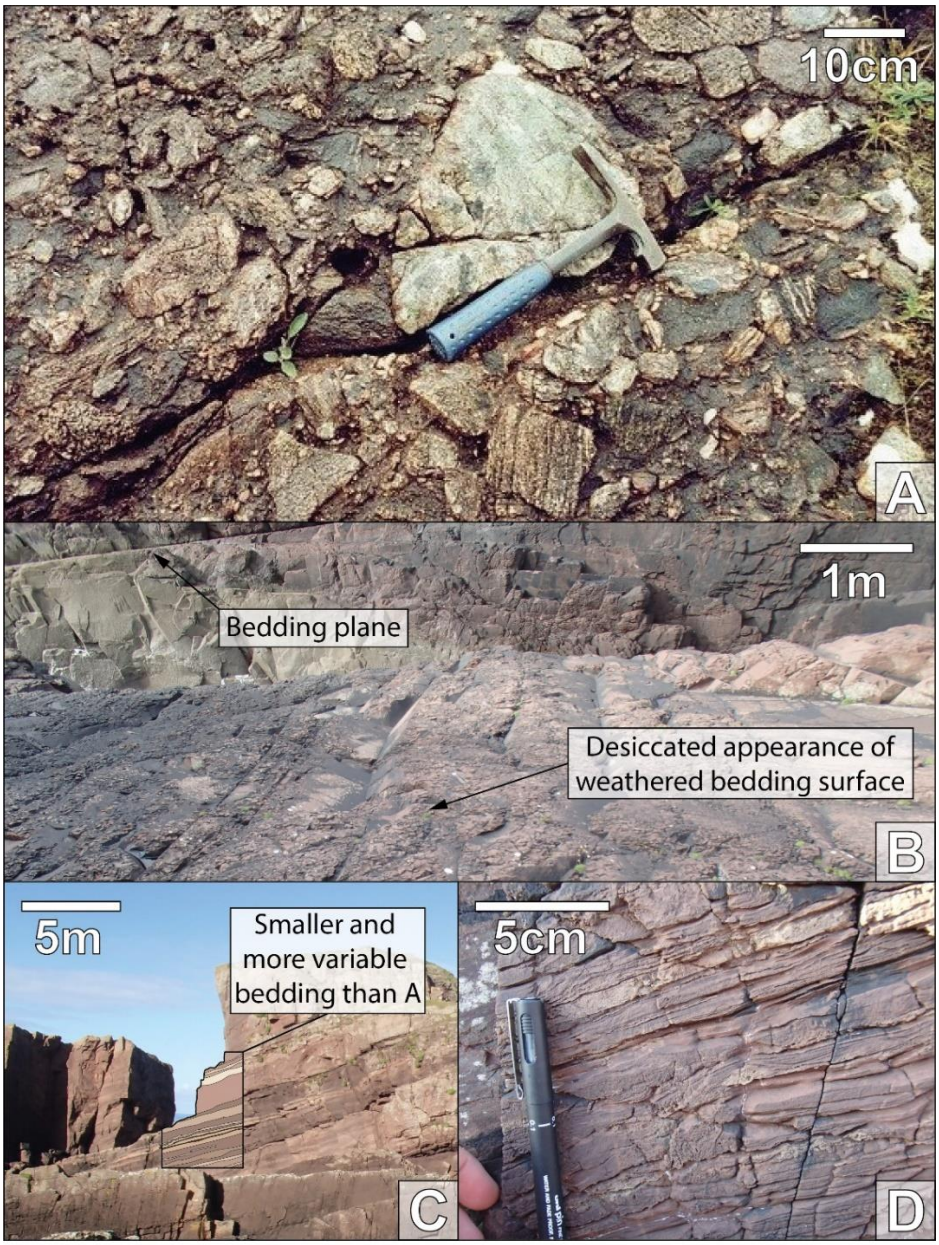

Figure 2.4.2. *Photograph A shows the appearance of the basal conglomerate at Clachtoll whilst photograph B shows the typical appearance of the middle to upper part of the Clachtoll formation in the study area. Photographs C and D show the typical appearance of the Bay of Stoer formation in the area. Photograph A is taken from Waters* (2003).

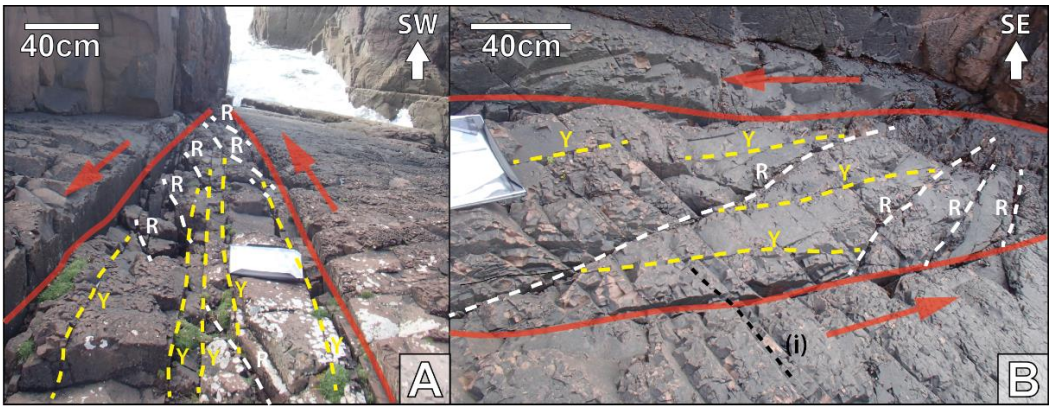

Figure 2.4.3. *The figure shows a fault with apparent strike slip displacement, representative of those found within the Stoer Group in the area of study. Photo A looks SW down the strike of the fault, whilst photo B looks approximately SE across the strike. A sinistral sense of shear is inferred from the orientation of Riedel fractures within the fault zone (white dashed lines). Y fractures (yellow) are observed running parallel to the margins of the fault zone (denoted in red). The black dotted line at (i) denotes the orientation of another set of fractures which in some places cross cut the fault zone, and in others truncate against it.*

Figure 2.4.4. *(1) Poles to bedding planes in the Stoer Group; (2a) Poles to faults and fractures in the Stoer Group, as they were measured in the field; (2b) poles to faults and fractures, back-rotated to pre tilting of bedding position; (3a) poles to faults in the Stoer Group by type of fault, as measured in the field; and (3b) poles to faults by type of fault, back-rotated to pre tilting of bedding position.*

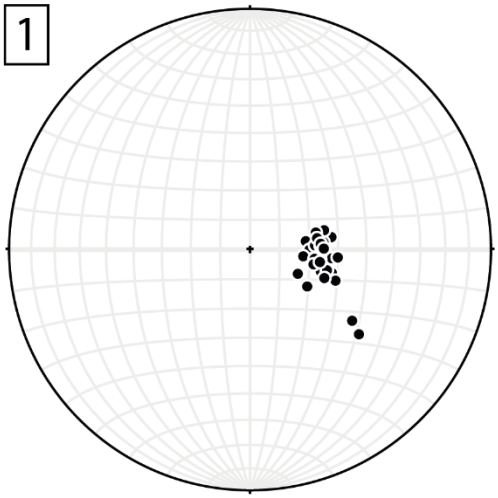

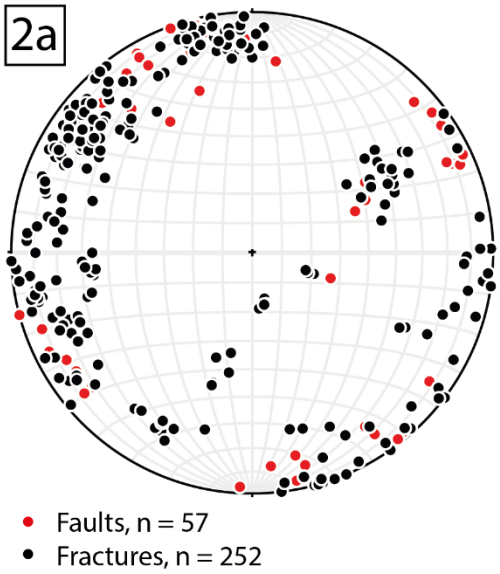

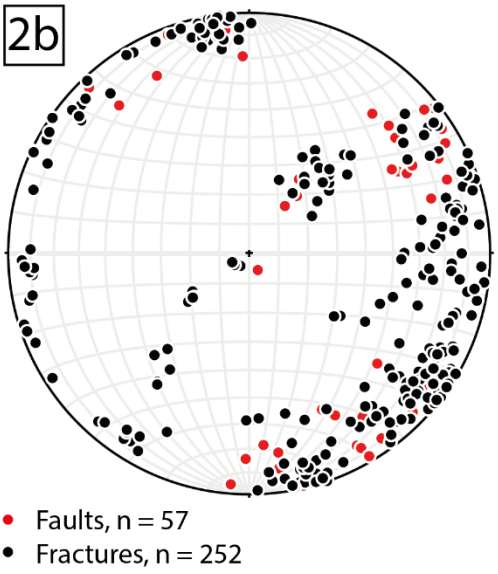

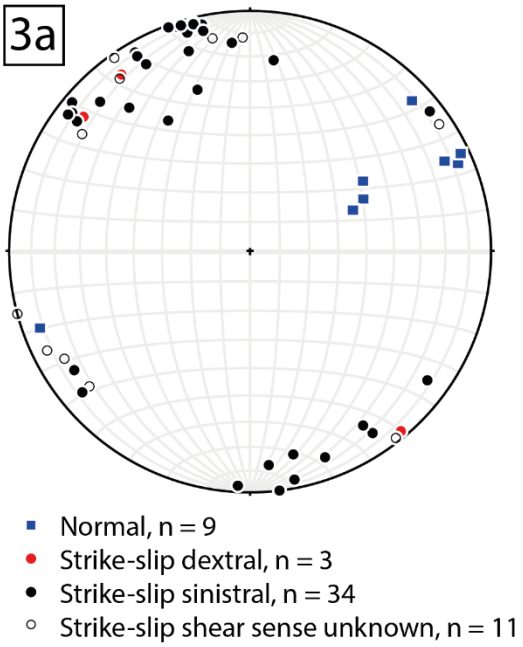

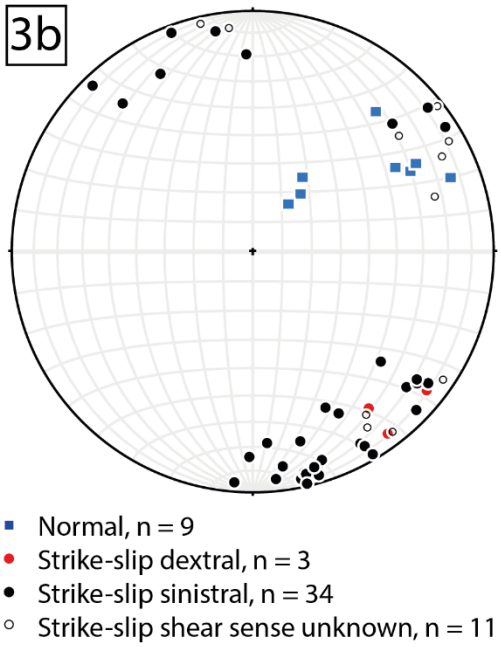

2.5. The contact between the Stoer Group and the Lewisian

UNCONFORMABLE CONTACT

On the Stoer Peninsula, the contact between the Stoer Group and the Lewisian is very irregular along its entire exposure (Fig. 2.5.1). The Stoer Group overlies the Lewisian, infilling the Lewisian topography to form a regional scale nonconformity. It is the high relief of the basement that has resulted in the abundance of palaeovalley fills that define the irregularity of the contact.

At Clachtoll, this relationship is clearly observable where a ~400 m^2, west dipping tongue of basal conglomerate lies on the Lewisian gneiss (Fig. 2.5.2). Erosion along the contact, directed towards the centre of the tongue, hints at the shape of the valley that the conglomerate has infilled. At Clachtoll, the basement at the time of Stoer Group deposition had a relief of up to about 150 m (Stewart 2002).

TECTONIC CONTACT

Small sections of stratigraphically higher units within the Stoer Group have been downthrown to the west to be juxtaposed against the Lewisian gneiss along inferred normal faults. Such an example is labelled in Figure 2.4.1. These faults are likely related to movement on the nearby Coigach fault which can be seen in Figure 2.5.1. Originally an east dipping normal fault during the time of Stoer Group deposition, the Coigach fault was reactivated as a west dipping normal fault after the Cambrian (Stewart 1993). The faulting responsible for the small sections where the Stoer-Lewisian contact is tectonic, also have an apparent downthrow to the west, and are therefore likely related to this later reactivation.

At Clachtoll, this faulting has also brought stratigraphically higher Stoer Group units into contact with the basal conglomerate. A potential geological history resulting in this relationship is presented in Figure 2.5.3.

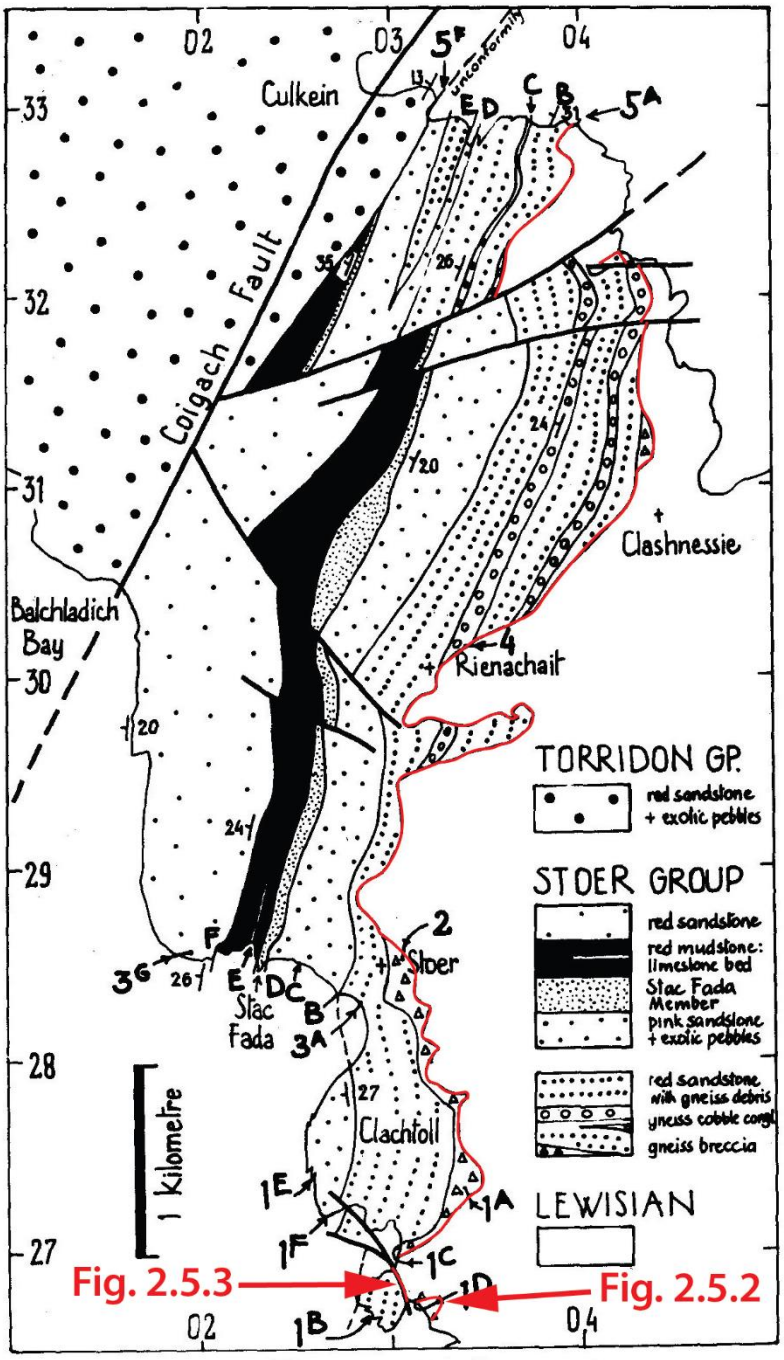

Figure 2.5.1. *Map drawn by A. D. Stewart, taken from Barber et al.* (1978 p.28) *showing the geology of the Stoer Group on the Stoer Peninsula. The Stoer Group – Lewisian contact (red line) observed in this study is seen at the very bottom of the map, but the contact is found to be very irregular, often infilling palaeovalleys, across the entirety of the region.*

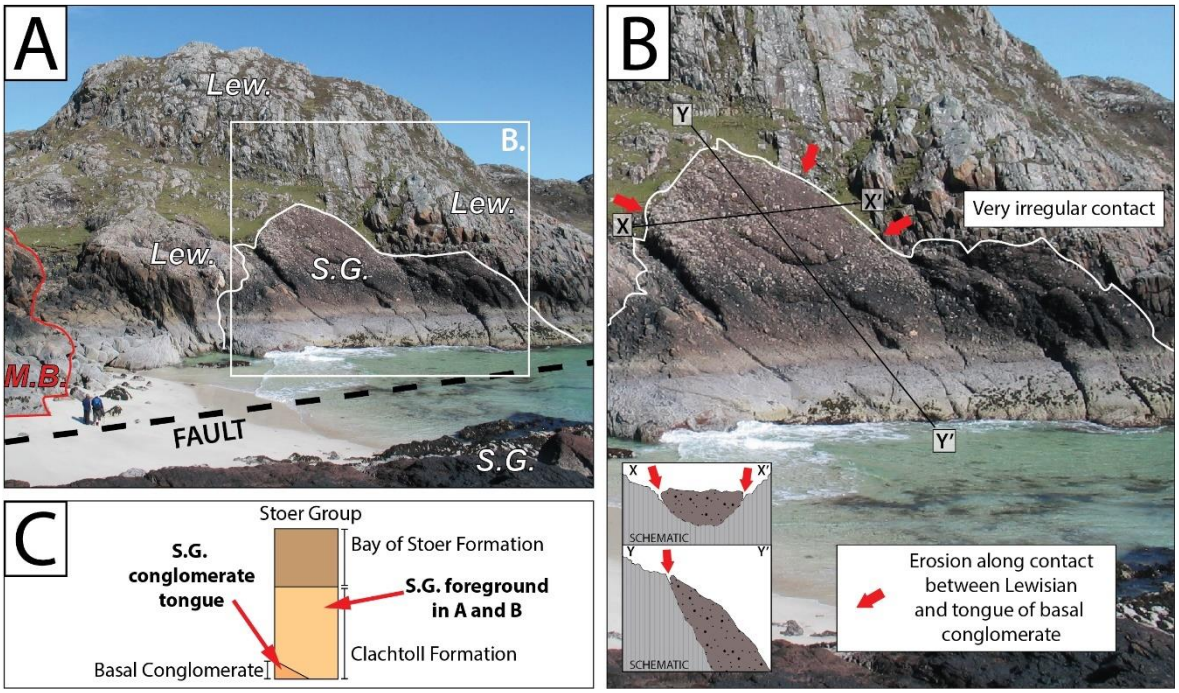

Figure 2.5.2. *(A) The unconformable contact between the Stoer Group and the Lewisian gneiss in the study area. (B) Close up of the conglomerate tongue representing a palaeo-valley, indicating the high relief of the landscape onto which the Stoer Group was deposited. The red arrows denote areas where erosion along the contact is clearly observable. (C) shows the relative positions of the Stoer Group lithologies observed in the photos, on a schematic stratigraphic column of the Stoer Group.*

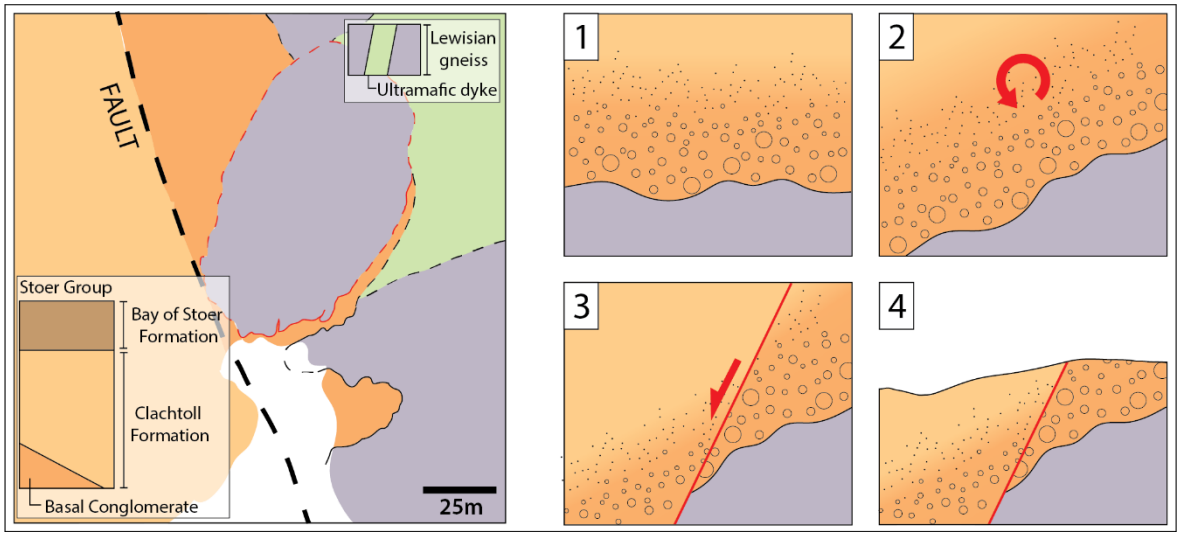

Figure 2.5.3. *(1) The relationships between the different facies of the Stoer Group are complex and frequently intercalated but are here schematically represented as a simple grading from the basal conglomerate into the higher, sand and mud rich facies. (2) The Stoer group is tilted to the west by approximately 25º. (3) Downthrow to the west occurred along a west dipping normal fault. (4) Erosion to present day topography.*

2.6. The Clachtoll Megablock

2.6.1. 3D Characterisation

The Clachtoll megablock has a roughly elliptical shape in plan view, with dimensions of approximately 100 m by 60 m. Its long axis is oriented NNE-SSW. Its vertical dimension appears to be much smaller, at approximately 15 m, giving the block a tabular shape in 3D. The gneiss comprising the block is identical in terms of lithology and texture to the adjacent basement, except for its foliation which strikes at 90° that in the main outcrop of the basement. Planes of foliation define two low cliff faces along the western edge of the block, shown in the far left of the top photo of Figure 2.6.1.1 and in the lower part of Figure 2.6.3.1. Henceforth, the southern and northern ends of the block are referred to as the front and back of the block respectively. Most of the western side of the megablock, and the western front edge of the megablock, form one contiguous block of gneiss; at least in its upper portion – the lowermost metre of outcrop is heavily cut by sediment filled fractures. The eastern side of the block, however, has a very brecciated appearance, and the degree of fragmentation increases towards the back of the block (Fig. 2.6.1.1). Foliation on the west side of the block consistently strikes NNE, whilst foliation on the east side is rather more irregular; though its average orientation is still NNE.

In a gulley to the east of the block, it is difficult to differentiate the brecciated gneiss of the Clachtoll megablock from the basal conglomerate of the Stoer Group. In some places, patches of basal conglomerate are plastered onto the side of the megablock. Previous studies attribute this gulley to the presence of a fault (Beacom, Anderson & Holdsworth 1999), however this study found insufficient evidence to infer a fault. Instead, the gulley follows the edge of a picrite dyke, which is seemingly more susceptible to erosion than the adjacent gneiss, forming a broad valley further inland (NC 0420 2675.

Treating the outline of the Clachtoll megablock as a contact, an attempt was made to use structure contours to determine the underground geometry of the basal surface of the block (Fig. 2.6.1.2). This resulted in a 25° dip to the southwest of the basal surface at the front of the block, decreasing to 10° at the back. It should be noted that in order to do this, it must be assumed that the basal contact is curviplanar about an axis parallel to strike. Then straight

structure contours could be drawn. If structure contours are used to plot this surface onto a cross section of the outcrop (Fig. 2.6.1.2), the basal surface is seen to exactly parallel the topography of the outcrop. This is not too surprising given that the upper surface is also a palaeosurface.

Inferred cross sections of the Clachtoll megablock in the context of the surrounding geology are presented in Figure 2.6.1.2.

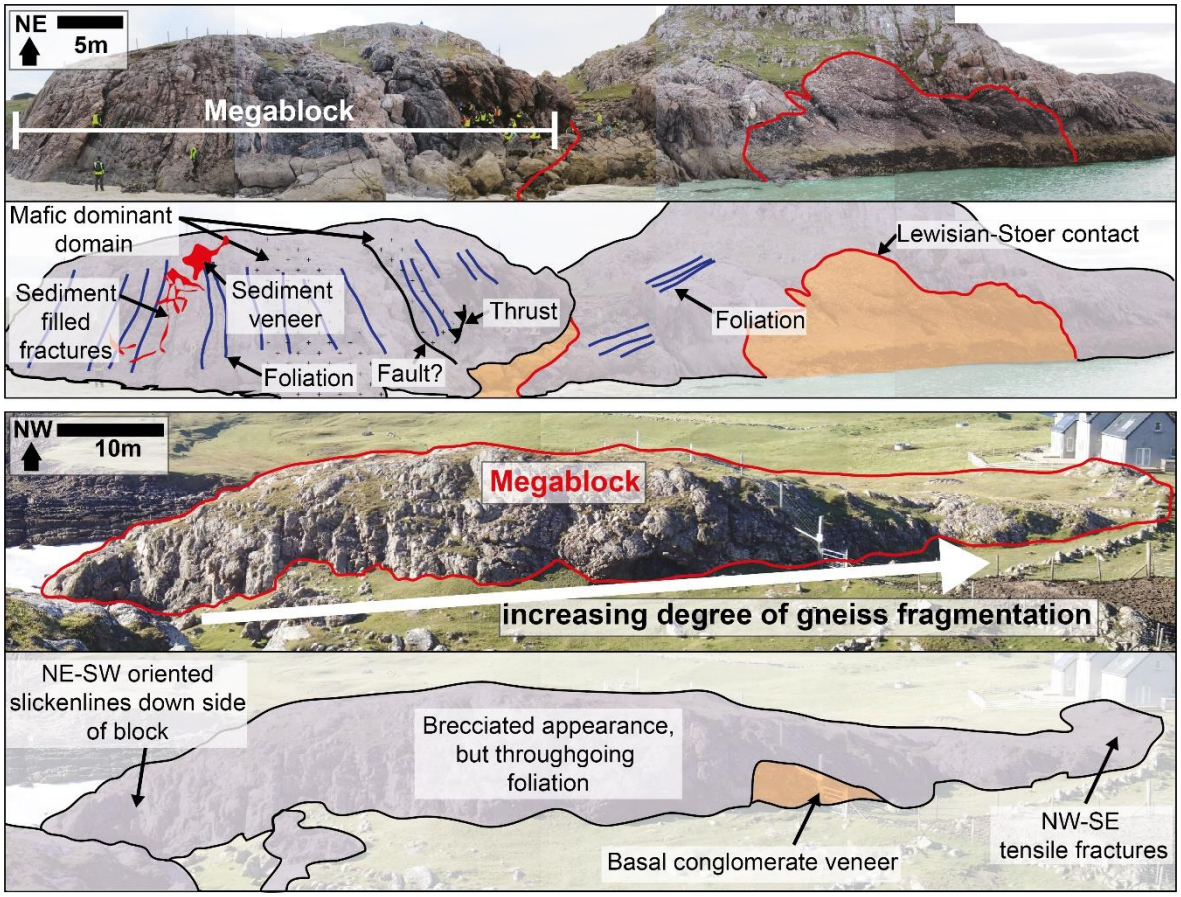

Figure 2.6.1.1. *(Top) Appearance of the front of the Clachtoll megablock and its relationship to the Lewisian-Stoer contact. (Bottom) Brecciated appearance of the eastern side of the Clachtoll megablock, with increasing fragmentation towards the NE.*

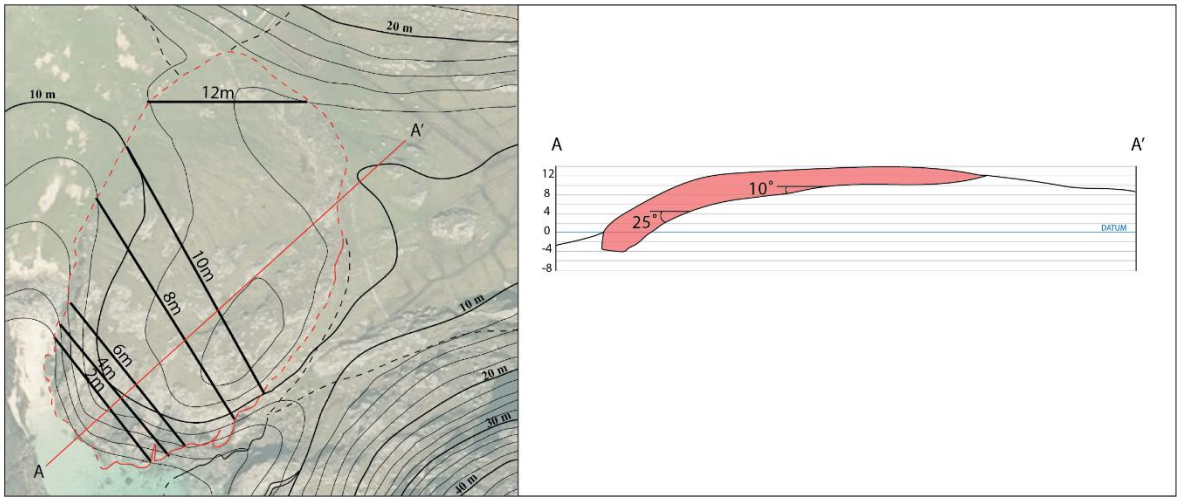

Figure 2.6.1.2. *Structural contours drawn using intersection between the outline of the Clachtoll megablock and the 2 m spaces topographic contours.*

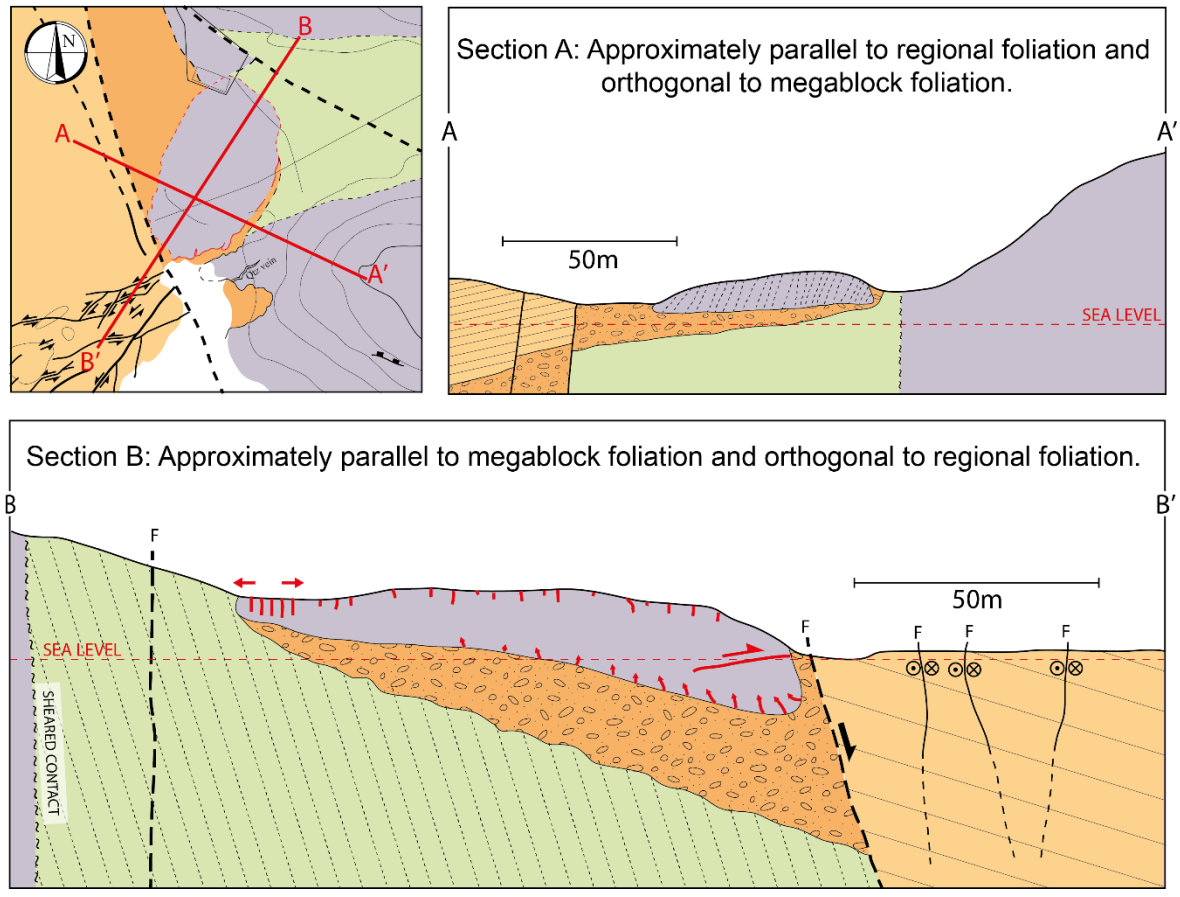

Figure 2.6.1.3. *Cross sections through the Clachtoll megablock. Section A is perpendicular to the foliation in the block, section B is parallel.*

2.6.2. Structural data and comparisons

The following structural data were recorded:

- Foliation in the Clachtoll megablock
- Foliation in the surrounding gneiss
- Faults and fractures in the Stoer Group
- Sediment filled fractures in the Clachtoll megablock
- Non-sediment filled fractures in the Clachtoll megablock

Other data recorded included:

- Apertures of the sediment filled fractures
- Laminations within the sediment filled fractures
- Bedding in the Stoer Group

Firstly, the foliation data for the Clachtoll megablock and the surrounding gneiss were plotted on a stereonet to ascertain the degree of misorientation between the two sets (Fig. 2.6.2.1). Using the mean foliation orientation for each set, the acute angle between the two foliations was found to be 87.9°. A misorientation of almost 90° compared to the regional foliation is especially significant given that it occurs very abruptly and only in a small area, with no evidence of the regional foliation being rotated by either folding or faulting into alignment with that in the area deemed to be the megablock.

Next, the orientations of the foliation in the megablock were compared with the orientations of the sediment filled fractures (Fig. 2.6.2.2). In this section, 'raw data' in figures denotes data that has been plotted in the orientation that it was measured in the field. 'Back-rotated data' denotes stereonets that have been corrected to represent the data as it would have been measured prior to tilting of the area. This correction involved rotating the data clockwise (looking N) about a horizontal axis with an azimuth of 007º, by 24º. (The Stoer Group bedding has an average strike and dip of 007/24 W.)

As the foliation contributes parallel planes of weakness to the gneiss, it was initially expected that fractures might follow the foliation. More often than not, this hypothesis was found to be false in the field. This is shown by the stereonet which, when contoured, gives a fracture

orientation which lies almost orthogonal to the foliation. Many of the fractures show no particular preferred orientation, but there is a clearly defined group of NW-SE trending, steeply dipping fractures. These fractures were seen to have a tensile opening direction, oriented NE-SW, which approximately parallels the long axis of the Clachtoll megablock. This preferred orientation of tensile fractures is especially well developed towards the northern, back end of the block (Fig. 2.6.3.6).

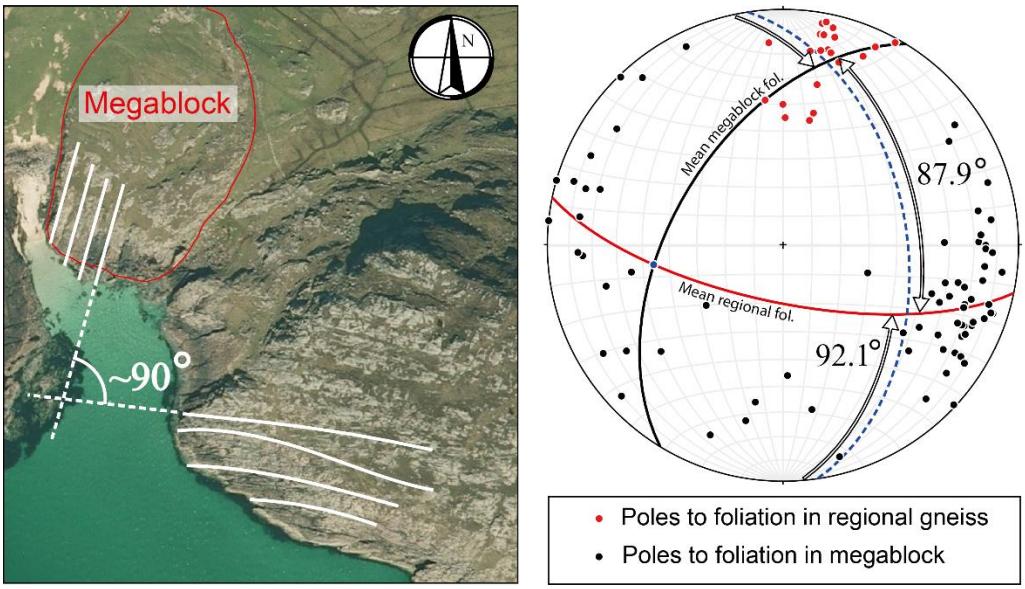

Figure 2.6.2.1. *The misorientation of the megablock foliation relative to the regional foliation, observable in the field and shown on a stereonet.*

This comparison of megablock foliation and sediment filled fracture orientations was then broken down by area of the block (Fig. 2.6.2.3). Localities were assigned to either the back, front, east, west or top of the block. The back of the block is where the most consistently NW-SE trending fractures occur. Fractures here are steep to vertical. Bar a few anomalies, the fractures at the front of the block are also fairly consistently NW-SE trending, but are more varied in their dip. A set of fractures on the west side of the block also has a general NW-SE trend, but additionally, many fractures are found with a N-S to NE-SW trend. Again, fractures here are variable in their dip, but none have a dip of less than 30º. The top of the block also has an approximately NW-SE oriented set of fractures and an additional NE-SW oriented set of fractures; both moderate to steeply dipping. Here, some of the fractures appear to parallel the foliation. Finally, fractures in the east side of the block are mostly random in

their strike and their dip. There is no obvious preferred orientation, and this is the only area where numerous sub-horizontal fractures are observed. There is also more significant variation in the gneissose foliation in the east side of the block; it is this side of the Clachtoll megablock that is seen to be the most brecciated and fragmented in the field. Foliation in the top, front and west of the megablock is consistently oriented NE-SW. Foliation at the back of the block is also more variable in its strike, though less so than that in the east side, and remains relatively steep.

The orientations of fractures with different apertures were also compared (Fig. 2.6.2.4). No clear correlation was observed, either between fracture aperture size and fracture orientation, or between fracture aperture size and position within the block. Though for fractures of known size, no fractures larger than 10 cm were found in the top of the megablock.

Next, orientations of laminated layers found in some of the sediment filled fractures, were compared to the bedding in the adjacent Stoer Group (Fig. 2.6.2.5a). The laminations show

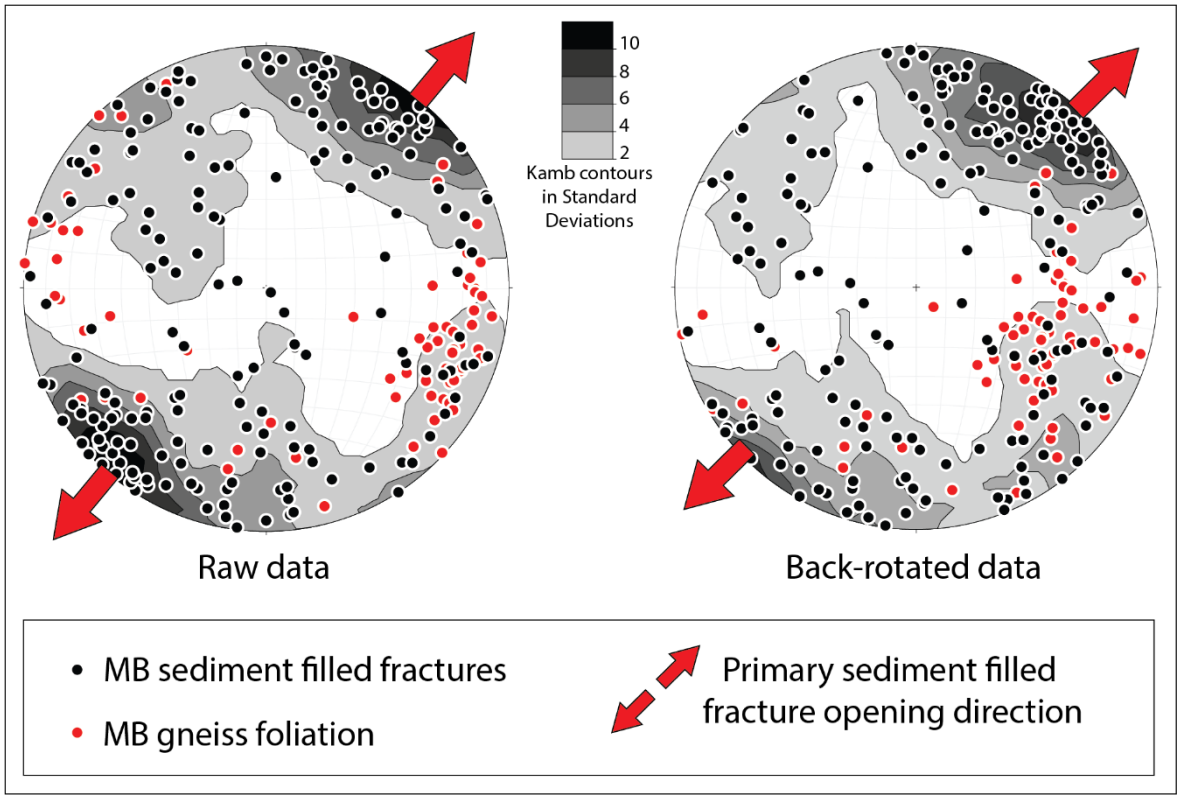

Figure 2.6.2.2. *Stereonets comparing the orientations of the foliation and the sediment filled fractures in the Clachtoll megablock. (Left) as measured in the field, (right) corrected to account for tilting of area.*

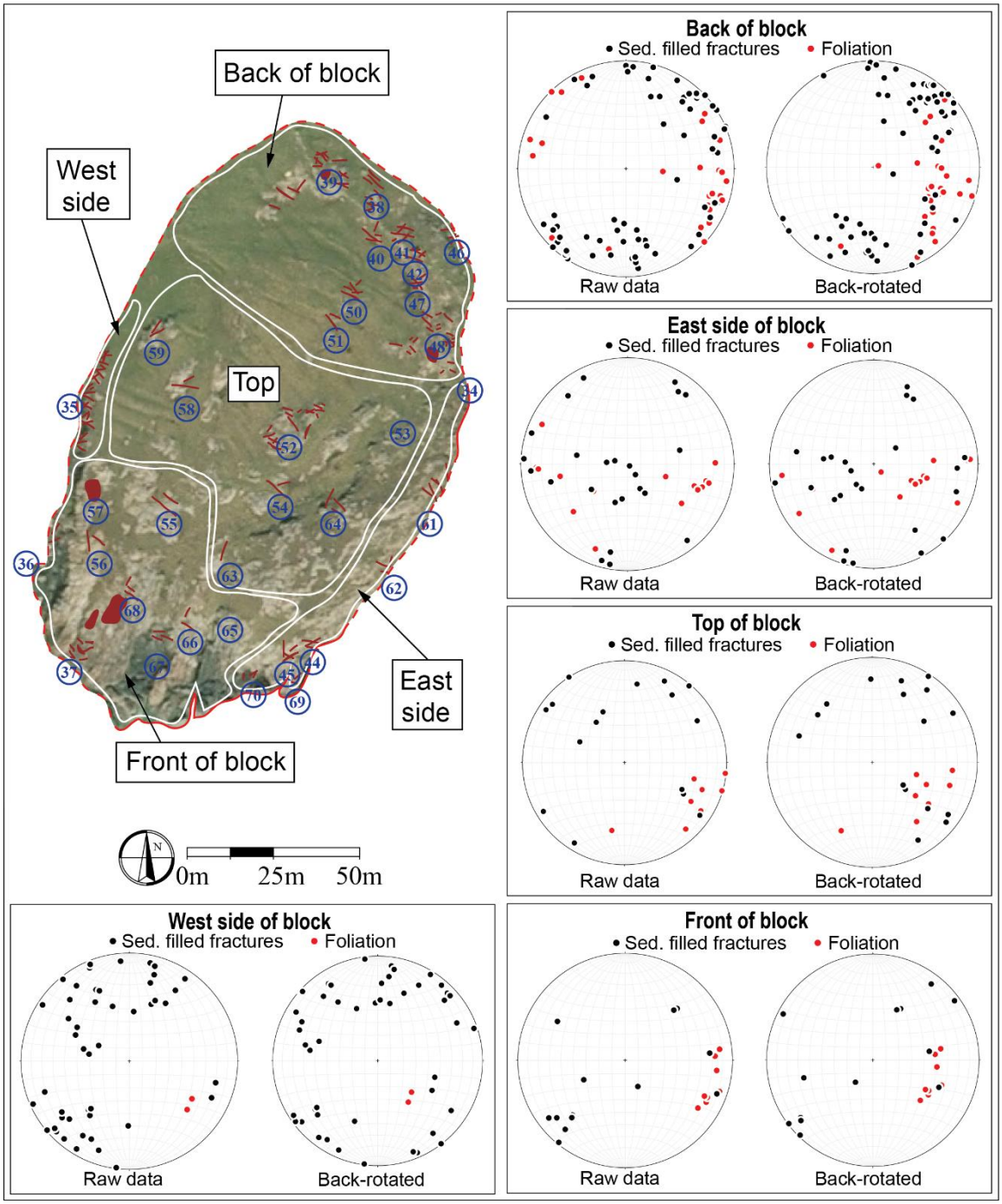

Figure 2.6.2.3. *Stereonets of Clachtoll megablock foliation and sediment filled fractures by area of the megablock.*

significantly more variation in their orientation compared to the bedding in the Stoer Group, but in general, the two sets are found to have a similar mean orientation. This suggests contemporaneous deposition of the sediments in the fractures of the Clachtoll megablock and the adjacent Stoer Group. It can cautiously be argued that the lamination data plots on a great circle, shown in Figure 2.6.2.5a, suggesting some sort of curvature to the laminations

(Fig 2.6.2.5b). This apparent curvature could be a depositional architecture; many fissure fills show this geometry (Walker, Holdsworth, Imber, *et al.* 2011). An alternative hypothesis could be that these laminations were planar when initially deposited but have since slumped in the middle as a result of later migration of fluids; as in Friese, Vollbrecht, Leiss, *et al.* (2011). More speculatively, it may be that WNW-ESE dilational fractures were late compressed in a NNE-SSW direction, soon after being deposited; possibly due to the deceleration and arrest of the sliding block. This is supported by the beta axis of the folded laminations being perpendicular to the inferred NNE-SSW sliding direction.

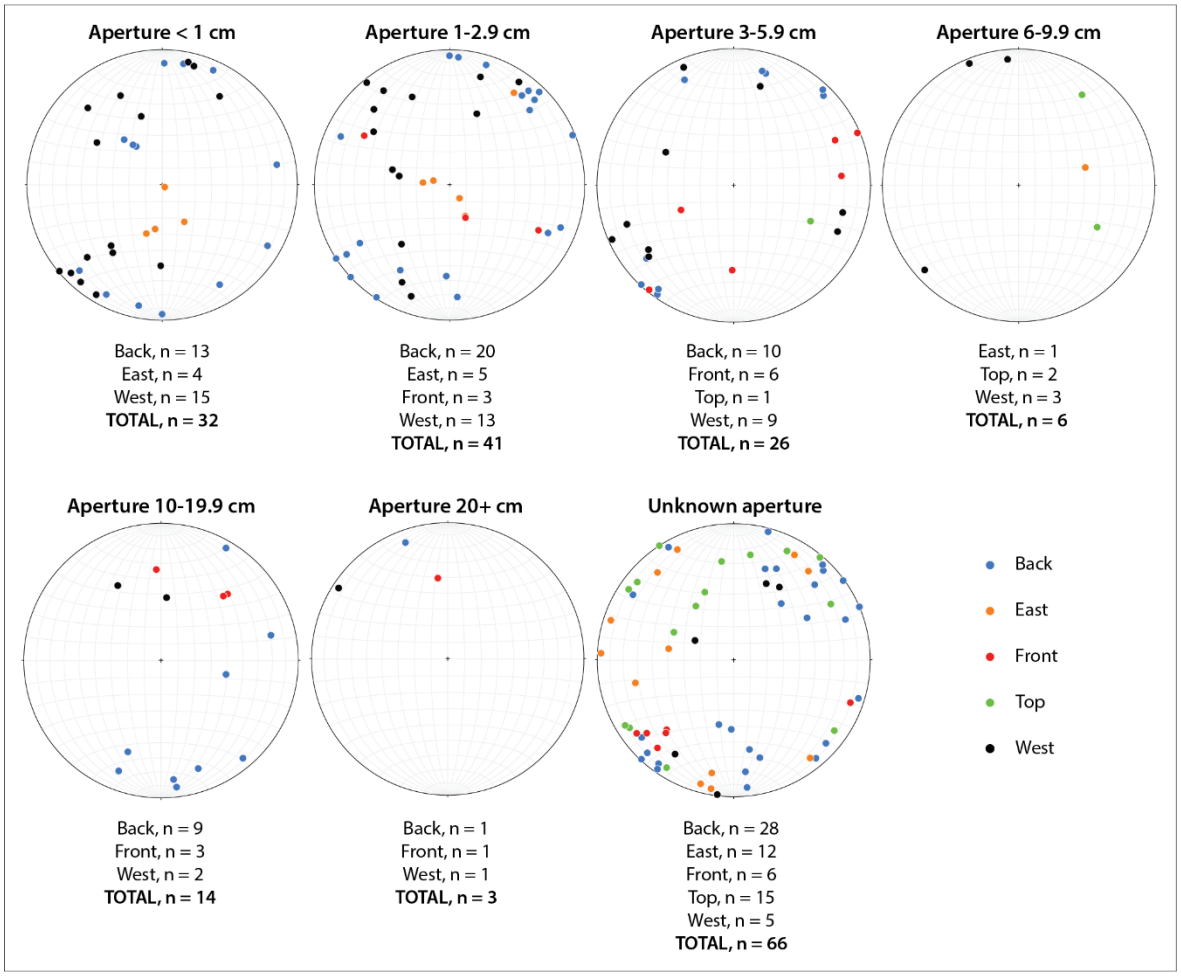

Figure 2.6.2.4. *Stereonets of sediment filled fractures by aperture. The colours denote where in the block the measurements have come from.*

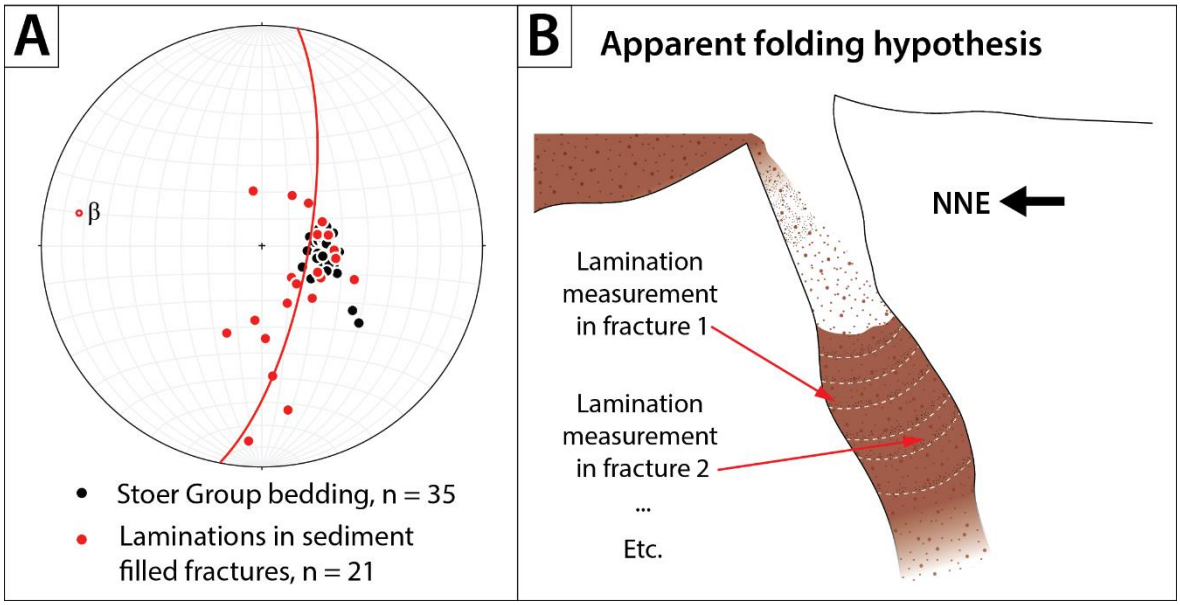

Figure 2.6.2.5. *(A) Stereonet comparing bedding in the Stoer Group south of the Clachtoll megablock to the orientation of laminations found in sediment filled fractures. (B) Hypothesis explaining the apparent fold observed from the lamination data.*

Finally, the orientations of the fractures in the Clachtoll megablock, both sediment filled and non-sediment filled, were compared to those in the Stoer Group. They show no obvious relationship to the fractures in the megablock, which are much more chaotic in orientation and distribution.

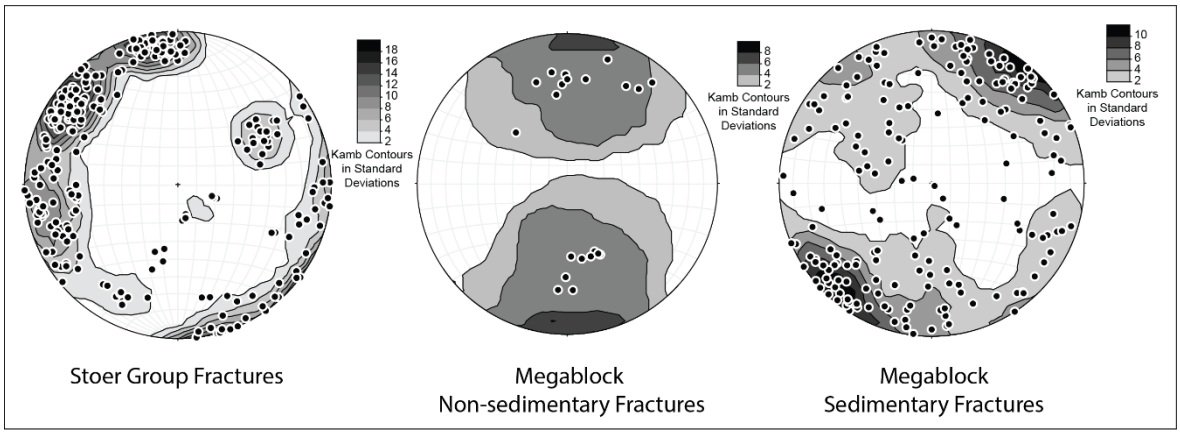

Figure 2.6.2.6. *Stereonets comparing the orientations of fractures in the Stoer Group to those in the Clachtoll megablock.*

2.6.3. The morphology and texture of the sediment filled fractures

The distribution and internal features of the sediment filled fractures varies throughout the Clachtoll megablock. Their morphologies and textures can broadly be assigned to 3 groups.

1. Fractures filled by bedded, fine to coarse sands, displaying sedimentary structures including lamination and clast imbrication. These fractures are only found in the top region of the Clachtoll megablock, and a few localities in the back region (denoted by a labelled dashed line in Figure 2.6.3.1). In some cases, the material in these fractures can be traced up into overlying veneers, plastering the surface of exposed sections of the block.
2. Mostly planar, fine sand filled fractures, found only around the margins of the block (see labelled dashed line in Figure 2.6.3.1). Most of these fills are structureless and massive and are interpreted to have been injected. Many contain matrix supported clasts of the host gneiss which have been detached from the fracture walls; akin to stoping in igneous intrusions. Some clasts have foliation that is misoriented relative to that in the host gneiss, but most contain foliation that parallels that in the wall rock. A small number of these sand-filled fractures (~5%) carry laminations of coarser and finer material, parallel to the fracture walls.
3. Forcefully injected zones of intensely fragmented gneiss containing planar to curviplanar, clastic fills, forming complex networks. A defining characteristic of these networks is the abundant presence of variably sized and oriented pockets of clastic material not confined to fractures.

Some fractures do occur along the pre-existing planes of foliation, but the vast majority crosscut it. Additionally, there are non-sediment filled fractures which were either pre-existing features or fractures that formed at the same time as the sediment filled fractures but weren't filled. Forcefully injected vs. passively infilled fractures have been identified on the basis of criteria outlined in Table 1.2.1.

FORCEFULLY INJECTED FRACTURE FILLS

All of the injected fracture fill material is comprised of sub-rounded to very angular grains of predominantly quartz and plagioclase, in addition to a significant clay component. The quartz and plagioclase grains are poorly sorted, but mostly still less than 0.5 mm. Larger grains do occur but are typically confined to coarser bands in fractures displaying wall parallel laminations. The appearance of these fracture fills is dark red in colour. The margins of all forcefully intruded, sediment filled fractures are very sharp, with no mineralisation present.

Fractures are present which contain variably sized, angular rafts of gneiss wall rock. Where these rafts have an elongated shape, their long axes are aligned parallel to the fracture walls. Foliation within these rafts is also typically parallel to that in the wall rock. Transport distance of these rafts is minimal; indeed some rafts can be matched to the location in the fracture wall that they were separated from, normally only millimetres to centimetres from where they are presently located (e.g. Fig. 2.6.3.2a, fig. 2.6.3.5).

Other fractures contain a layering that runs parallel to the fracture wall. These layers are relatively gradual where defined by changes in grainsize (Fig. 2.6.3.2b) and sharp where defined by a change in colour, possibly reflecting composition (Fig. 2.6.3.3). Clast size in these layers varies from 1 – 10 mm, and elongated clasts are again aligned with their long axes parallel to the fracture walls. Grain size is not normally related to position within the fracture, but occasionally, the largest grains are observed to occupy a position down the centre of the fracture fill material. These are possibly analogous to the distribution of variably sized phenocrysts within an igneous dyke, resulting from the parabolic velocity profile across the fracture at the time of intrusion/injection. Subtle, wall parallel laminations also occur along the outer portions of some sediment filled fractures (Fig. 2.6.3.3).

Larger fractures are associated with and connected by a complex network of smaller fractures (Figs. 2.6.3.2, 2.6.3.3). These are sometimes observed to branch off from larger fractures and then terminate, much like the injection structures observed in pseudotachylytes (Figs. 2.6.3.2, 2.6.3.4). Such structures are also observed intruding wall rocks surrounding, or clasts within, larger pockets of injected material (e.g. Fig. 2.6.3.7).

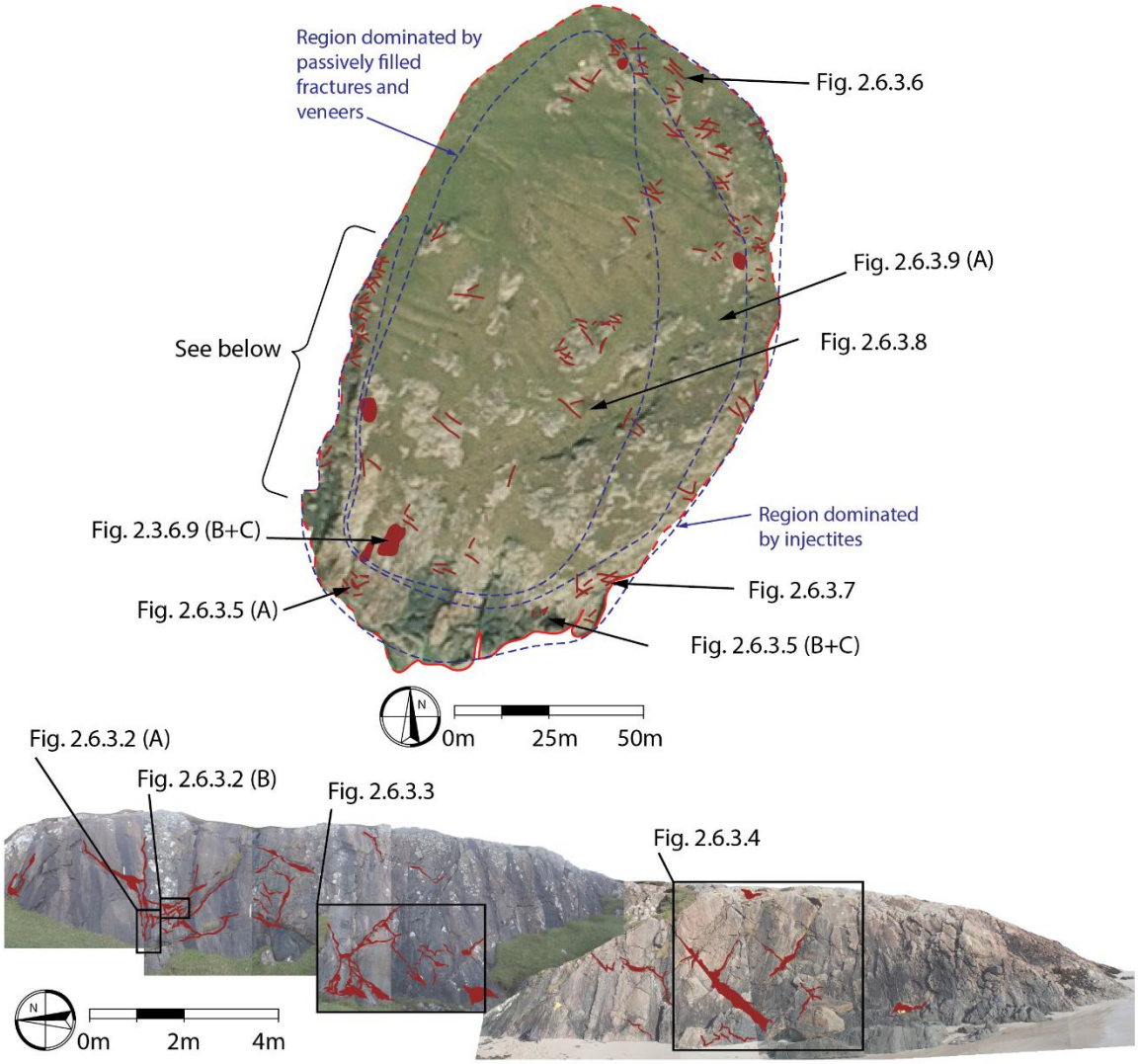

Figure 2.6.3.1. *Locations of sediment filled fractures pictured in subsequent figures. The blue dashed lines denote the general distribution of forcefully injected vs. passively infilled fractures.*

Tensile opening directions can sometimes be found by matching points on opposing sides of the fracture walls, as in Figs. 2.6.3.3., 2.6.3.5., 2.6.3.7.

On the western side of the megablock (lower part of Figure 2.6.3.1), fractures up to 30 cm in aperture, penetrate for 2-3 m up the outcrop. Smaller fractures, less than 20 mm in aperture, are confined to the bottom metre of the outcrop, and the lowermost 30cm is abundant in small, 2 – 5 mm thick fractures. It is on this side of the megablock that the sediment filled fractures are observed to sometimes intrude along an apparently conjugate set of non-sediment filled fractures or joints. Here a fracture with an aperture of nearly 50 cm at its observable base, closes upwards, terminating 2 – 3 m away. The upper part of the

fracture is filled with fine, homogeneous, massive sand, whilst the wider base contains poorly sorted, randomly oriented, angular to sub-rounded clasts of gneiss. It is variably clast supported and matrix supported. Small injections branch off the base of the fracture, filled by fine, homogeneous, massive sand (Fig. 2.6.3.4).

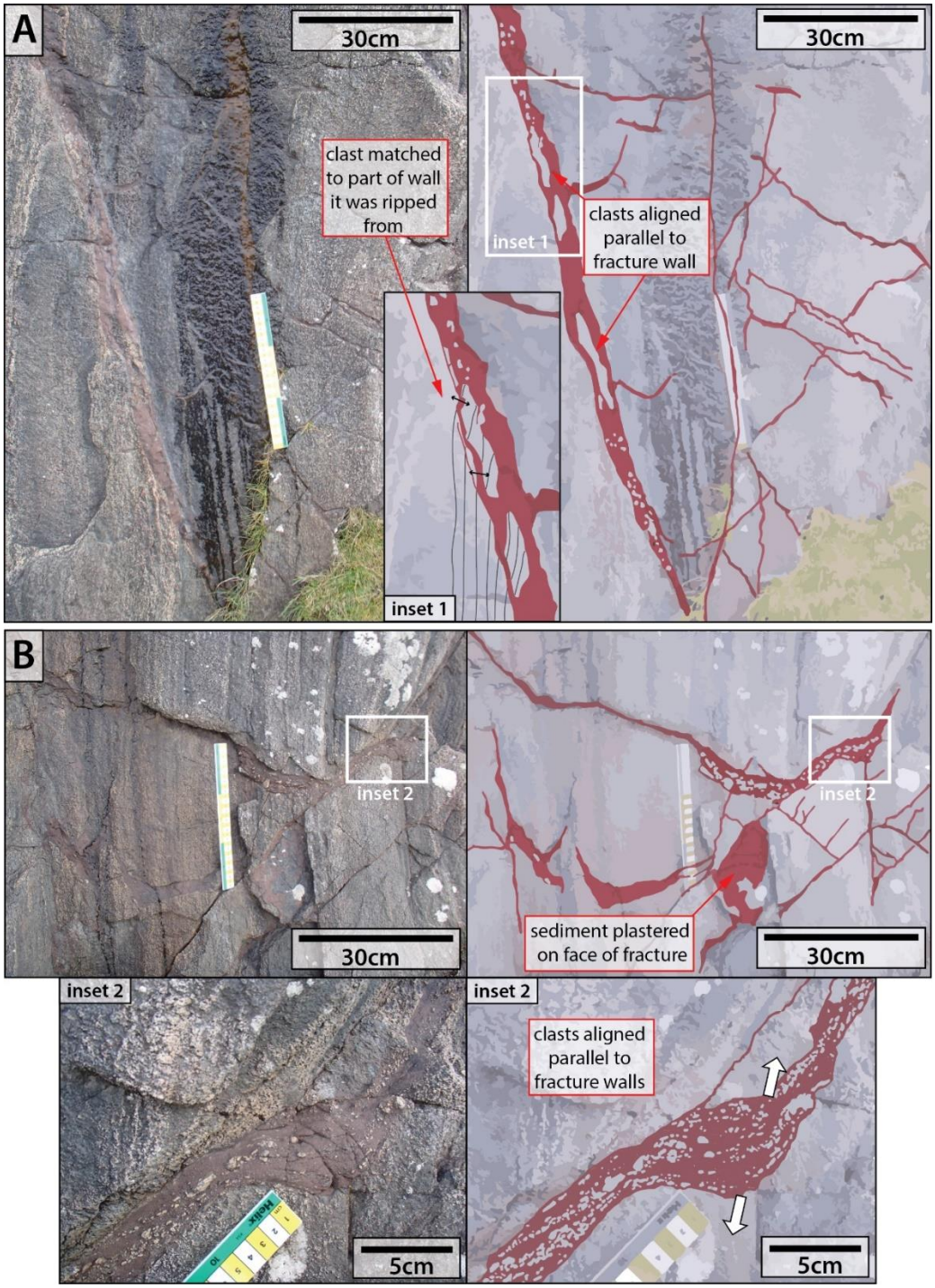

Figure 2.6.3.2. *Forcefully intruded sediment filled fractures on the west side of the Clachtoll megablock. (A) Fracture containing stoped wall raft, (B) Fracture wall parallel banding with sediment fill.*

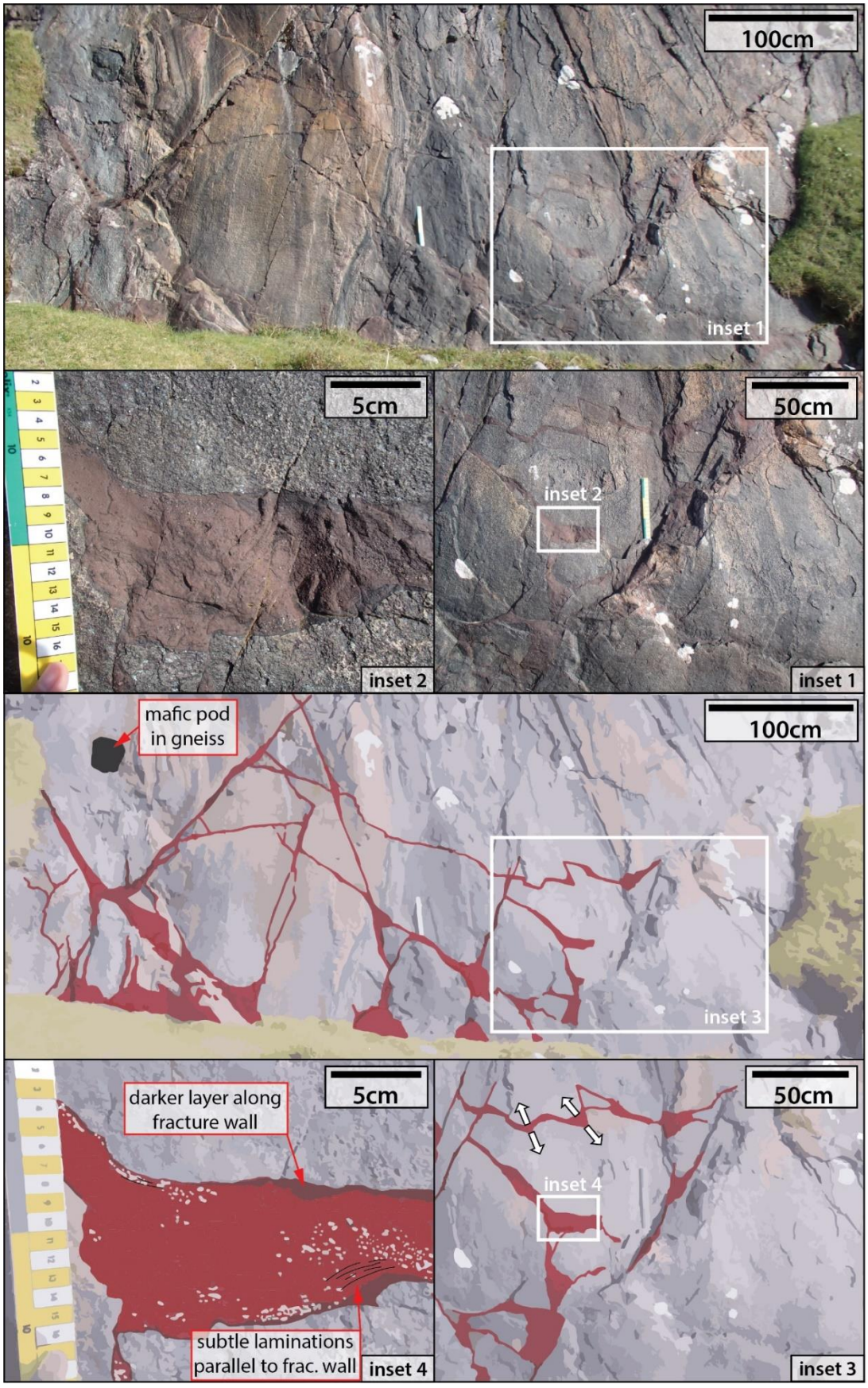

Figure 2.6.3.3. *Forcefully intruded sediment filled fractures on the west side of the Clachtoll megablock, showing complex networks and occasional laminations parallel to fracture wall.*

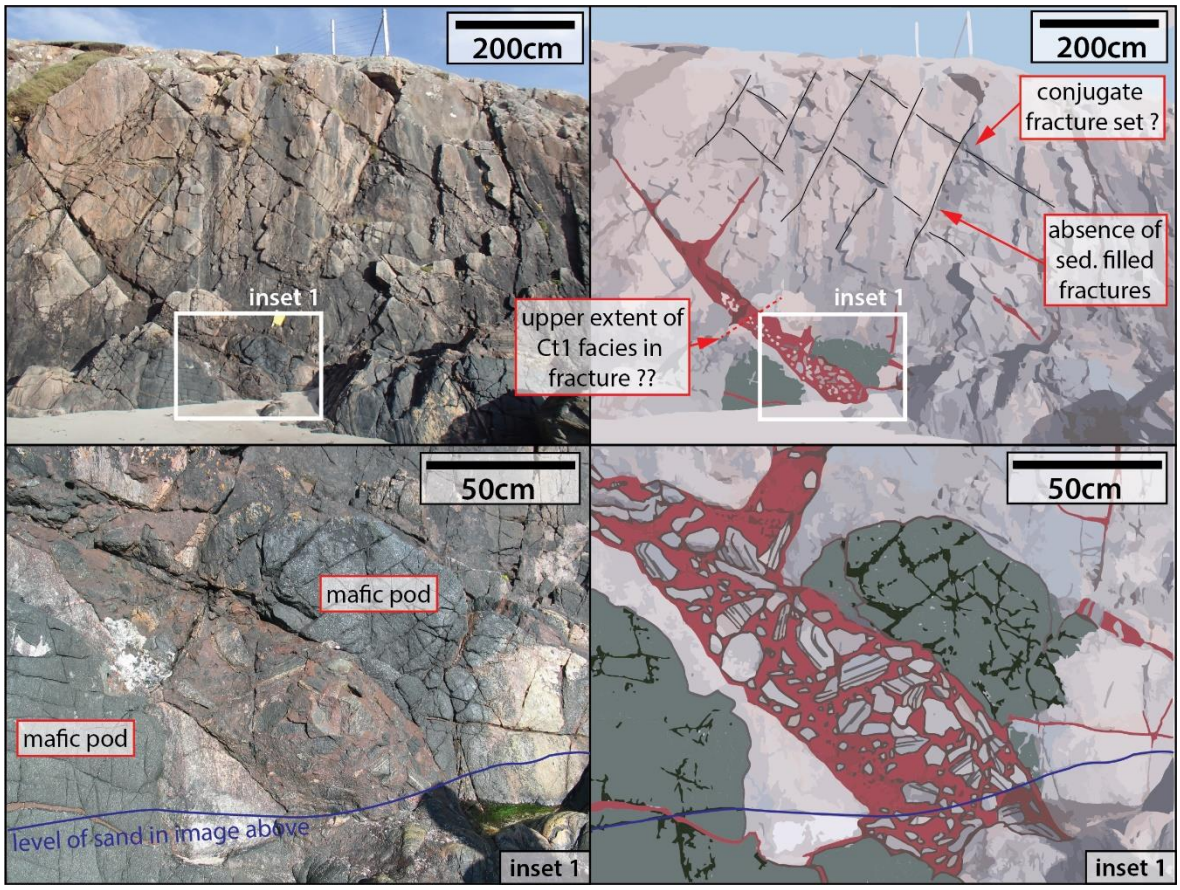

Figure 2.6.3.4. *Wide aperture fracture on the west side of the Clachtoll megablock with several smaller injections coming off it. These fractures appear to follow a set of (apparently) conjugate, non-sediment filled fractures.*

At the back of the Clachtoll megablock, fractures are observed with a clear NW-SE trending orientation. Here the gneiss is very fragmented. These clasts of gneiss have clearly been held in position by rapidly emplaced, fluidized sediments, coeval with brecciation, as very little rotation of the clasts is found. In general, the foliation in the gneiss of the Clachtoll megablock can be traced right through such fracture zones (Fig. 2.6.3.6). Additionally, the sandstone in the fractures is massive and homogeneous, with no internal stratification. This preferred orientation is also observed in localized areas in the front portion of the block; as in Figure 2.6.3.5a.

The front portion of the east side of the megablock contains a zone of intense fracturing and brecciation of the gneiss. Here, the sandstone is not confined to fractures, but also occupies irregular shaped voids within the gneiss (Fig. 2.6.3.7). Jigsaw breccias are a common occurrence (Fig. 2.6.3.7. b and parts of c). The term jigsaw breccia is used to loosely cover

breccias that could be described as crackle breccias or mosaic breccias, as defined by Woodcock and Mort (2008). The clasts of gneiss are very angular and little to no rotation has occurred. The sandstone matrix surrounding the clasts is mostly massive, though in some places there appears to be subtle layering defined by changes in grain size (Fig. 2.6.3.7c). The emplacement of this matrix must have been instantaneous and explosive, as evidence by the jigsaw breccia, so this layering cannot result from gradual deposition. Instead it may indicate high velocity flow.

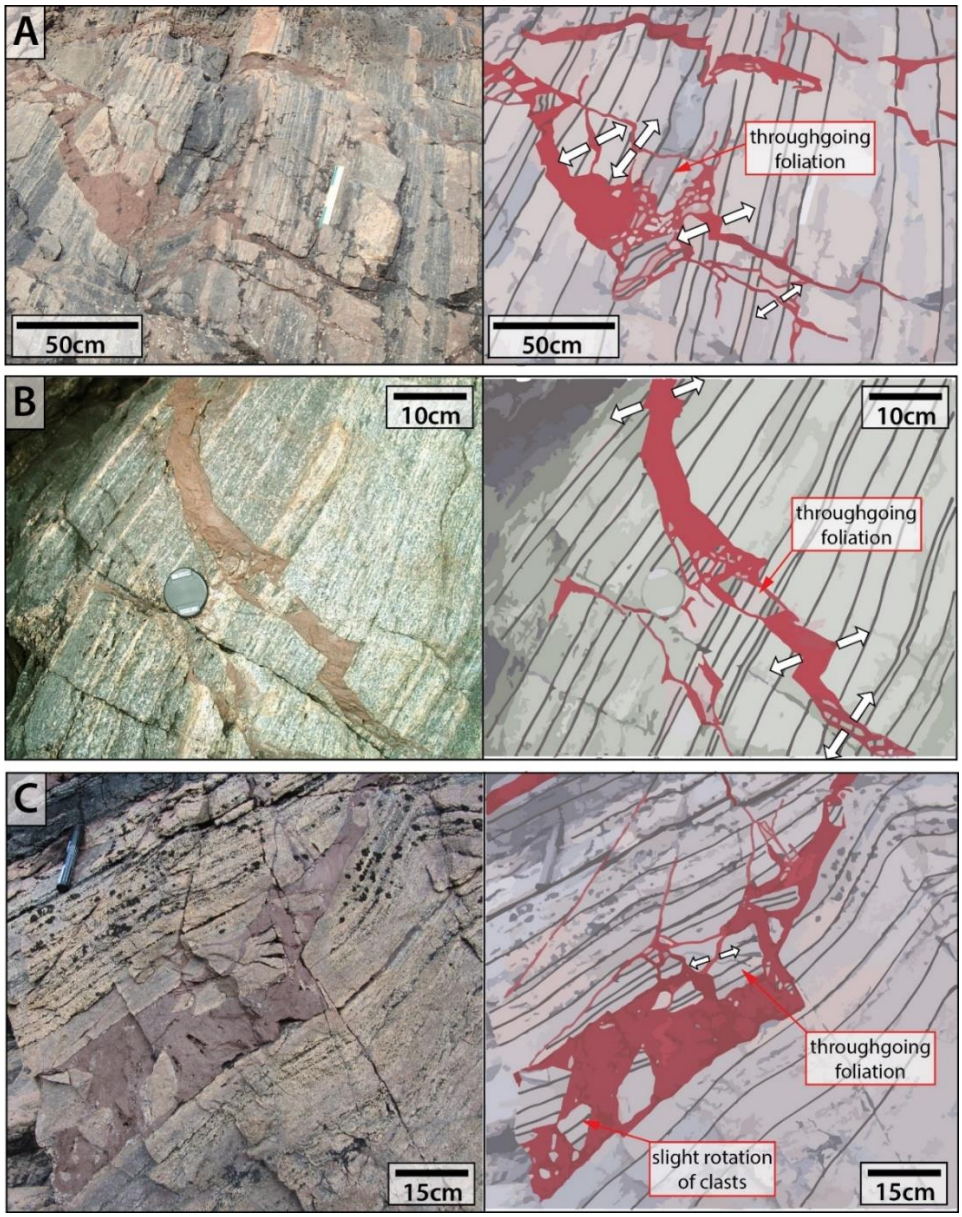

Figure 2.6.3.5. *Forcefully intruded sediment filled fractures on the front of the Clachtoll megablock. Tensile opening directions can sometimes be observed.*

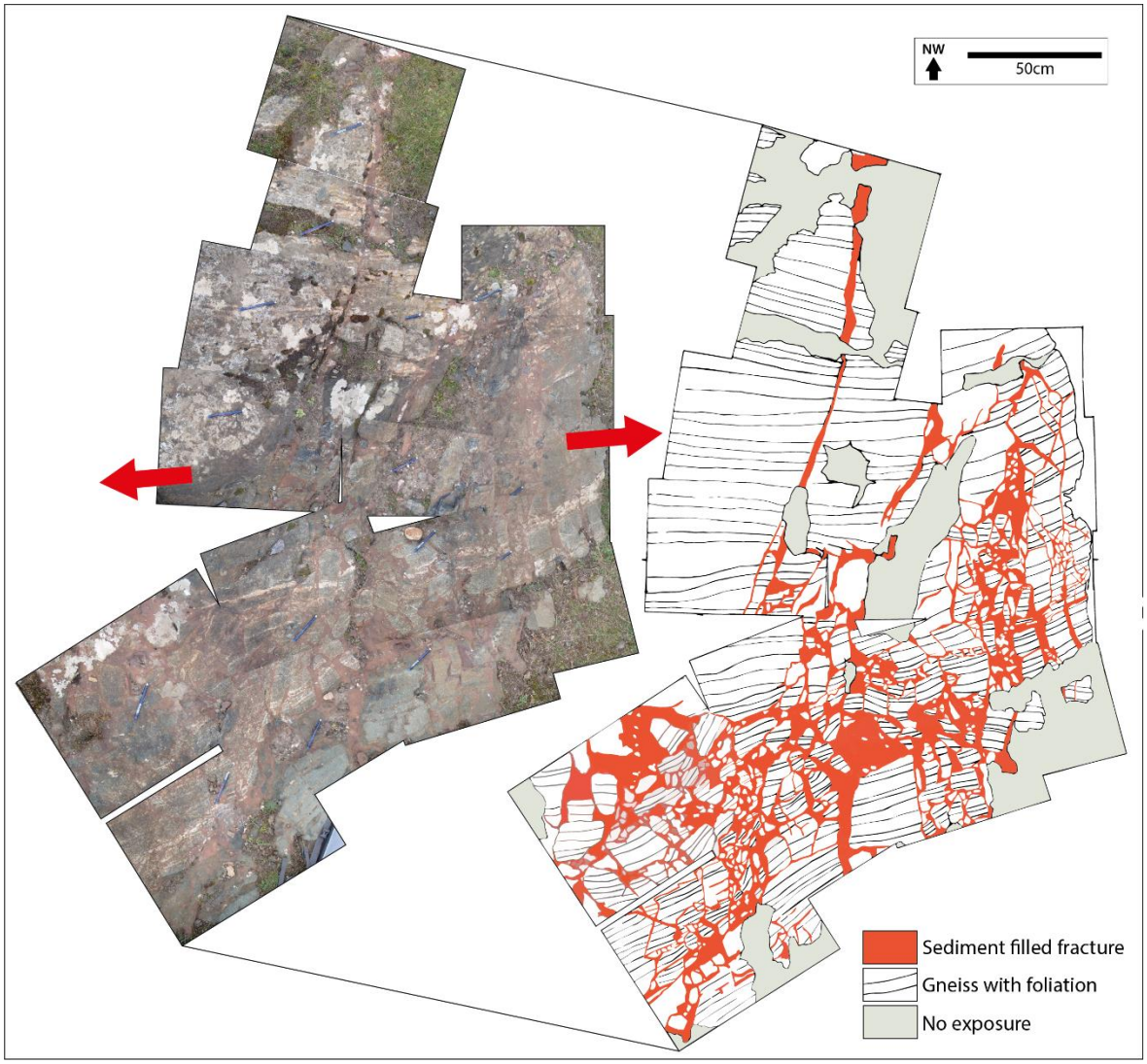

Figure 2.6.3.6. *Composite photograph and diagram of locality 38, at the back of the Clachtoll megablock, showing preferred NW orientation of fractures and through-going foliation in gneiss clasts. Tensile opening direction denoted by arrows.*

Also, in the front portion of the east side of the Clachtoll Megablock, a small (<5 m length exposed) fault is observed (Fig. 2.6.3.8.). This is the fault zone of Beacom, Anderson and Holdsworth (1999). The fault trends NNE-SSW and dips by approximately 45º. It appears to terminate at its NNE end against a folded band of foliation in the gneiss. The fault seems to have approximately followed the axial plane of this fold. In the footwall, sparse, discreet sediment filled fractures are found, around half of which follow the foliation, and half crosscut it. With distance from the fault, zones of more intense brecciation and complex fracture networks start appearing again. The hanging wall, however, is composed of an

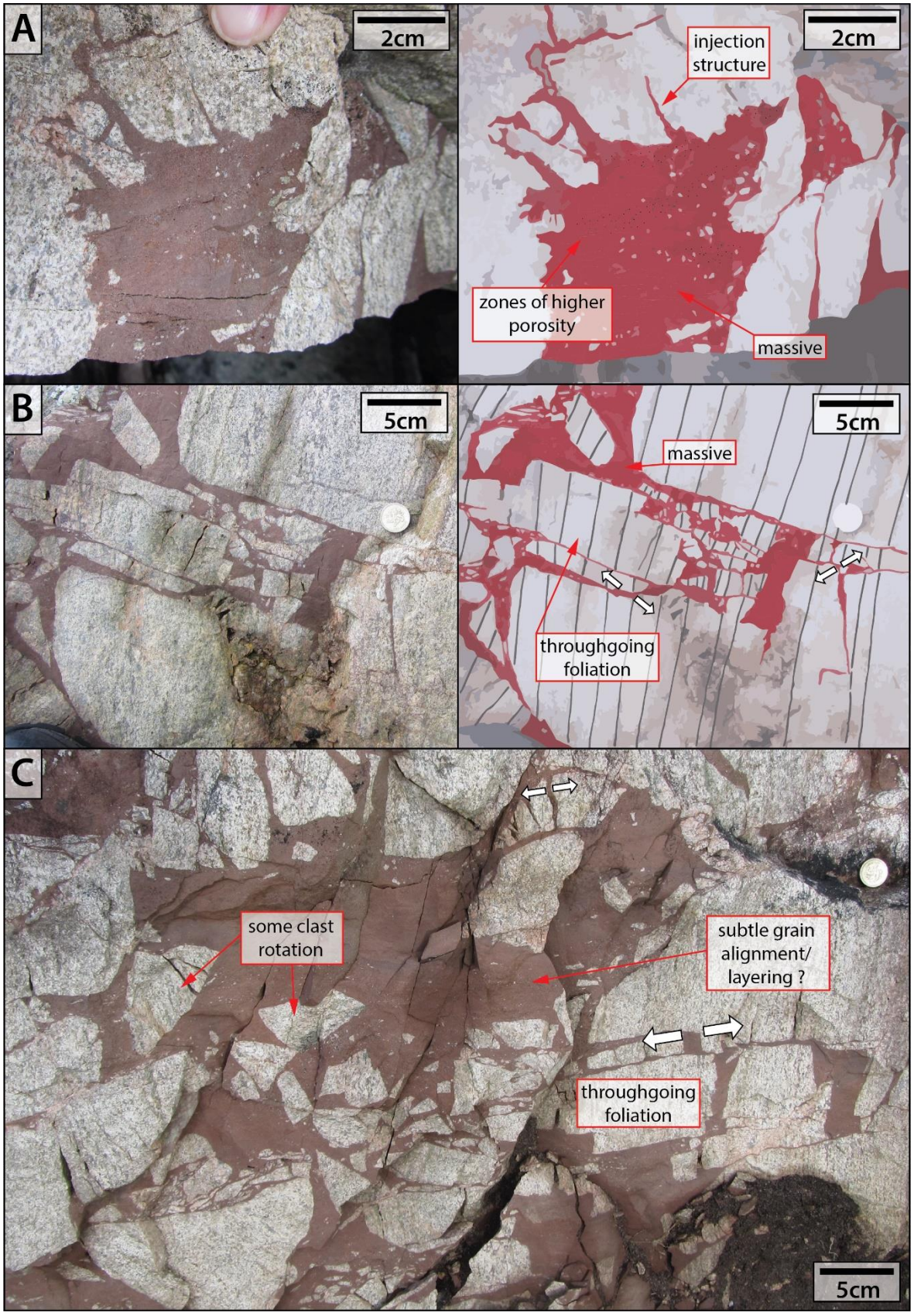

Figure 2.6.3.7. *High energy, explosive structures on the front edge of the east side of the Clachtoll megablock. (A) Injection structure analogous to those in pseudotachylytes, (B) Jigsaw Breccia, (C) Exploded gneiss.*

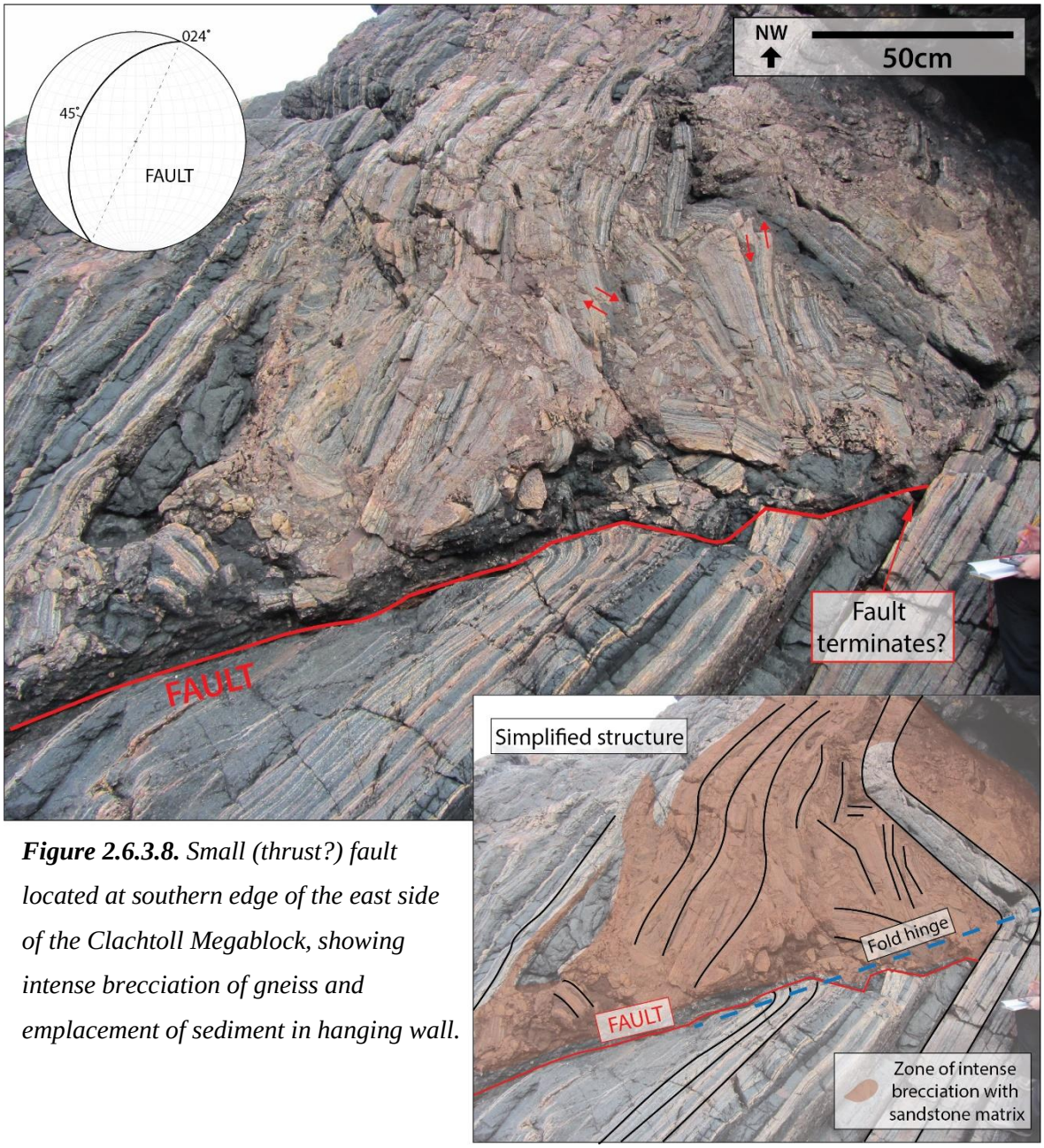

Figure 2.6.3.8. *Small (thrust?) fault located at southern edge of the east side of the Clachtoll Megablock, showing intense brecciation of gneiss and emplacement of sediment in hanging wall.*

intensely fragmented section of gneiss. Superficially, it has the appearance of a clast supported breccia, with patches of smaller, matrix supported clasts. On closer inspection, however, almost all of the clasts are surrounding by at least a film of fine sandstone matrix. The fold in the gneiss can roughly be traced through this zone of brecciation, with relatively little rotation of the clasts. Bands of gneiss in the hanging wall have been broken and vertically compressed. It appears that the section of gneiss in the hanging wall has been shunted upwards, partly accommodated by the fault, and partly by compression of a simultaneously formed breccia, resulting from rapid emplacement of fluidised sediment.

PASSIVELY INFILLED FRACTURE MATERIAL

The bedded material within fractures is confined to the top region and part of the front region of the block (fig. 2.6.3.1.) and is typically lighter in colour than the injected material. Grain size is also much more variable, and grain shape is rounded to sub-angular. Depositional laminations within these fractures are widespread, and numerous types of primary sedimentary structures are observable, often within the same fracture. These fills are completely different to the texturally and compositionally much more homogeneous injections described above.

Towards the front of the top of the megablock, NE-SW trending, moderately dipping fractures are found, containing clear bands and laminations of variable sized grains. Unlike the forcefully intruded sediment filled fractures, these laminations do not run parallel to the fracture walls but instead truncate against them (Fig. 2.6.3.9). In some examples, coarser grains (2-10 mm, but up to 50mm) are found at the bottom and are imbricated in an orientation suggesting flow towards the southwest (Fig. 2.6.3.9a). Many bands up to 2 cm thick also display normal grading, with grain sizes of 1-2 mm at the bottom, and <0.5 mm at the top. One particular fracture also shows undulate, discontinuous laminations which truncate against one another (Fig. 2.6.3.9b). These were initially interpreted as ripples but could equally result from interaction between the sediment laden fluid and the fracture wall, or later diagenetic processes.

On the top of the block and the high part of the front of the block, large patches of sedimentary veneer occur, which plaster the surface of the gneiss. These are also clearly stratified (Fig. 2.6.3.10a), with possible evidence of cross bedding ([i] of Fig. 2.6.3.10a). The larger patches of veneer (Fig. 2.6.3.10b), up to approximately 2 m by 5 m, resemble Stewart's (2002) Ct1 facies (fig. 1.1.3), found in the conglomerate tongue to the south of the Clachtoll Megablock. Subrounded to subangular clasts of gneiss, 1-40 cm in size, are randomly oriented within a fine to coarse, red sandstone matrix. The angular, ultramafic clasts found in the lower part of the conglomerate tongue are absent here, indicated a slightly higher position within the Stoer Group stratigraphy. The lithology is variable clast supported and matrix supported, though matrix supported volumes significantly dominate. Additionally, there are patches where stratification is again obvious (Fig. 2.6.3.10c). These patches contain shallowly westward dipping laminations, defined by changes in grain size.

Within these areas, some preferential clast orientation is observed, including possible imbrication of smaller clasts.

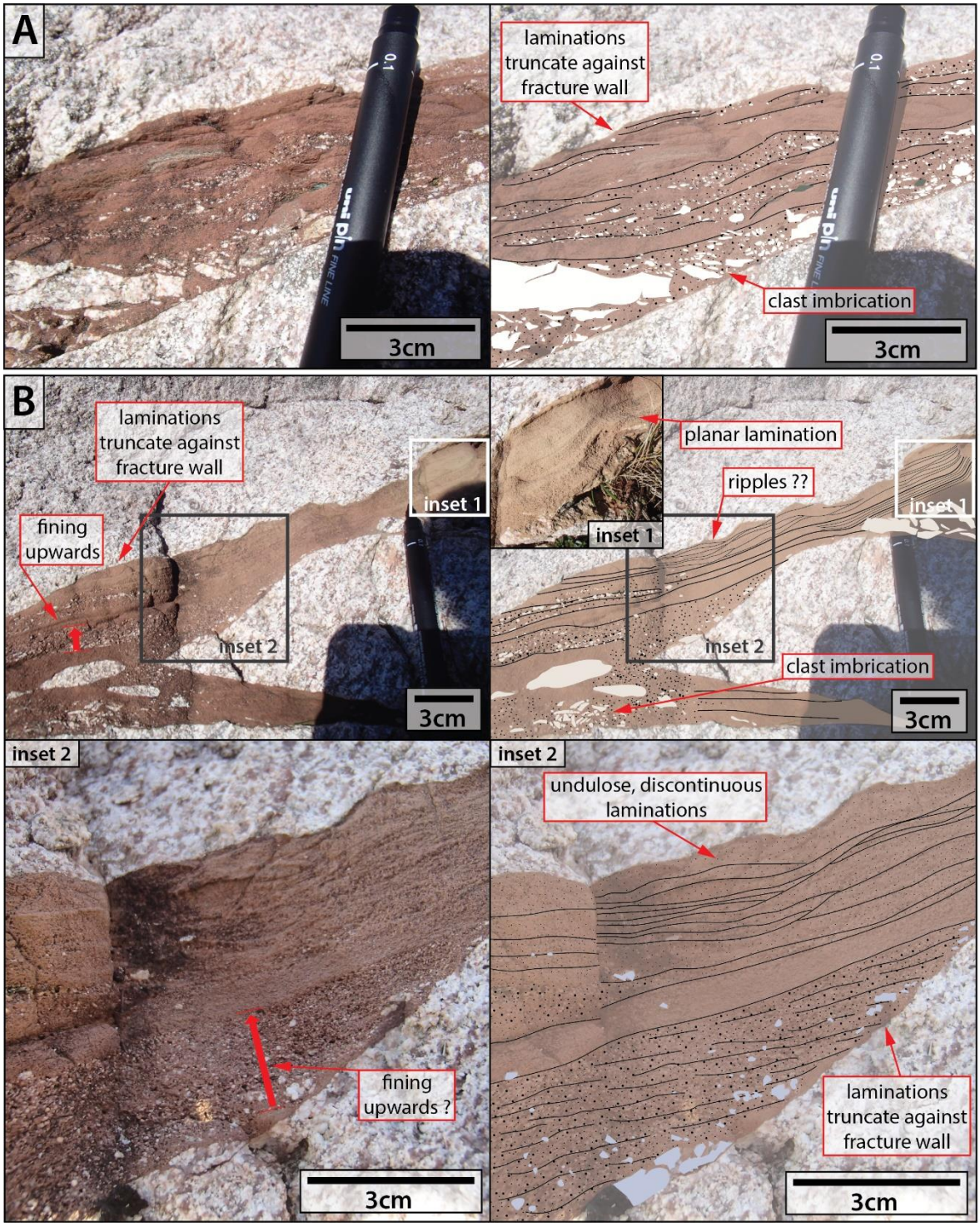

Figure 2.6.3.9. *Passively infilled fractures on the top of the Clachtoll megablock, displaying laminations, graded bedding and clast imbrication.*

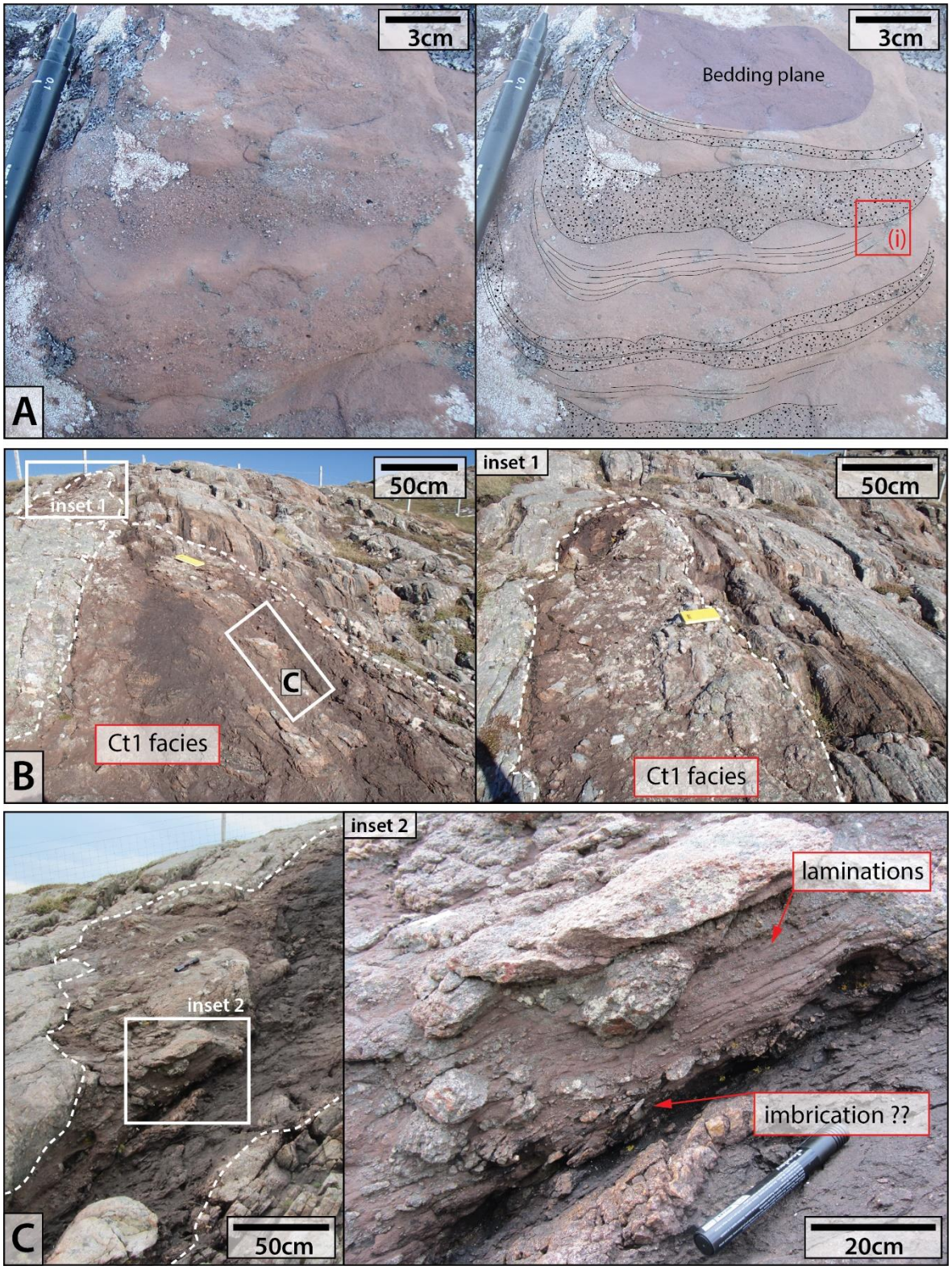

Figure 2.6.3.10. *Stoer Group veneers plastering patches of the surfaces of the top of the Clachtoll megablock. In photo A, (i) denotes an area where laminations appear to truncate against an overlying, coarse layer – possible cross bedding?*

2.7 Key observations for discussion

- The misorientation of the foliation in the gneiss of the Clachtoll Megablock compared to the surrounding gneiss.

- The relative locations of the forcefully intruded fractures, seemingly in the base of the Clachtoll Megablock, vs. the passively infilled fractures found on the top.

- The orientations of the fractures which more frequently cut the foliation in the gneiss despite this representing a plane of weakness.

- The relative positions of a compressional structure (the inferred thrust fault and folds) and the 'explosive' jigsaw breccias in the front of the block vs. the tensile fractures with preferred orientation in the back.

- The increased degree of fragmentation observed on the east side of the megablock when compared to the west side.

- The lack of evidence for larger faults or fault zones running through or down the sides of the Clachtoll Megablock.

CHAPTER 3
Discussion

3.1. Model/hypothesis

The working hypothesis of this study is that the Clachtoll Megablock represents a fallen block that has impacted into fluid laden sediment causing overpressuring of the fluid and subsequent hydrofracturing of the block. The block possibly has a flat or subtly curviplanar base; evidenced by structure contours in section 2.6.1. The production of predominantly tensile fractures upon impact would also have opened up fractures on the surface of the block, higher than intruded material was able to reach, which were then gravitationally filled by sediment as the block was progressively buried. The main evidence for this is the misorientation of foliation in the block compared to the surrounding gneiss, and the presence of intruded fracture fill material in the base of the block, vs. passively infilled material in the top. This hypothesis is diagrammatically represented in its simplest form in Figure 3.1.1.

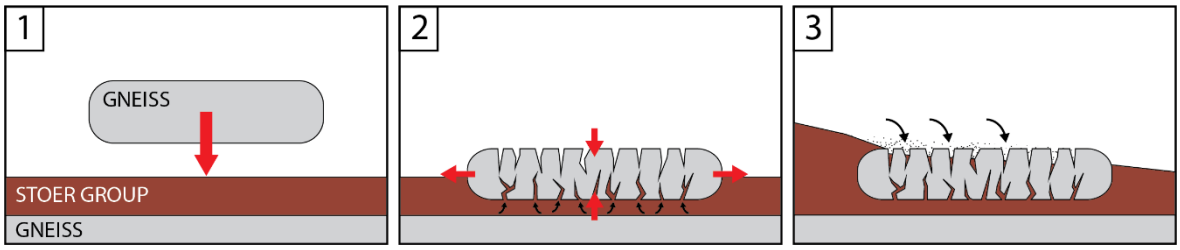

Figure 3.1.1. *Simple rock fall model hypothesised for the Clachtoll Megablock (1) Vertical falling of a detached block onto unconsolidated sediments. (2) Impact forces vertically compress and horizontally extend the block. This creates open tensile fractures, certainly in the top of the block, but possibly also to some degree in the bottom of the block. The main mechanism of fracturing in the base, however, is hydraulic due to rapid overpressure of the underlying sediment. Sediment is forcefully injected into these fractures as they form. (3) Continued sedimentation passively infills the open fractures on the top of the block under gravity.*

A lack of evidence for larger faults or fault zones running through or down the side of the Clachtoll Megablock precludes Beacom, Anderson and Holdsworth's (1999) theory that the sediment filled fractures result from brittle deformation processes within a trans-tensional fault zone. This is discussed further in section 3.3.

The height that the block had to fall to overcome the tensile strength of the gneiss must be feasible. Calculations estimating this height are presented in section 3.4.

In reality, the block cannot have just fallen out of the sky as implied by Figure 3.1.1. Instead, the block may have slid, fallen or toppled into its current position (Fig. 3.1.2). The block must be locally sourced and cannot have fallen far. One need only watch videos of modern rockfalls in progress to see that rocks of all strengths and other mechanical properties rapidly fragment and disaggregate with transport distance and successive impacts (e.g. (euronews (in English) 2014; Storyful Rights Management 2017; yosemitenationalpark 2010). Types of landslide phenomena and emplacement mechanism are summarised in section 3.2.1. Possible models for the detachment and emplacement of the block are discussed in more detail in section 3.5, whilst section 3.6 deals with processes that could have triggered the emplacement of the Clachtoll Megablock.

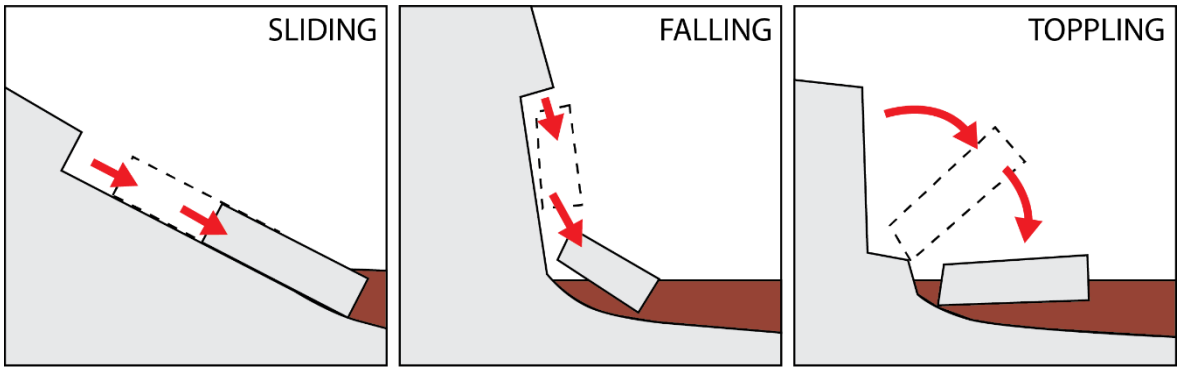

Figure 3.1.2. *Simplified but physically feasible transport and emplacement processes, as opposed to the pure vertical emplacement seen in figure 3.1.1.*

Certain features within the Clachtoll Megablock indicate that the processes involved in emplacement were more complex than have just been described. The block displays

extensional features at its rear in the form of parallel tensile fractures, and compressive features at the front, in the form of a small thrust fault and brittle folding. Such features could result from the downslope sliding motion of a block, where drag acts on the back of the block to pull it apart, whilst the front of the block undergoes compression due to deceleration resulting from friction (Fig. 3.1.3). This idea is further discussed in section 3.5. A similar situation is described from a contemporary rock slide in Canada in section 3.2.2.

Further adding to the complexity, the most dominant orientation of the sediment filled fractures within the Clachtoll Megablock is perpendicular to the foliation in the block. This seems counterintuitive given that the foliation should provide planes of weakness. Additionally, the west side of the megablock appears to have undergone a greater degree of fragmentation compared to the east side. Possible causes for these features are again discussed in section 3.5.

Figure 3.1.1. and 3.1.3. represent two end member processes. Emplacement of the Clachtoll Megablock likely resulted from a combination of these processes. Ultimately, a more detailed model must be found which can reconcile all of the features observed at Clachtoll.

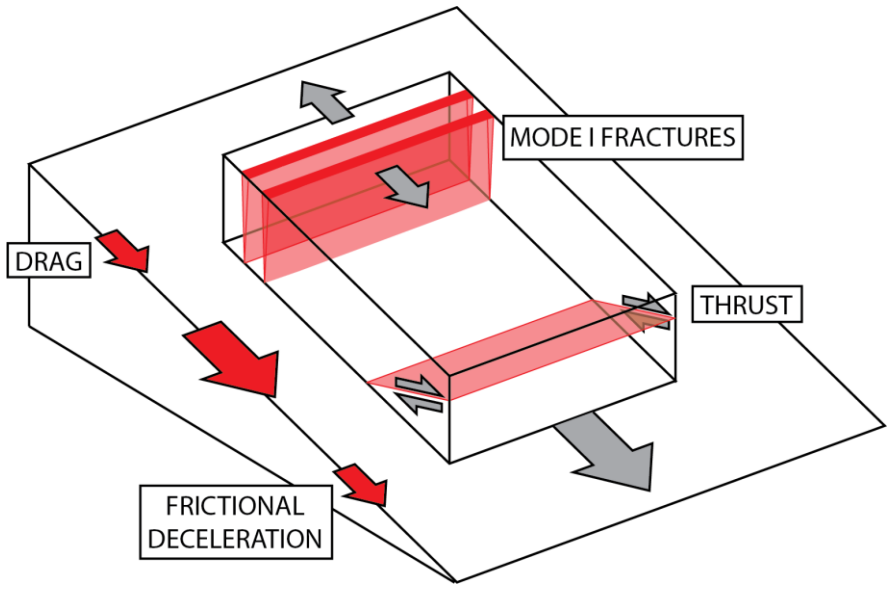

Figure 3.1.3. *Schematic diagram of tensile and compressional forces acting in a sliding block and the structures associated with them. The size of the red arrows indicates the relative velocities of portions of the block.*

3.2. Landslides and other megablocks

3.2.1. Landslide terminology and processes

The word landslide is frequently used to refer to a number of processes involving the gravitational movement of material at the Earth's surface in a downwards or outwards motion (Terzaghi 1950). Landslide evolution involves pre-failure deformations, the failure event itself, and post-failure displacements (Hungr, Leroueil & Picarelli 2014). The most widely used classification system for such processes is that of Varnes (1978). Under this classification, a two-part naming system is utilised to describe any manner of landslide. The first part refers to the type of material involved, and the second refers to the type of movement. For example, falls involving bedrock are termed rock falls, slides involving predominantly fine soil are termed earth slides, and flows involving predominantly coarse soil are termed debris flows. This classification is summarised in table 3.2.1. and represented diagrammatically in figure 3.2.1.

<table>
<tr><th colspan="2" rowspan="3">TYPE OF MOVEMENT</th><th colspan="3">TYPE OF MATERIAL</th></tr>
<tr><th rowspan="2">BEDROCK</th><th colspan="2">Engineering soils</th></tr>
<tr><th>DEBRIS
Predominantly coarse</th><th>EARTH
Predominantly fine</th></tr>
<tr><td colspan="2">Falls</td><td>Rock fall</td><td>Debris fall</td><td>Earth fall</td></tr>
<tr><td colspan="2">Topples</td><td>Rock topple</td><td>Debris topple</td><td>Earth topple</td></tr>
<tr><td rowspan="2">Slides</td><td>Rotational</td><td rowspan="2">Rock slide
Also called a block slide</td><td rowspan="2">Debris slide</td><td rowspan="2">Earth slide</td></tr>
<tr><td>Translational</td></tr>
<tr><td colspan="2">Lateral spreads</td><td>Rock spread</td><td>Debris spread</td><td>Earth spread</td></tr>
<tr><td colspan="2">Flows</td><td>Rock flow
(deep creep)</td><td>Debris flow
(soil creep)</td><td>Earth flow</td></tr>
<tr><td colspan="2">Complex</td><td colspan="3">Combination of two or more principal types of movement</td></tr>
</table>

Table 3.2.1.1. *Varnes' classification of slope movements (Varnes 1978).*

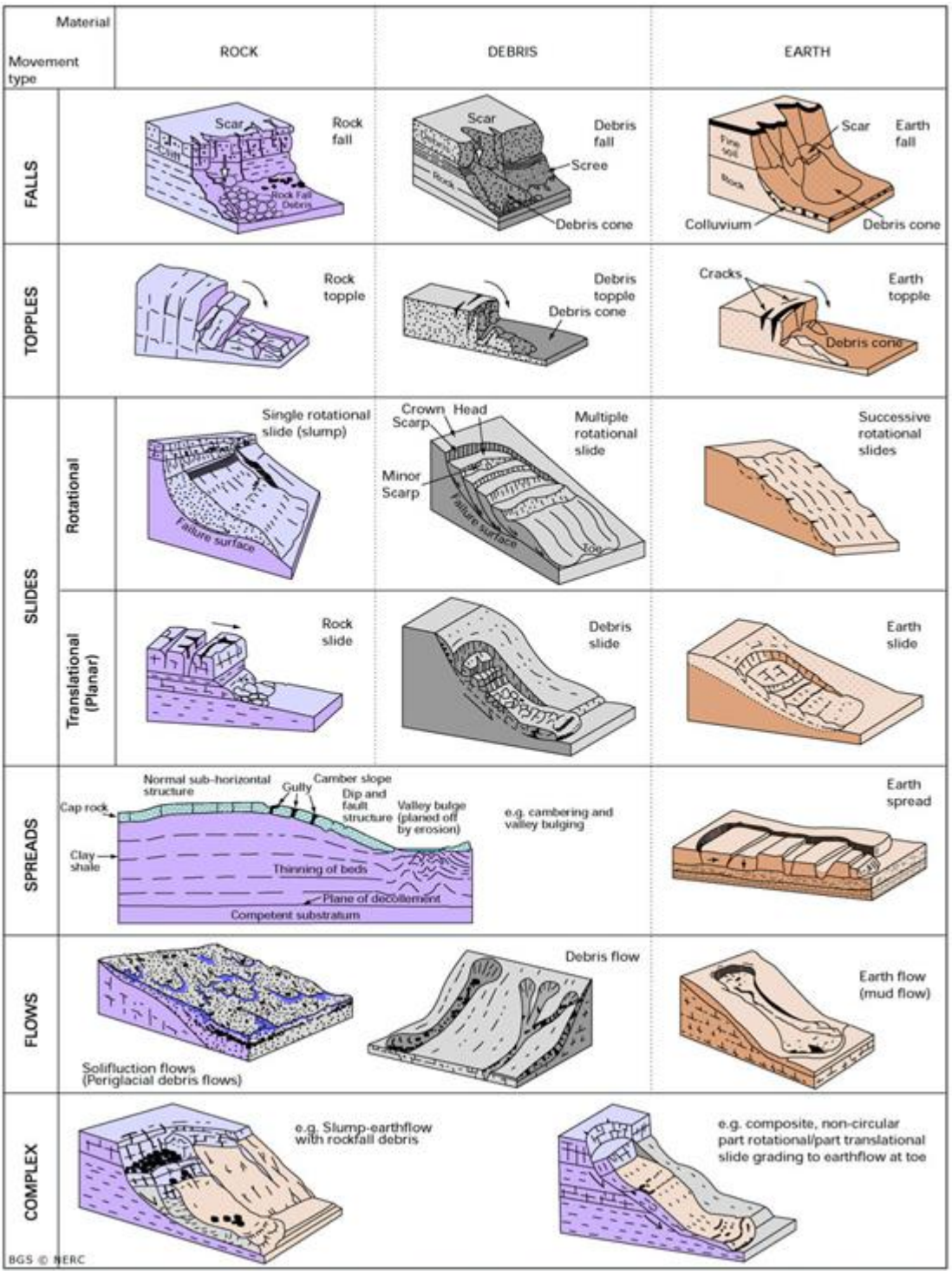

Figure 3.2.1.1. *Landslide classification. Diagram produced by BGS (©NERC) after Varnes (1978) and Cruden & Varnes (1996).*

Hungr, Loreoueil and Picarelli (2014) have since developed an updated version of this classification to allow compatibility with geotechnical terminology and easier categorisation of complex slides. For the purposes of this study however, Varnes' (1978) original classification will suffice.

The Clachtoll Megablock is comprised of the local gneiss, so we can ignore the 'debris' and 'earth' columns in Table 3.2.1.1. The megablock is too intact to be described as a flow (or more specifically a rock avalanche), and the geology and geomorphology would not have suited lateral spreading; lateral spreads typically occur on gentle slopes or flat terrain and are accommodated by liquefaction in an underlying, less coherent material (Highland & Bobrowsky 2008). This leaves rock falls; rock topples and rock slides.

Highland and Bobrowsky (2008) define rock falls as:

"…abrupt, downward movements of rock or earth, or both, that detach from steep slopes or cliffs. The falling material usually strikes the lower slope at angles less than the angle of fall, causing bouncing. The falling mass may break on impact, may begin rolling on steeper slopes, and may continue until the terrain flattens."

The slope gradient must exceed 70º before falling, instead of bouncing or rolling, occurs (Dorren 2003).

Highland and Bobrowsky (2008) define rock topples as:

"…the forward rotation out of a slope of a mass of rock around a point or axis below the centre of gravity of the displaced mass."

Hungr, Leroueil and Picarelli (2014) explain that:

"…rotation occurs on well defined basal discontinuities. Movement may begin slowly, but the last stage of failure can be extremely rapid. Block rotation is often initiated by water pressure in tension cracks, yielding of a weak foundation, or by earthquake acceleration."

Rock slides can either be rotational or translational. Rotational slides involve the rotational movement of the mass, along a concave-upwards rupture surface, and about an axis parallel to the strike of the slope (Highland & Bobrowsky 2008). They typically involve little internal deformation, and only occur in very weak rock masses (Hungr, Leroueil & Picarelli 2014). Varnes' (1978) diagram outlining landslide nomenclature is based on this type of slide (Fig.

3.2.1.2). Translational rock slides involve the movement of rock along a planar rupture surface. Failure occurs along a discontinuity such as a bedding plane, fault, joint or plane of schistosity (Highland & Bobrowsky 2008). These slides disintegrate rapidly during downward motion (Hungr, Leroueil & Picarelli 2014).

Events can also be classified as one type of landslide in their initial stages and then develop into another type. For example, slabs may break off of and slide down a rock face, before an increase in slope angle causes them to start falling.

When it comes to impact processes, fragmentation is found to be facilitated by discontinuities within the rock volume (Giacomini, Buzzi, Renard, *et al.* 2009).

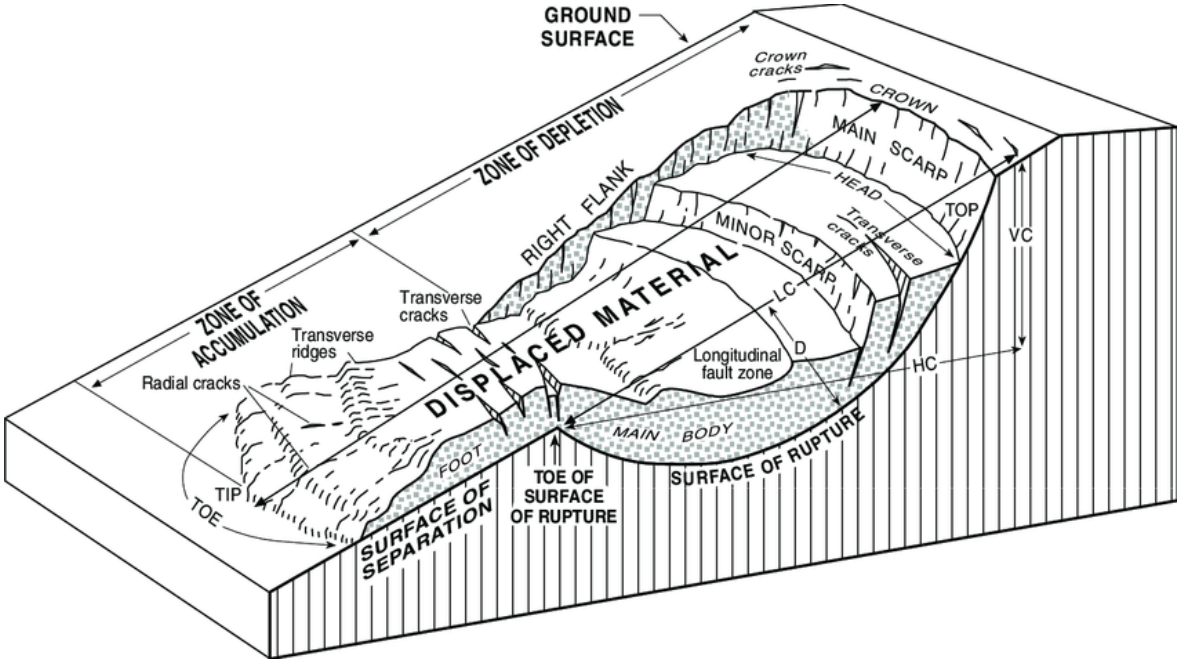

Figure 3.2.1.2. *Rotational slide diagram showing terminology used to describe landslides; taken from Varnes* (1978).

3.2.2. Other megablocks

The definition of a megablock varies between sources. Most descriptions come from volcanology, where mass wasting into subsiding calderas produces so called megabreccias (Branney & Acocella 2015). Branney and Acocella (2015) define a megabreccia as a

"deposit of rock fragments, where each megablock is too large to be seen at a field exposure without mapping". Each megablock may itself be internally brecciated and can be several km in size. Troll, Emeleus & Donaldson (2000) on the other hand, describe megablocks as clasts with dimensions larger than 25 m.

Descriptions of large, intact megablocks are hard to come by in the literature. Most bedrock landslide events involve the fragmentation of the volume of rock into numerous smaller constituents which may be widely distributed. Most work on landslide concerns the slumping of unconsolidated material, or the movement and impact processes of multiple, relatively small constituents in rock falls, avalanches and flow. Large, intact blocks tend to be mentioned in passing but not described in any detail (e.g. the 'Fallen Stack' in the upper Jurassic 'Boulder Beds of NE Scotland,(Pickering 1984)).

Here, three examples of megablocks are discussed, chosen because they have characteristics shared by the Clachtoll Megablock.

The fall of Threatening Rock

All information comes from Schumm and Chorley (1964).

In 1941, a monolith of rock 150 feet long, 100 feet high, and 30 feet thick, toppled from the side of Chaco Canyon, northwestern New Mexico. Movement of the rock had been monitored for the previous five years. The rock belonged to the mechanically weak and permeable Cliff House Sandstone and rested on the underlying shales of the Menefee Formation. Prior to falling, the difference in distance between the smaller gap between the rock and canyon wall at the bottom, and larger gap at the top, was due to weathering, not just tilting. The space between the rock and canyon wall was partially filled with loose rocks. In places, the undercutting of the rock was almost to the gravity axis (14-16 feet when width of block at mid-height was 34 feet).

Similarities to the Clachtoll Megablock:

- Environmental setting
- Movement of one massive block

Differences to the Clachtoll Megablock:

- Different (and weaker) material involved
- Greater fall distance than proposed for Clachtoll Megablock, causing severe fragmentation.

Of particular interest is the description of the actual failure event itself, and the deduced cause of movement and subsequent failure, given the similarity in environmental setting to that of the Clachtoll Megablock.

Eyewitnesses described the failure in the following way:

"…heard the rock groan and looked up to see dust shooting out of cracks in it. The slab leaned out about 30 or 40 feet from plumb, settled sharply, and when it hit solid bottom, rocks from the top of it were broken loose and propelled into the ruin. The lower two thirds then pivoted on its outer edge and fell down the slope towards the ruin. The whole mass broke into many fragments and an avalanche of rocks catapulted down the slope…"

This description is very similar to what is seen in a video of a rock fall above Evolène in the canton of Valais in Switzerland in 2015 (Editions Le Nouvelliste 2015). Screen shots of this video are annotated in Figure 3.2.2.1.

Both the topples observed at Chaco Canyon and at Evolène, involved first the breaking loose of rocks from the top of the block. In the case of the topple at Evolène, this breaking appeared to occur along layers that were oriented sub-horizontal prior to failure. The lithologies involved at both Chaco Canyon and Evolène have a sub-horizontal fabric. This is not true for the gneiss at Clachtoll, so perhaps this initial breakage of rocks from the top of the block would not have occurred at Clachtoll? In the video of the rock fall above Evolène, crushing of the rock is observed about the axis of pivoting. This is something also noted by Hungr, Leroueil & Picarelli (2014) to occur in topples. Should the block not fall far and manage to stay relatively intact, is it possible that evidence of this crushing could be preserved, perhaps as a zone of rubble or more intense brecciation?

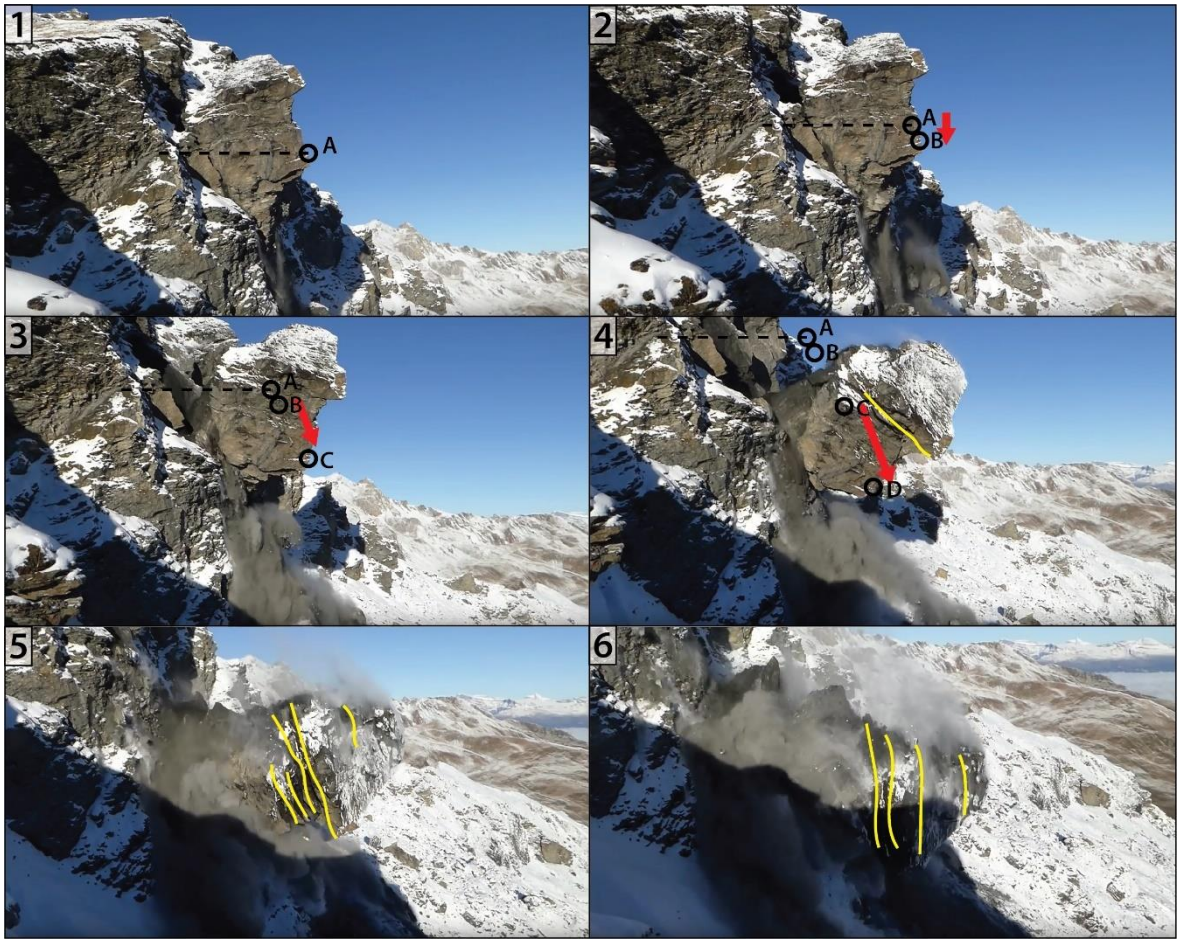

Figure 3.2.2.1. *Screenshots of rock fall above Evolène (Editions Le Nouvelliste 2015). Lettered, black circles serve as reference points to track movement. Yellow lines are developing fractures along which the block is disaggregating. (1) Failure has just initiated. Streams of dust and small rubble fall from cracks developing at the bottom of the block. (2) There is continued crushing and fragmentation at the base of the block and the block has slid downwards – movement from reference point A to reference point B. (3) There is significant downward sliding and settling from reference point B to reference point C, and outward rotation has begun. (4) Some downward slipping is still occurring, but forward rotation is becoming the dominant process, accompanied by further crushing about a pivot axis. Prominent fractures within the top part of the block are developing. (5) Downward slipping seems to have stopped, and movement is now purely accommodated by forward rotation. The once top portion of the block is disaggregating along an originally sub-horizontal fabric in the rock. (6) The block continues to fall and disaggregate.*

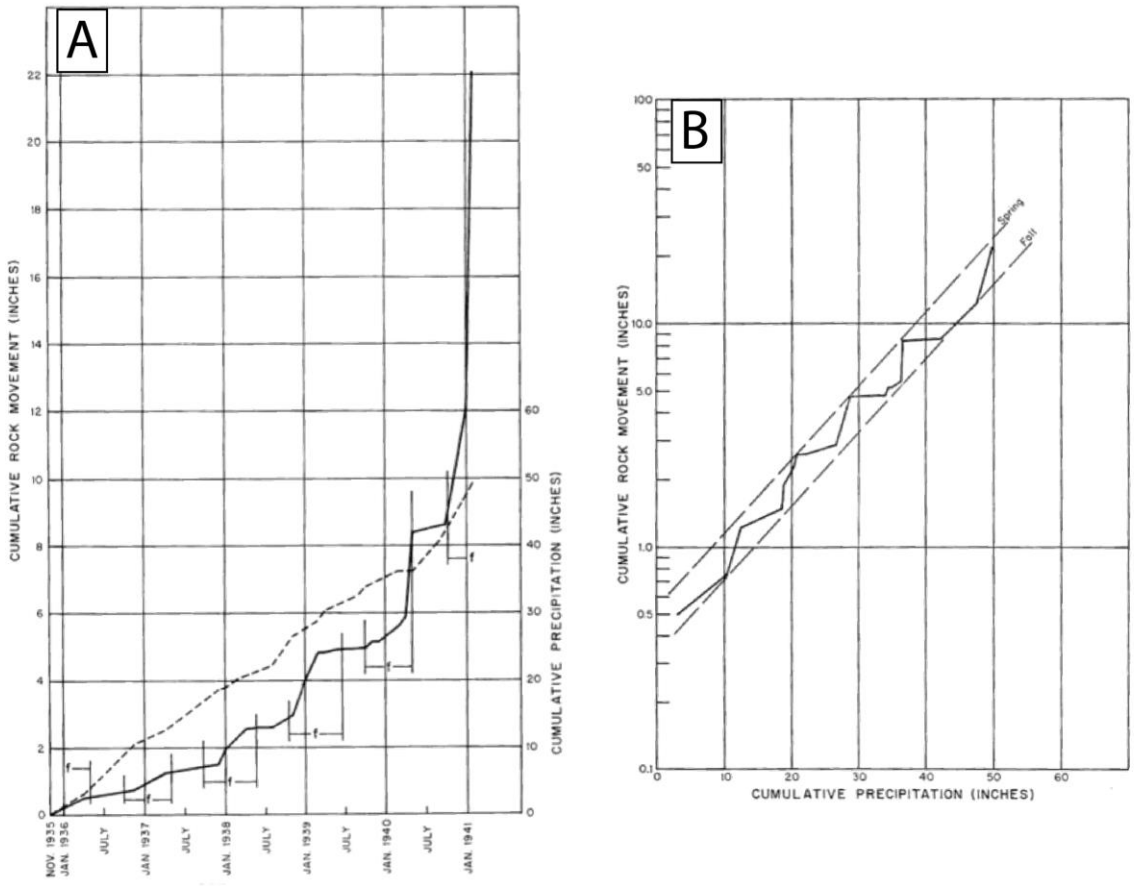

Figure 3.2.2.2. *(A) Schumm and Chorley's* (1964) *Figure 2 showing cumulative rock movement over time (solid line) and cumulative precipitation over time (dashed lines). Period of most movement occur in the sections labelled 'f' corresponding to the period of time between the first and last killing frost of each season. (B) Schumm and Chorley's* (1964) *Figure 3 showing cumulative rock movement plotted logarithmically against cumulative precipitation plotted linearly.*

Schumm and Chorley (1964) used cumulative precipitation data and cumulative rock movement data (Fig. 3.2.2.2a) to infer precipitation and weathering to be the cause of movement. To a first order, when cumulative rock movement vs. cumulative precipitation is plotted on semi-logarithmic paper, cumulative movement appears to be an exponential function of cumulative precipitation (Fig. 3.2.2.2b). In reality, the situation is more complicated than the amount of precipitation being the only influencing factor. Periods of greater movement are punctuated by periods of little to no movement. Periods of greater movement always coincide with winter months; particularly the time between the first and last killing frost of the season. It seems that the most important parameters controlling movement of the block were freeze-thaw weathering and wetting by snow melt. The climate

of Chaco Canyon is arid with approximately 200 mm of rainfall per year (Anon 2019). Similarly, the environment of deposition of the Stoer Group is described by Stewart (1990) as arid to semi-arid with an annual precipitation of around 300 mm. If this environment underwent the same daily temperature fluctuations and seasonal variations as the present day Chaco Canyon, then the action of freeze-thaw may have played an important role in the movement of the Clachtoll Megablock.

The 'Brèche Rouge of Carboneras'

All information comes from Montenat, Ott d'Estevou, Leyrit, *et al.* (2000).

Montenat, Ott d'Estevou, Leyrit, *et al.* (2000) describe a large rockslide, resulting from the collapse of one or several Miocene volcanic cones in a deep marine setting, which occurred in the Carboneras area of southern Spain. The event occurred in the context of sinistral wrench tectonics within the northeastern segment of the Trans-Alboran shear zone, during the late Miocene. The rockslide material is described as "massive, fissured, and cut by sedimentary dykes". These dykes are not found in the underlying lithology. The degree of brecciation and presence of sedimentary dykes increases towards the top of the block, and dykes formed by injection close upwards.

Similarities to the Clachtoll Megablock:

- Movement of massive block of rock
- Proximity to active faulting
- Presence of sediment filled fractures – both injected and passively filled

Differences to the Clachtoll Megablock:

- Different material involved
- Fracturing and brecciation is more intense towards the top of the block rather than the bottom.
- Different climatic and depositional setting

The brecciation of the rock volume was caused by the development of neptunian (passively filled) and injected dykes, resulting from two different processes which alternated during multiphase movement of the rock volume (Fig. 3.2.2.3). Tractional movement caused the

opening of tensile fissures oriented perpendicular to the direction of movement, into which sediment was deposited. When sliding stopped, these fissures were compressed, inducing hydrofracturing and sediment injection. These dykes form a random, reticulate network which outline the brecciated clasts that have undergone little relative displacement (i.e. formed a jigsaw breccia). Successive phases of dykes cross-cut each other, indicating the 'stop-start' nature of the sliding.

Hydraulic fracturing requires the sudden overpressuring of fluids. Most instances of hydraulic fracturing result from overburden, fault movement, seismic shock or the sudden influx of more fluid. Here, however, it is demonstrated that overpressure may be produced by the breaking action of a body in motion. This is the mechanism inferred for the development of forcefully injected sediments in the Clachtoll Megablock.

The then active tectonic setting of the Brèche Rouge of Carboneras is cited as the trigger for its emplacement. The setting of the Clachtoll Megablock was also tectonically active at the time of emplacement, so it's possible that the same trigger can be invoked.

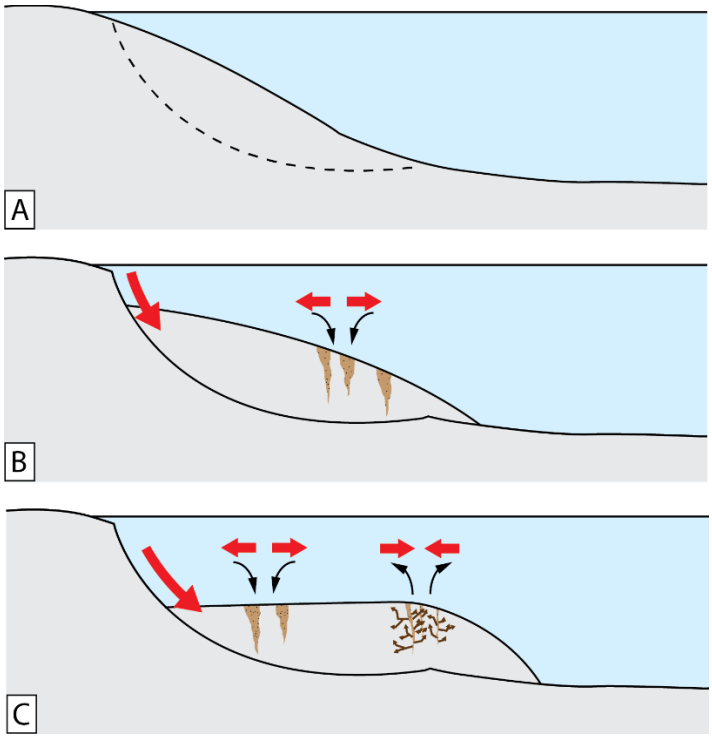

Figure 3.2.2.3. *Simplified version of Montenat, Ott d'Estevou, Leyrit, et al.'s (2000) Figure 10.6. (A) Pre-failure. (B) Sliding occurs. Traction results in the opening of tensile fractures which are filled with fluid and sediment. (C) Further sliding results in the opening of more tensile fractures towards the back of the block, whilst the base of the front of the block is locked causing compression of the fluid in previous tensile fractures and subsequent hydrofracturing and injection.*

The Mitchell Creek Landslide

All information comes from Clayton, Stead, Kinakin, *et al.* (2017).

Clayton, Stead, Kinakin, *et al.* (2017) describe a bedrock slide occurring in foliated and altered volcanics on the steep southern slope of Mitchell Valley in British Columbia, Canada. The slide initiated between 1956 and 1972. They have used historical aerial photographs, digital photogrammetric modelling and point cloud analysis, and geomorphological mapping to study the evolution of this ongoing slide. This has allowed identification of a rear, sliding zone exhibiting extensional features, a middle transitional zone with extensional features, and a front, toppling zone, exhibiting bulging and complex deformational features (Fig. 3.2.2.4).

Similarities with the Clachtoll Megablock:

- Movement of one massive block
- Steep to vertically oriented foliation
- Tensional structures to the rear of the block and complex deformation at the front.

Differences with the Clachtoll Megablock:

- Different material involved
- Foliation is orientated perpendicular to movement direction of block. This may or may not be different to the Clachtoll Megablock. In Section 3.5, a possible sliding motion in a direction parallel to the foliation is discussed.
- Different climatic setting

The front third of the landslide is defined by a mass of toppling rocks, resulting in compression and bulging of the rock. Movement rates are the fastest in this zone, and there is significant variation in displacement rates throughout the zone, consistent with the complex deformation occurring. The middle third of the landslide, termed the transition zone, marks a region between sliding rock above, and toppling rock below. It is moving slower than the toppling zone, resulting in tension and extensional features such as normal faults. These are especially present in the top part of this area where the transition zone is moving away from the sliding zone above. This middle zone may either be down-dropping into space behind the front zone or may be causing the movement of the front zone by pushing against it. The uppermost third of the landslide is undergoing translational sliding

as a largely intact block along a rupture surface, at rates slower than in either of the other two zones.

The Mitchell Creek Landslide is an example of an event that is significantly slower to evolve and far less catastrophic than the event proposed to explain the Clachtoll Megablock. Of interest however, is the presence of both extensional and compressional features and their spatial relationship. In both the Mitchell Creek Landslide and the Clachtoll Megablock, compressional features are observed at the front and inferred front of the masses respectively, and extensional features at the back. Tensional stretching of the block opens up these extensional features (normal faults in the Mitchell Creek Landslide and Mode I fractures in the Clachtoll Megablock), whilst an impediment to movement at the front results in compression. The spatial relationship between these features indicates that the Clachtoll Megablock may have undergone translational sliding in some form, rather than just simple vertical emplacement.

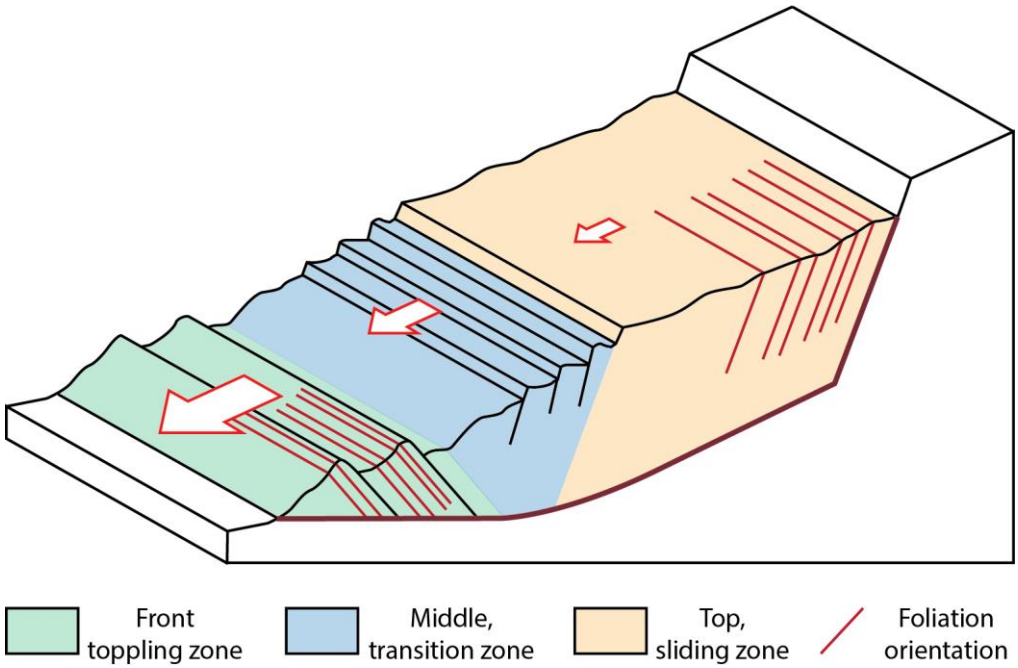

Figure 3.2.2.4. *Simplified version of Clayton, Stead, Kinakin, et al.'s (2017) Figure 12, highlighting the different deformational and geomorphological zones within the Mitchell Creek Landslide.*

3.3. Alternative hypotheses

In order to prove that the Clachtoll Megablock represents an ancient rock fall, not only must there be sufficient evidence, but there must also be a lack of, or lesser degree of, evidence supporting alternative hypotheses. These alternative hypotheses are discussed below.

Folding in the gneiss as a cause for the misorientation of foliation within the Clachtoll Megablock

This hypothesis is immediately problematic in that, whilst it can explain the misorientation of foliation, there is no conceivable way in which it can explain the presence of the sediment filled fractures at Clachtoll. This could be resolved by invoking a two-phase process in which folding within the ductile crust, significantly predates subsequent exhumation to brittle crustal levels, where an entirely different process facilitated the emplacement of sediment filled fractures in the already misoriented gneiss. Decametre to kilometre scale folds are found in the gneiss between Clachtoll and Achmelvich (Fig. 3.3.1), but no appropriately scaled folds are recorded in the immediate vicinity of the Clachtoll Megablock. Using a map

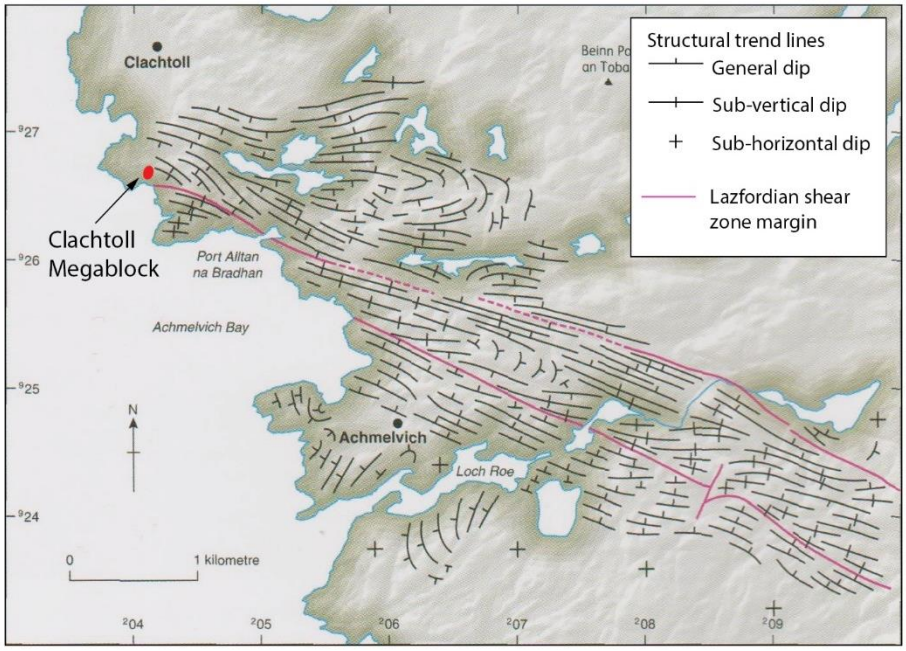

Figure 3.3.1. *Foliation trends between Clachtoll and Achmelvich. Image taken from Wilson, Holdsworth & Wightman (2011 p.54) after Attfield (1987).*

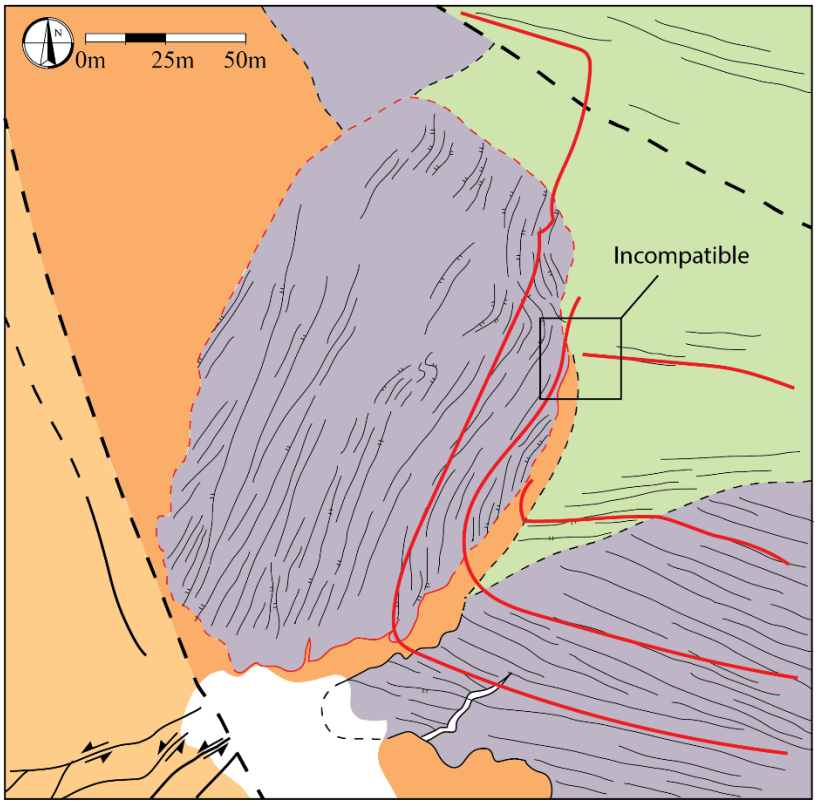

Figure 3.3.2. *Using the map of foliation form lines from figure 2.2.3. to attempt to reconcile the misorientation of foliation in the Clachtoll Megablock by folding (red lines).*

of foliation form lines in the Clachtoll Megablock and surrounding gneiss, it is difficult to find a fold structure that seems geometrically compatible (Fig. 3.3.2). Indeed, it seems more likely that sections of the foliation in the surrounding gneiss abut against the Clachtoll Megablock.

Beacom, Anderson & Holdsworth's (1999) Clachtoll Fault Zone and tectonic opening of fractures

As discussed in chapter 1, Beacom, Anderson and Holdsworth (1999) infer brittle deformation around an ENE-WSW oblique sinistral normal fault in the underlying basement as a mechanism for emplacement of hybrid and tensile fractures filled with Stoer Group sediment. They posit that fractures filled gravitationally from above were then cross-cut by the tectonically-driven forceful injection of fluidised sediment. They use tensile opening directions and slickenline data from Clachtoll, Canisp and the Gairloch region to deduce WNW-ESE oriented extension during rifting.

During this study however, numerous problems with Beacom, Anderson and Holdsworth's (1999) interpretations were identified:

- Problem 1 – this 'Clachtoll fault' isn't where they say it is.

- Problem 2 – the fault is too small and localized to be responsible for all of the sediment filled fractures observed at Clachtoll. It also appears to be a thrust fault not a normal fault.

- Problem 3 – the larger E-W fault on their figure 1, and annotated here in Fig. 3.3.3, is actually south not north of the 'Clachtoll Fault Zone' and there's no evidence that it's actually a fault.

- Problem 4 – The features observed at Clachtoll, Canisp and Gairloch, thought to be contemporaneous at the time, are now known not to be.

- Problem 5 – this study didn't find the different types of fracture fill to ever cross-cut one another.

- Problem 6 – Beacom, Anderson and Holdsworth (1999) do not address or offer an explanation for the misorientation of foliation in the gneiss.

<u>Problem 1:</u>

Beacom, Anderson and Holdworth (1999) identify the location of this 'Clachtoll fault zone' on their figure 1, here presented in figure 3.3.3. Photographs of the fault zone (their figure 5) come from a location 150-200 m north of where they label the fault zone. Whilst this may be a simple case of mislabelling, it is of concern that the fault is shown to occur on the south side of the tongue of Stoer Group conglomerate, when it in fact is found to the north.

<u>Problem 2:</u>

This study found the fault to only be about 5 m long in exposed length, with its termination

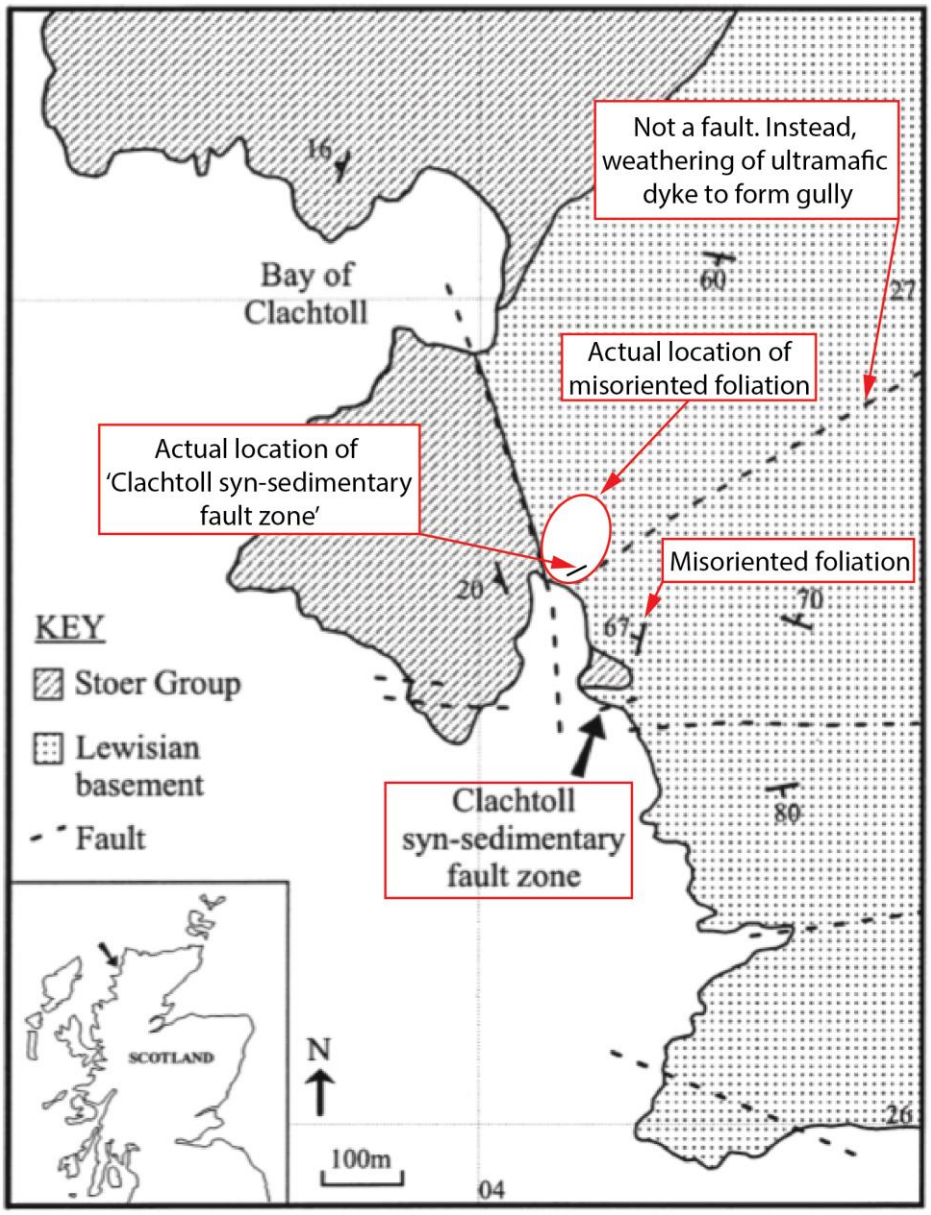

Figure 3.3.3. *Annotated version of Beacom, Anderson & Holdsworth's (1999) Figure 1.*

observed at one end. Deformation that could clearly be attributed to the fault is only found locally within a ~3 m zone around the fault. It seems highly unlikely that this fault could explain the development of the sediment filled fractures throughout the rest of the Clachtoll megablock, e.g. those located at the back of the block, ~100 m to the north. Beacom, Anderson and Holdsworth (1999) focus on the 'Clachtoll fault' but mention that it is one of several ENE-WSW oriented faults in the vicinity. One which they show on their figure 1 is considerably larger than the 'Clachtoll fault' and could conceivably cause fracturing and the development of sediment filled fractures over a much wider area. The inference of this fault is problematic in itself, however, as is discussed in problem 3. Beacom, Anderson and

Holdsworth (1999) do acknowledge the presence of sediment filled fractures outside of the vicinity of the fault, and attribute these to fluid overpressure during Stoer Group deposition. Some of these fractures, i.e. those at the back of the Clachtoll Megablock, have a clear preferred orientation and therefore are unlikely to be attributed to hydraulic fracture resulting from overburden alone.

Problem 3:

Following on from problem 2, on their figure 1, Beacom, Anderson and Holdsworth (1999) show a large ENE-WSW trending fault to the north of the Stoer Group conglomerate tongue, which parallels the 'Clachtoll fault'. Assuming that they have inferred this fault from the gully observed here, then it is correctly located on the map. It is located ~10 m south of the 'Clachtoll fault', however, not ~150 m north of it. During the present study, no evidence could be found to indicate that this feature is actually a fault. No fault plane, or anything that could be described as a fault zone is observed, though admittedly this is not uncommon. Additionally, the only fracturing that occurs is that within the Clachtoll Megablock. There isn't any pervasive or dominant fracturing observed in the gneiss on the south side of this feature, and nothing that could obviously be described as antithetic or synthetic structures is found on either side of the feature. Instead, this linear gully is occupied by a sheared, ultramafic dyke. It is proposed that this feature in the landscape instead results from the preferential weathering and erosion of the ultramafic dyke compared to the more intermediate gneisses, rather than the presence of a fault.

Problem 4:

At the time of Beacom, Anderson and Holdworth's (1999) study, the structures observed at Clachtoll, Canisp and Gairloch were believed to be contemporaneous with each other. They therefore used the similarity in tensile opening direction and slickenline orientation observed at Clachtoll and Gairloch as evidence of a more regional scale extensional setting. It is now known however, that the structures at Canisp are much older than those seen at Clachtoll (Hardman 2019), whilst those at Gairloch are ~200 Myr younger (Jonk, Kelly & Parnell 2004). Beacom, Anderson and Holdsworth (1999) also state that a sinistral-normal movement on their Clachtoll fault is shown by slickenlines on the fault surface. During the fieldwork conducted for this study however, no slickenlines on the fault surface could be found. In fact, no clearly identifiable fault surface could be found. All of the slickenlines in

the vicinity, were instead found on a large boulder toppling from the southeast side of the Clachtoll Megablock, and no longer in situ.

Problem 5:

This study proposes that instantaneous injection of fluidised sediments in the base of the block, was later followed by gravitational filling of sediment into open fractures on the top of the block, over a much longer period of time. Conversely, Beacom, Anderson and Holdsworth (1999) state that injection 'veins' cross cut the fractures that have been passively filled and therefore occur later. In this study, the cross cutting relationships described by Beacom, Anderson and Holdsworth (1999) could not be found. Cross cutting relationships were not observed in general, implying that the two fracture filling mechanisms occurred spatially separated from one another.

Problem 6:

On their figure 1, Beacom, Anderson and Holdsworth (1999) show a data point representing the misoriented zone of gneiss, albeit too far south on their map (Fig. 3.3.3). They do not however, refer to this in the text or offer an explanation as to how it might relate to the 'Clachtoll fault zone'.

Whilst there is evidence in other localities (e.g. Canisp and Gairloch) for the tectonic opening and filling of fractures within an extensional setting, overall, the present study found little evidence to indicate that this process was responsible for the structures observed in and around the Clachtoll Megablock, as is described by Beacom, Anderson and Holdsworth (1999).

The Clachtoll Megablock as a glacial erratic or dropstone

Despite Stewart (1997) and Young (1999) strongly disputing a glacial environment for the basal Stoer Group, for the sake of argument, a glacial provenance for the Clachtoll megablock is here considered. Subglacial hydrofracturing has previously been mentioned in chapter 1, but this process would not explain the misorientation of foliation. Instead, two hypotheses are considered which allow the Clachtoll Megablock to be a detached (not in situ) block of gneiss.

The first hypothesis is that the Clachtoll Megablock represents a large glacial erratic. Erratics have been recorded with dimensions of up to approximately 50 m along their longest axis (Stalker 1956). Rock volumes of varying sizes become entrained in glaciers in a number of different ways (Benn & Evans 2013). Broadly speaking, debris is transported within a glacier in either basal tractive zone (active transport), where it undergoes significant crushing and abrasion, or at higher levels (passive transport), where little to no modification occurs (Boulton 1978). A block of rock the size of the Clachtoll Megablock would likely have been disaggregated in the basal tractive zone. Alternatively, if transported at higher levels, the block would either move into the basal tractive zone and become deformed, simply come to rest on the bedrock as the glacier gradually melted, or be expelled (probably from the Snout of the glacier (Benn & Evans 2013)), thus essentially invoking the rockfall hypothesis proposed by this study.

The second hypothesis is that the Clachtoll Megablock is a large glacial dropstone. Therefore, the sediment filled fractures result from the vertical emplacement of a volume of rock and subsequent overpressuring of fluidised sediments beneath, as in the primary hypothesis of this study – it is the emplacement process that is different. No information could be found regarding the largest drop stones recorded, so instead, some simple calculations were performed.

For a block of gneiss to float, the combined density of the gneiss and the ice it is incorporated in must be less than the density of water. First, the volume of ice required to support a 1 m^3 block of gneiss was calculated:

$$\frac{\rho_g + (\rho_i x)}{x + 1} < \rho_w$$

Where, x is the volume of ice in m^3, ρ_g is the density of the gneiss (2700 kg/m^3), ρ_i is the density of ice (917 kg/m^3), and ρ_w is the density of water (1000 kg/m^3).

$$\frac{2700 + 917x}{x + 1} < 1000 \Rightarrow x > 20.5\ m^3$$

So, for a 1 m^3 block of gneiss to stay afloat, it needs to be incorporated in a >20.5 m^3 block of ice. The Clachtoll Megablock has a volume of ~90,000 m^3, so a volume of at least 1,845,000 m^3 of ice is needed. The minimum size of the combined volume of rock and ice is 1,935,000 $m^{3.}$ This is by no means a huge amount of ice when you consider the scale of ice sheets observed around the world at present.

However,

$$fraction\ of\ floating\ object\ above\ water = \frac{(\rho_{liquid} - \rho_{object})}{\rho_{liquid}}$$

Depending on the ratio of rock to ice, this ultimately yields a below water percentage of 83 - 99.9 %. Stewart (2002) attributes the non-fluvial or alluvial portions of the Stoer Group to deposition within shallow lakes; certainly above fair weather wave base. Assuming a maximum fair-weather wave base of 15m (though it's actually more like 10 m (Johnson & Baldwin 2002 p.246)), at 99.9% submersion, the Clachtoll Megablock barely fits (the block is thought to be ~15 m thick) and there is certainly no room for it to drop. At 83% submersion (12.45 m of block below surface) this leaves a gap of only 2.55 m. In section 3.4. this is proven to be an insufficient fall height to produce hydrofracturing. It also seems implausible that an ice sheet of sufficient size to carry the Clachtoll Megablock could have fit within the confines of the palaeotopography. Within the limitations imposed by these assumptions, it is therefore not possible for the Clachtoll Megablock to be a glacial drop stone.

3.4. Rockfall calculations

The premise than an impact resulting in subsequent injection of wet sediments into a fallen block of gneiss is dependent on the impact generating sufficient overpressure to overcome the tensile strength of the fallen block. It is therefore important to know the minimum height from which the block has to fall to achieve this. If this height seems unreasonable, then the hypothesis breaks down. A fall height of 100 m for example, would seem implausible given the unlikelihood of a 100m free fall with no obstacles or impacts that would break the block into much smaller constituents.

In order to simplify the problem enough for calculations to be undertaken, several assumptions must be made. Firstly, we assume a simple, vertical free fall of the block, with no rotations or translations besides the vertical displacement. We also assume the block itself to be homogeneous. Finally, we assume a flat impact of the block, where all of the underlying surface impacts the ground at the same time. The merits and limitations of these assumptions are further elaborated on in section 3.5.

This section outlines the mathematics and methodology involved in performing this calculation, along with the sourcing of the required parameters to input into said calculation.

3.4.1. Calculations methodology – dynamic stress and fracturing upon rockfall impact

1 – Problem outline and assumptions

Impact consequences can be analysed globally (i.e. in terms of the conversion of kinetic energy from whole colliding mass) or locally (i.e. in terms of waves generated in the vicinity of the object boundaries immediately after impact). In terms of dynamic fracturing, initiation and propagation will occur at a local scale within short time intervals, in the immediate vicinity of the impact surface, therefore the second approach is applicable here.

Usually such analysis is restricted to cases where both objects are solid elastic and have similar impedance[1]. Here we extend the analysis to collision of media with contrasting properties – elastic stress wave on the impacting object[2], and acoustic pressure waves[3] on the target medium. Since the soil is saturated, we may describe the propagation of an acoustic wave using the properties of water incompressibility and density.

At initial times after the collision, we can reduce analysis to one dimension – considering any point where the waves diffracted from the outer borders of the object, and propagating laterally, have not yet arrived. For a rock boulder of linear dimension 15 m, the centre of the impact surface will be reached by lateral waves only at times of the order of $\approx$ 1 ms after impact. Later developments of the stress wavefield will be more complex, but after about 1 ms, dynamic tension fractures will already have nucleated and propagated up to a few metres within the boulder.

Our analysis also considers sections of the impacting object whose surface is parallel to the ground, and we assume that the ground is relatively flat. Under those assumptions, the elastic strain within the block, immediately after impact, will be reduced to shortening parallel to the vertical (fall) direction. Both stress and pressure waves, within the impacting boulder and within saturated soil, respectively, will propagate away from the impact surface at

---

[1] Mechanical impedance is a measure of how much a structure resists motion when subjected to a harmonic force. The mechanical impedance of a point on a structure is the ratio of the force applied at a point to the resulting velocity at that point.

$$\boldsymbol{F}(\omega) = \boldsymbol{z}(\omega)\boldsymbol{v}(\omega)$$

Where $\boldsymbol{F}$ is the force vector, $\boldsymbol{z}$ is the impedance matrix, $\boldsymbol{v}$ is the velocity vector, and ω is the angular frequency.

[2] Elastic stress wave velocity or P-wave velocity is given by:

$$V_P = \sqrt{\frac{K + \frac{4}{3}\mu}{\rho}} = \sqrt{\frac{\lambda + 2\mu}{\rho}}$$

Where K is the bulk modulus, λ is Lame's first parameter, μ is the shear modulus, and ρ is the density of the material through which the wave is propagating.

$$K = \lambda + \frac{2}{3}\mu$$

[3] Acoustic wave propagation speed of sound, c.

$$V_w = c = \sqrt{\frac{K}{\rho}}$$

Pressure wave velocity is dependent on density, ρ, and elasticity, K, λ, μ.

typical velocity of P-waves in the rock (circa 5000 m/s) and of acoustic waves in water (circa 1500 m/s).

2 – Solid collision

We start our analysis with the classic problem of the collision between two elastic solid bodies of identical impedance. In the case of a rockfall, this may equate to a rock boulder falling on a rock ground of same composition.

It is known that the initial wave due to the impact will produce a constant displacement gradient

(1)

$$\frac{\partial u}{\partial z} = -\frac{v_b}{V_P}$$

in the target object, within the thickness reached by the propagating wave, i.e., $z_c = V_P\, t$ at time t after impact[4]. Here v_b is the displacement velocity of the target surface due to impact. If the projectile and the target share the same impedance, then v_b is half the projectile velocity. V_P is the longitudinal (P) wave velocity, u is the particle displacement perpendicular to the boundary with respected to the unstrained position, and z is the collision direction (vertical for a falling boulder).

Derivation of equation (1):

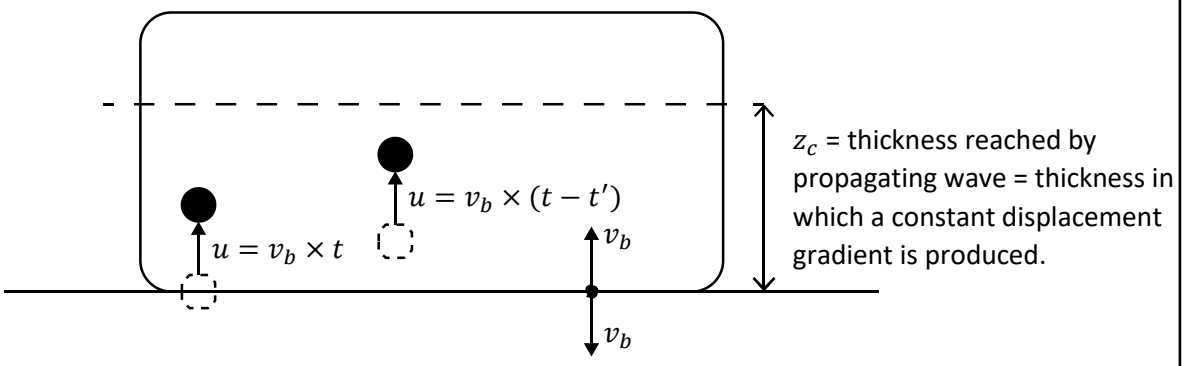

[4] This comes from the simple equation, distance = velocity x time. Hence, $z_c = V_P\, t$.

Derivation of equation (1), continued:

The boundary is moving at velocity v_b, so the displacement of the boundary at time t after impact is given by

$$u = v_b \times t$$

Away from the boundary, points will only start to move when the wave from the impact reaches them, at a time

$$t' = z/V_P$$

The displacement at any point z will therefore be

$$u(z) = v_b \times (t - t') = v_b(t - \frac{z}{V_P})$$

$$u = v_b\left(t - \frac{z}{V_P}\right) = v_b t - v_b \frac{z}{V_P}$$

We can take the derivative of u with respect to z to find the displacement gradient $\frac{\partial u}{\partial z}$

$$\frac{\partial u}{\partial z} = -\frac{v_b}{V_P}$$

Using positive compressive stress convention, the stress due to unidirectional compression along z is

$$\sigma_{zz} = -(\lambda + 2\mu)\frac{\partial u}{\partial z}$$ [5]

Substituting $\frac{\partial u}{\partial z} = -\frac{v_b}{V_P}$ gives

$$\sigma_{zz} = (\lambda + 2\mu)\frac{v_b}{V_P}$$

Also,

$$\sigma_{xx} = \sigma_{yy} = -\lambda\frac{\partial u}{\partial z} = \lambda\frac{v_b}{V_P} = \frac{\lambda}{\lambda + 2\mu}\sigma_{zz} \quad (2)$$

[5] This comes from Hooke's Law $\sigma = -c\varepsilon$, where c is the elastic parameters and ε is strain, $\varepsilon = \frac{\partial u}{\partial z}$.

where λ, μ are Lame's parameters for an isotropic elastic solid. Generation of fractures may then be diagnosed as a function of v_b using the two stress components and rock tension or shear fracturing stress, or, assuming pre-existing cracks, using material toughness values.

3 – Matching traction and displacement for mixed media collision

We will treat the water-saturated soil as a fluid with the properties of water. Matching traction and displacement continuity produces the well-known result that traction perpendicular to the impact boundary (σ_{zz} for the solid, pressure P for the soil) will be the same.

$$\sigma_{zz} = P$$

However, if the impedance of the boulder (projectile) and the soil (target) are unequal, the boundary displacements with respect to unstrained conditions of either objects will be unequal, therefore instead of a unique boundary velocity v_b, we should define v_r as the boundary deflection with respect to the unstrained rock of the boulder, and v_w as the boundary deflection with respect to the unstrained soil (note that v_r and v_w are in different kinematic referentials). In terms of wave propagation analysis, v_r corresponds to the reflected particle velocity inside the boulder, and v_w corresponds to the transmitted particle velocity in the soil.

After impact (but before any rebound) the boundary will be joined, therefore we have to match the boulder falling velocity v_i and the respective boundary velocities in each medium referential such that:

$$|v_i| = |v_w| + |v_r|$$

Adopting a referential in each media which is pointing away from the boundary (positive z up in the boulder, positive z down in the soil) and recalling that v_w, v_r are defined relative to the unstrained position of both media, we can write

$$v_i = v_w + v_r \tag{3}$$

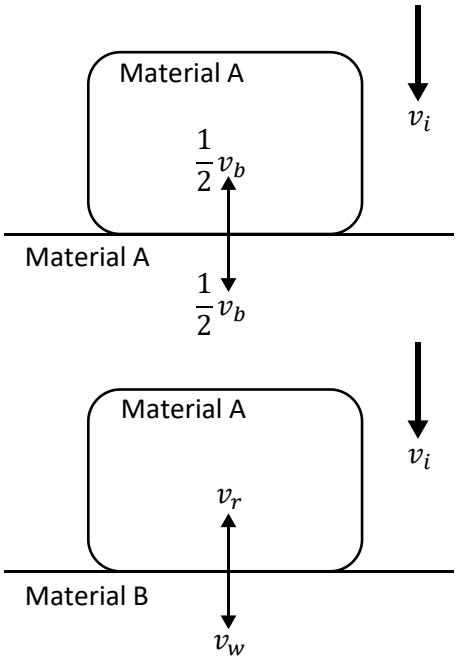

$$v_i = v_b$$

$$|v_i| = |v_w| + |v_r|$$

$$v_i = v_w + v_r$$

Proceeding in similar fashion as for equations (1) and (2), we can equate pressure in the unconsolidated soil to

$$P = K\frac{\partial u_z}{\partial z} = K\frac{v_w}{V_w} \tag{4}$$

where K is water incompressibility (bulk modulus) and V_w is the pressure wave velocity in the soil.

Remember:

$$\sigma_{zz} = (\lambda + 2\mu)\frac{v_b}{V_P} \tag{5}$$

Now matching P and σ_{zz} for traction continuity, we obtain

$$P = \sigma_{zz} \implies \frac{K}{V_w}v_w = \frac{(\lambda + 2\mu)}{V_P}v_r$$

Both sides of this equation are a force, and remembering that,

$$\boldsymbol{F = Zv}$$

This equates to,

$$v_w Z_w = v_r Z_r \tag{6}$$

We define the impedances Z and the wave velocities V such that,

$$Z_w = \sqrt{\rho_w K} = K/V_w$$

$$Z_r = \sqrt{\rho_r(\lambda + 2\mu)} = \frac{\lambda + 2\mu}{V_P} \tag{7}$$

Where,

$$V_P = \sqrt{\frac{\lambda + 2\mu}{\rho_r}}$$

$$V_w = \sqrt{\frac{K}{\rho_w}}$$

and ρ_r and ρ_w are mass densities for rock and water respectively.

Check step to see where this comes from/show that it works:

$$Z_w = \frac{K}{V_w} = K \Big/ \sqrt{\frac{K}{\rho_w}} = \frac{K\sqrt{\rho_w}}{\sqrt{K}} = \sqrt{K}\sqrt{\rho_w} = \sqrt{\rho_w K}$$

$$Z_r = \frac{\lambda + 2\mu}{V_P} = \lambda + 2\mu \Big/ \sqrt{\frac{\lambda + 2\mu}{\rho_r}} = \frac{(\lambda + 2\mu)\sqrt{\rho_r}}{\sqrt{\lambda + 2\mu}} = \sqrt{\rho_r(\lambda + 2\mu)}$$

Also,

$$\sigma_{zz} = (\lambda + 2\mu)\frac{v_r}{V_P} \quad \Rightarrow \quad Z_r = \frac{\boldsymbol{F}}{\boldsymbol{v}} = \frac{\sigma_{zz}}{v_r} = \frac{\lambda + 2\mu}{V_P}$$

$$P = K\frac{v_w}{V_w} \quad \Rightarrow \quad Z_w = \frac{F}{v} = \frac{P}{v_w} = K\frac{v_w}{V_w} \Big/ v_w = \frac{K}{v_w}$$

Remember equation (3)

$$v_i = v_w + v_r$$

and equation (6)

$$v_w Z_w = v_r Z_r$$

Jointly solving these equations gives:

$$v_r = \frac{Z_w}{Z_r + Z_w} v_i \tag{8}$$

$$v_w = \frac{Z_r}{Z_r + Z_w} v_i$$

Workings for this step:

$$v_i = v_w + v_r \quad \Rightarrow \quad v_w = v_i - v_r \quad \Longrightarrow \quad v_r = v_i - v_w$$

$$v_w Z_w = v_r Z_r \quad \Longrightarrow \quad v_w = v_r \frac{Z_r}{Z_w} \quad \Longrightarrow \quad v_r = v_w \frac{Z_w}{Z_r}$$

$$v_i - v_w = v_w \frac{Z_w}{Z_r} \quad \Rightarrow \quad v_i = v_w \frac{Z_w}{Z_r} + v_w \quad \Rightarrow \quad v_i = v_w \left(\frac{Z_w}{Z_r} + 1\right)$$
$$= v_w \left(\frac{Z_w + Z_r}{Z_r}\right)$$

$$\Rightarrow v_w = {v_i}\Big/{\frac{Z_w + Z_r}{Z_r}} = \frac{Z_r}{Z_r + Z_w} v_i$$

$$v_i - v_r = v_r \frac{Z_r}{Z_w} \quad \Rightarrow \quad v_i = v_r \frac{Z_r}{Z_w} + v_r \quad \Rightarrow \quad v_i = v_r \left(\frac{Z_r}{Z_w} + 1\right) = v_r \left(\frac{Z_r + Z_w}{Z_w}\right)$$

$$\Rightarrow v_r = {v_i}\Big/{\frac{Z_r + Z_w}{Z_w}} = \frac{Z_w}{Z_r + Z_w} v_i$$

We can now substitute equations (8) for v_r and v_w into

$$P = \sigma_{zz} \implies \frac{K}{V_w} v_w = \frac{(\lambda + 2\mu)}{V_P} v_r$$

to obtain,

$$P = \sigma_{zz} = \frac{K}{V_w} \frac{Z_r}{Z_r + Z_w} v_i = \frac{(\lambda + 2\mu)}{V_P} \frac{Z_w}{Z_r + Z_w} v_i$$

From equation (7) we know that

$$Z_w = \frac{K}{V_w}$$

So equation (9) becomes

$$P = \sigma_{zz} = Z_w \frac{Z_r}{Z_r + Z_w} v_i = \frac{Z_w Z_r}{Z_r + Z_w} v_i = \frac{1}{\frac{Z_r}{Z_w Z_r} + \frac{Z_w}{Z_w Z_r}} v_i \qquad (9)$$

$$= \frac{1}{\frac{1}{Z_w} + \frac{1}{Z_r}} v_i = \left(\frac{1}{Z_w} + \frac{1}{Z_r}\right)^{-1} v_i$$

If we now define the harmonic mean[6] of the impedances as

$$\overline{Z} = \frac{1}{2}\left(\frac{1}{Z_r} + \frac{1}{Z_w}\right)^{-1} \qquad (10)$$

[6] The harmonic mean of a set of n numbers is given by

$$\overline{H} = \frac{n}{\frac{1}{x_1} + \frac{1}{x_2} + \cdots + \frac{1}{x_n}} = \frac{1}{n}\left(\frac{1}{x_1} + \frac{1}{x_2} + \cdots + \frac{1}{x_n}\right)^{-1}$$

Or in words: add the reciprocals of the numbers in the set, divide the sum by n, then take the reciprocal of the result.

We can then write

$$\sigma_{zz} = P = 2\overline{Z}v_i$$

$$\sigma_{xx} = \sigma_{yy} = \frac{\lambda}{\lambda + 2\mu} 2\overline{Z}v_i \tag{11}$$

Recall equation (2) to do this step:

$$\sigma_{zz} = -(\lambda + 2\mu)\frac{\partial u}{\partial z}$$

$$\sigma_{xx} = \sigma_{yy} = -\lambda\frac{\partial u}{\partial z} = \frac{\lambda}{\lambda + 2\mu}\sigma_{zz}$$

4 – Hydrofracturing criterion

If the dynamic tensile strength of gneiss is σ_c, we can write as an Hydrofracturing criterion

$$P > \sigma_c + \sigma_{xx} \tag{12}$$

$$2\overline{Z}v_i > \sigma_c + \frac{\lambda}{\lambda + 2\mu} 2\overline{Z}v_i$$

Which means that the fluid pressure should overcome the tensile strength plus the compressive horizontal stress (for vertical hydrofractures), resulting in

$$v_i = \frac{\sigma_c}{2\overline{Z}\left(1 - \frac{\lambda}{\lambda + 2\mu}\right)} \tag{13}$$

The σ_{xx} component of the Hydrofracturing criterion:

Following impact, the block will compress in the vertical direction and want to expand in the horizontal direction. Immediately after impact, particles away from the edges of the block are confined by surrounding particles and are therefore unable to undergo this lateral extension, thereby setting up a horizontal stress that opposes extension. Extension first occurs at the edges of the block where the particles are unconfined, then migrates inwards. This results in the pressure required for Hydrofracturing to occur, to not only exceed the tensile strength of the gneiss, but also the horizontal stress, hence:

$$P > \sigma_c + \sigma_{xx}$$

Once the value of the initial velocity, v_i has been obtained, this value can be put into the free fall equation shown below to determine the minimum height the block must fall from to provide a pressure great enough to overcome the tensile strength and the horizontal stress.

$$v_i = \sqrt{2gh}$$

Where h is the fall height and g is acceleration due to gravity.

How is the free fall equation derived?

We can derive the free fall equation as follows:

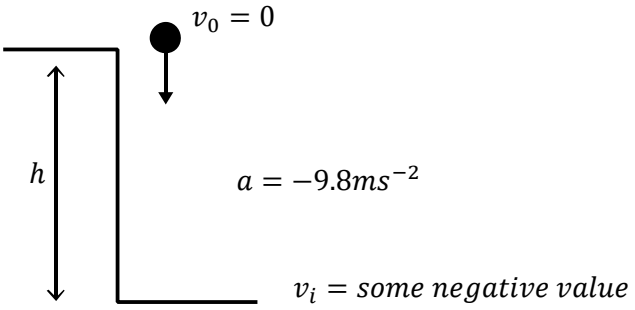

$v_0 = initial\ velocity$

$v_i = impact\ velocity\ (final\ velocity)$

$a = acceleration\ due\ to\ gravity$

Firstly we can define the average velocity:

$$v_{avg} = \frac{v_i + v_o}{2}$$

We can also define the change in time:

$$\Delta t = \frac{\Delta v}{a}$$

Where $\Delta v = v_i - v_o$

Remember, distance = velocity x time, so:

$$h = v_{avg}\Delta t = \frac{v_i + v_o}{2}\frac{\Delta v}{a}$$

We know that $v_0 = 0$ so h becomes:

$$h = \frac{v_i}{2}\frac{v_i}{a}$$

Finally, we simply rearrange this equation to obtain the free fall equation.

$$h = \frac{v_i}{2} \quad \Rightarrow \quad 2ah = {v_i}^2 \quad \Rightarrow \quad v_i = \sqrt{2ah}$$

$a = g$, so:

$$v_i = \sqrt{2gh}$$

3.4.2. Brazil test

Determining the fall height of the block using the free fall calculation methodology, requires inputting the tensile strength of the gneiss as a known parameter. In order to ascertain the tensile strength of the gneiss, the Brazil test was performed on a selection of cores, using the methodology outlined by Part 2 of Bieniawski & Hawkes (1978). The test measures the indirect uniaxial tensile strength of a specimen. Measuring the indirect strength is important for realistically modelling the impact event – it is the downward motion being impeded by impact that results in the opening of tensile fractures (indirect), rather than an active pulling apart of the block (direct).

Experiment methodology

1. **Apparatus**

(i) A pair of steel loading jaws intended to grip a disc-shaped specimen at diametrically-opposed surfaces (Fig. 3.4.2.1).

(ii) A machine appropriate for the application and measurement of compressive loads applied to the specimen, preferably with a fitted load/displacement recorder. Here, the biaxial loading apparatus in Durham University's Rock Mechanics Laboratory was utilised.

(iii) Not required, but used in this case: a high speed camera, used to verify that rupture initiated in the centre of the specimen, not the perimeter, which would be the result of edge effects and wouldn't give a true tensile strength. In addition to the high speed camera, a bright lighting set-up is required to sufficiently illuminate the specimen, given the high frame rate of the camera.

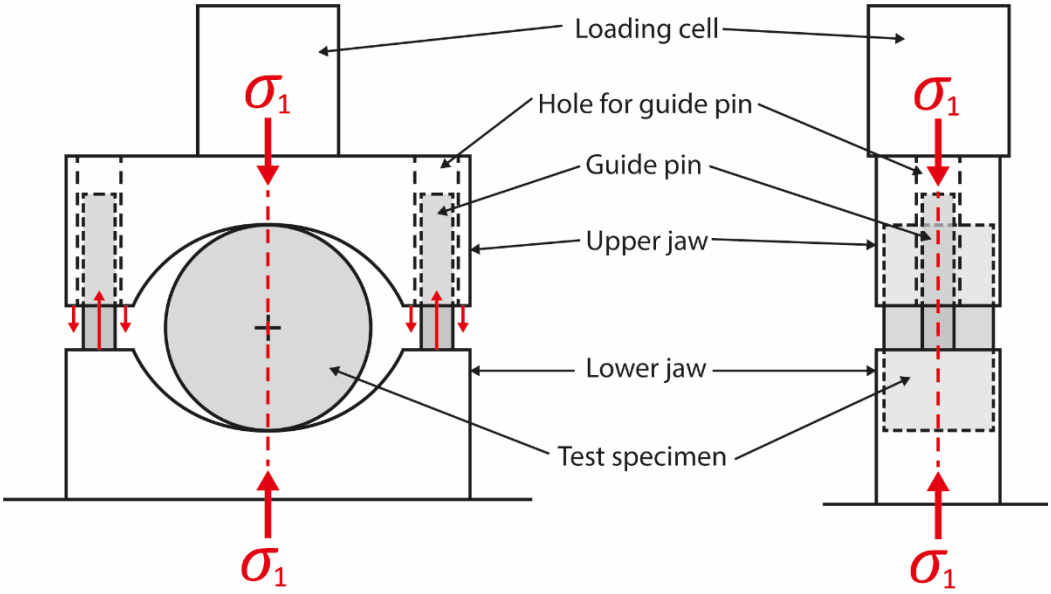

Figure 3.4.2.1. *Set-up for loading jaws, specimen and loading cell. As laid out Bieniawski and Hawkes (1978), "the critical dimensions are the radius of curvature of the jaws (1.5 x specimen radius); the clearance and length of the guide pins coupling the two jaws (they must not permit rotation of one jaw relative to the other out of plane by more than 4 x* 10^{-3} *rad) and the width of the jaws (1.1 x specimen thickness)."*

2. Specimens

An in situ sample of the Lewisian gneiss was taken from the hillside approximately 100 m southeast of the Clachtoll megablock. Four cores with a diameter of 20 mm were taken from the sample, two parallel to the foliation of the gneiss, and two perpendicular. These cores were then sliced to obtain discs with a thickness varying from 13 to 20 mm. In total, four discs were made with the axes of the core running parallel to foliation (P1-P4), and four perpendicular (O1-O4) (Fig. 3.4.2.2. and Table 3.4.2.1). The remaining core was designated 'spare'. As required by the method detailed Bieniawski & Hawkes (1978), the cylindrical surfaces were free from tool marks, and irregularities across the thickness of the specimen did not exceed 0.025mm. End faces were flat to within 0.25mm and square and parallel to within 0.25°.

Specimen	Diam. 1 (mm)	Diam. 2 (mm)	Diam. 3 (mm)	Diam. Mean (mm)	Length 1 (mm)	Length 2 (mm)	Length 3 (mm)	Length Mean (mm)
P1	20.04	20.06	20.05	20.05	15.55	15.51	15.53	15.53
O1	19.97	19.98	19.99	19.98	20.89	20.91	20.90	20.90
P2	20.18	20.15	20.06	20.13	13.56	13.56	13.53	13.55
P4	20.05	20.02	20.07	20.05	18.95	18.89	18.93	18.92
P3	20.04	20.06	20.06	20.05	17.46	17.49	17.45	17.47
O2	19.99	19.98	19.99	19.99	14.42	14.43	14.43	14.43
O4	20.01	19.82	19.77	19.87	15.47	15.41	15.42	15.43
O3	19.99	19.99	19.99	19.99	13.13	13.11	13.17	13.14

Table 3.4.2.1. *Specimen orientations (relative to foliation in sample) and dimensions. Each specimen's diameter and length were measured three times using digital callipers to calculate a mean value.*

3. Procedure

(a) The test specimens were cut and prepared using clean water, then stored in a sealed plastic bag until use, as the sample had been prior to coring.

(b) The loading jaws, with first specimen in place were squarely positioned in the biaxial loading apparatus, such that the load was applied to the specimen diametrally (Fig. 3.4.2.3). Upon inserting the specimen into the jaws, the orientation of its foliation relative to the loading direction was recorded (Fig. 3.4.2.4).

(c) The high speed camera and appropriate lighting were then set up and the camera focused.

(d) A continuous load was then applied to each specimen in turn, at a constant rate, until failure occurred. The load/displacement recorder was used throughout to precisely determine the load at primary fracture.

(e) After each test, the footage captured by the high speed camera was reviewed to ensure that the fracture nucleated in the centre of the specimen (Fig. 3.4.2.6).

4. Conversion of results to tensile strength

The following formula is used to determine the tensile strength of the specimen:

$$\sigma_t = 0.636\, F/Dt$$

Where σ_t is tensile strength, F is the load at failure (N), D is the diameter of the specimen (mm) and t is the thickness of the specimen (mm).

Figure 3.4.2.2. *Specimens prepared for testing. (a) Specimens O1 – O4, with cores cut orthogonal to foliation in gneiss – circular surface of cylinder displays plane of foliation; (b) Specimens P1 – P4, with cores cut parallel to foliation in gneiss – circular surface of cylinder cross-cuts foliation.*

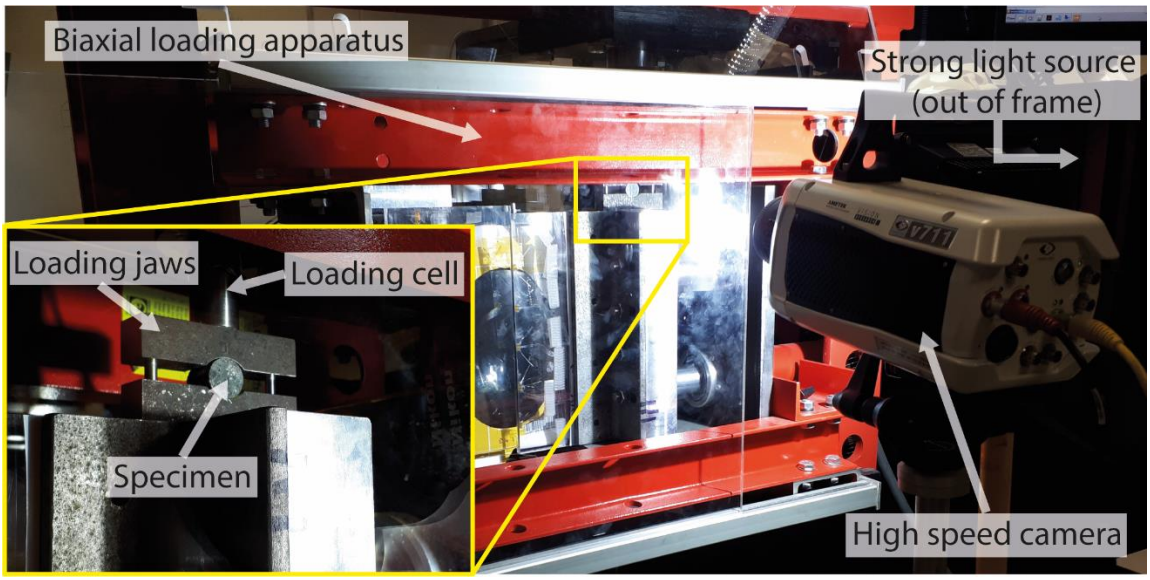

Figure 3.4.2.3*. Apparatus set-up for Brazil test. Note that although the loading apparatus is capable of loading a specimen biaxially, this is unnecessary for performing a Brazil test, and the specimens were only uniaxially loaded.*

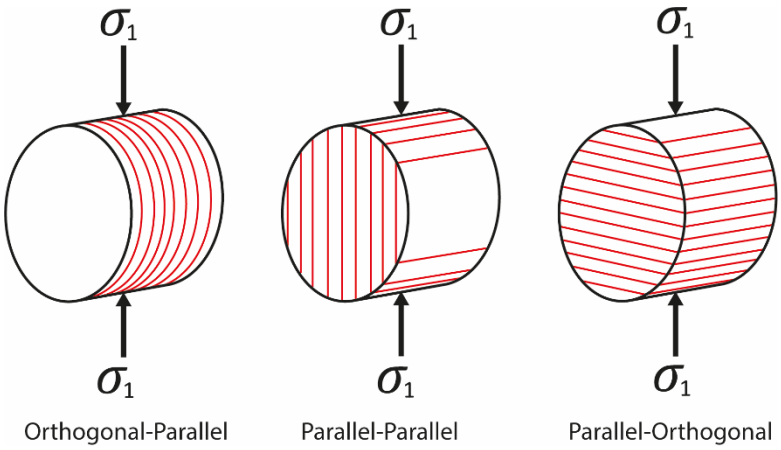

Figure 3.4.2.4. *Specimen loading orientations. Orientations are noted in two parts, each part of which can either be parallel or orthogonal. The first part refers to the orientation of the foliation with respect to the core cutting direction of the sample, whilst the second part refers to the orientation of the foliation with respect to the loading direction. Thus specimens O1 – O4 are all designated Orthogonal-Parallel, whilst samples P1 – P4 can either be loaded such that they are Parallel-Parallel or Parallel-Orthogonal.*

Results

Calibration

Prior to testing of the specimens, a known load was applied to the loading cell and jaws and the resulting voltage recorded, such that a slope for load vs volts could be calculated (Fig 3.4.2.5). This relationship can then be used to ascertain the load for each test, given the voltage recorded at failure.

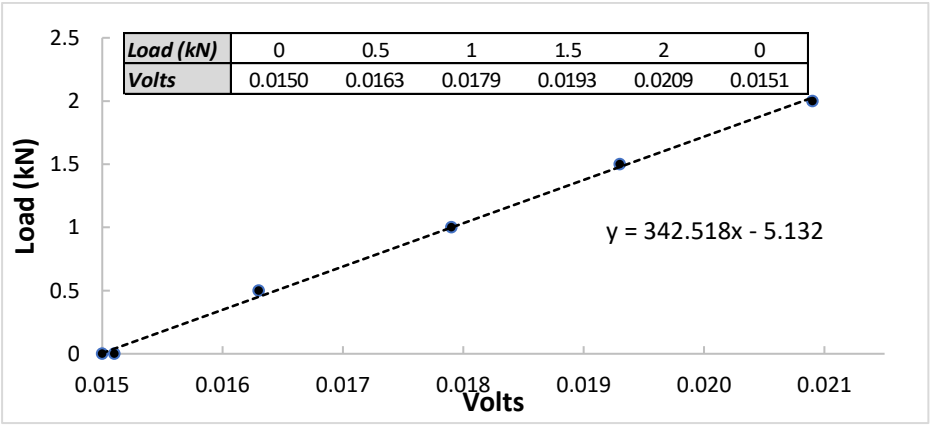

Figure 3.4.2.5. *Experiment calibration, applying a load of 0 to 2 kN at 0.5 kN intervals yielded a slope of 342.518.*

Verification of initial fracture rupture location

To be sure that a true tensile strength was found, it was necessary to verify that a mode I fracture nucleated within the centre of the test specimen. In order to do this, the high speed camera footage was carefully reviewed after each test to identify the location of fracture nucleation. An example of images from this process, for each of the three possible specimen orientations, is shown in Figure 3.4.2.6. Example (A) is of interest because it contains a pre-existing weakness oriented approximately perpendicular to both the foliation and the loading direction. Fracturing did initially occur in the centre of the specimen, but was immediately followed by fracturing around the edges of the sample, in the vicinity of, and parallel to this existing weakness.

Also of note, was the difference in the fracture sets generated in specimen P1 and P4. Both specimens were oriented parallel-parallel, but whilst P1 failed along multiple parallel fractures, P4 failed along one, centrally located, discreet fracture (Fig. 3.4.2.7). Inspection of the specimens indicates that this difference in failure behaviour is likely due to the relative abundance of micaceous minerals in P1, defining numerous planes of anisotropy when compared to P4.

Results and conversion to force and stress

The initial results of the Brazil tests are shown in Table 3.4.2.2. Two steps were required to convert these results to tensile strength. The first step uses the results of the experiment calibration to convert the recorded voltages to force, using the following equation (multiplying by 10^3 converts from kN to N):

$$F = slope \times (peak\ V - zero\ V) \times 10^3$$

The second step uses the equation outlined in the experiment methodology to convert from force to stress:

$$\sigma = 0.636\ F/Dt$$

The load vs time graphs recorded during the tests are presented in Figure 3.4.2.8. The variable responses observed in the stress drop curves are considered to be a result of heterogeneities in fabric spacing, mineral modalities and grain size within the specimen, rather than specimen orientation or experimental effects. It is expected that with a larger sample size, patterns would emerge that would more clearly identify variable responses in relation to the specimen orientation.

In some cases, after an initial stress drop, taken as the point of failure, stress then continues to rise. This is to be expected, given that the specimen should theoretically fail along its weakest layer. It then follows that the resulting two halves will each then individually be stronger than the original whole, having eliminated the weakest layer.

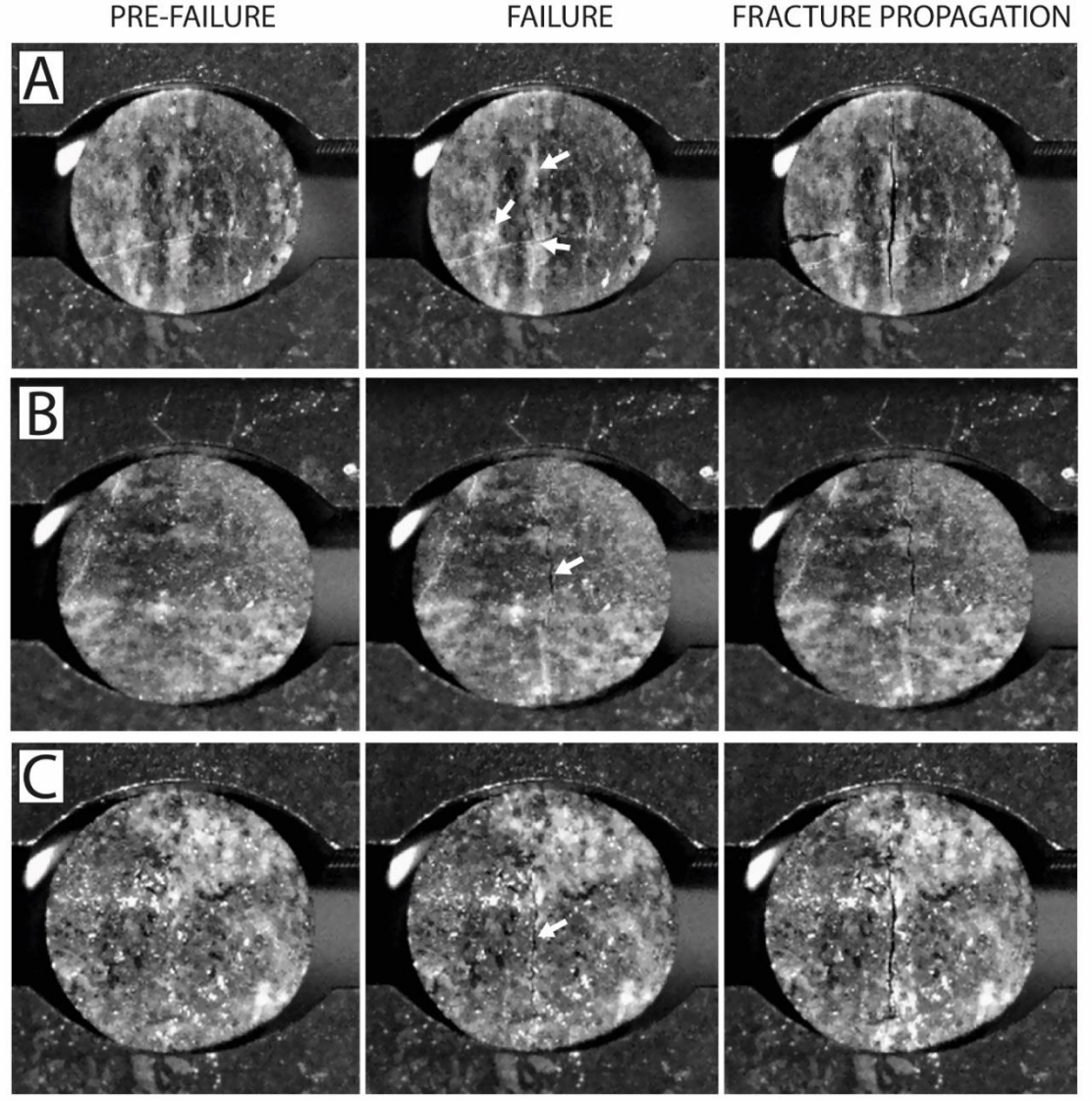

Figure 3.4.2.6. *High speed camera stills of fracture initiation. (A) shows an example of fracture initiation in a parallel-parallel oriented specimen, (B) a parallel-orthogonal oriented specimen, and (C) an orthogonal-parallel oriented specimen. The first column shows the specimens in their pre-failure state. The second column shows the frame recorded in which fracturing is first observed, denoted by the white arrows. Here, specimen (A) has three white arrows, highlighting a diffuse whitening of the sample in specific localities which then formed obvious fractures in one frames time (column 3).*

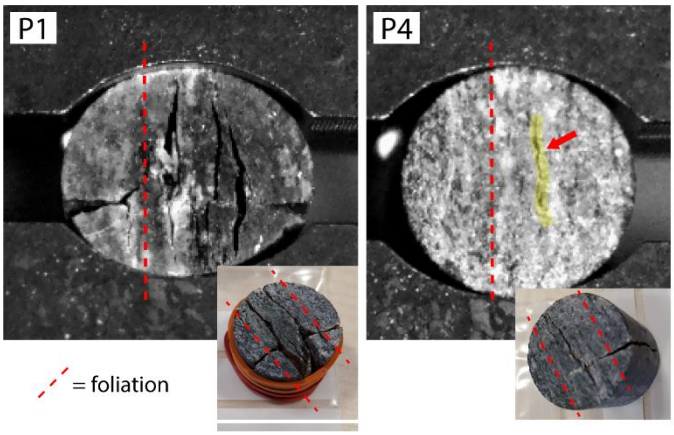

Figure 3.4.2.7. *High speed camera stills of fracture development in specimens P1 and P4, along with photos of the specimens after the experiment. P1 clearly shows fracturing along numerous parallel fractures, whilst P4 failed along one main foliation parallel fracture.*

Experiment #	*Video file name*	*Specimen*	*Orientation*	*Diam. Mean (mm)*	*Length Mean (mm)*	*Zero V (V)*	*Peak V (V)*	*Force (N)*	*Stress (Mpa)*
1	Z01	P1	//	20.05	15.53	0.0131	0.0177	1575.58	3.21566
2	Z02	O1	-	19.98	20.90	0.0164	0.0296	4521.24	6.89284
3	Z03	P2	T	20.13	13.55	0.0148	0.0231	2842.90	6.60751
4	Z04	P4	//	20.05	18.92	0.0124	0.0236	3836.20	6.42148
5	Z05	P3	T	20.05	17.47	0.0136	0.029	5274.78	9.58781
6	Z06	O2	-	19.99	14.43	0.0135	0.0331	6713.35	14.81216
7	-	O4	-	19.87	15.43	0.0138	0.0211	2500.38	5.13719
8	Z07	O3	-	19.99	13.14	0.0144	0.0273	4418.48	10.70663

Table 3.4.2.2. *Brazil test results. // denotes a parallel-parallel specimen orientation, T a parallel-orthogonal orientation, and – an orthogonal-parallel orientation.*

The mean tensile strength was calculated for each of the three possible specimen orientations (Table 3.4.2.3).

As expected, the parallel-parallel specimens had the lowest tensile strength, being optimally oriented to form fractures parallel to foliation. The orthogonal-parallel specimens are the most accurate representation of the Clachtoll megablock, with fractures forming parallel to the maximum principal stress, but orthogonal to the foliation. It was therefore initially decided to input this measurement into the fall height calculation. However, given the similarity in mean tensile strength of the orthogonal-parallel and parallel-orthogonal specimens, and their overlap when considering error, it was decided to group these specimen orientations so that a result could be used that derived from a larger sample size.

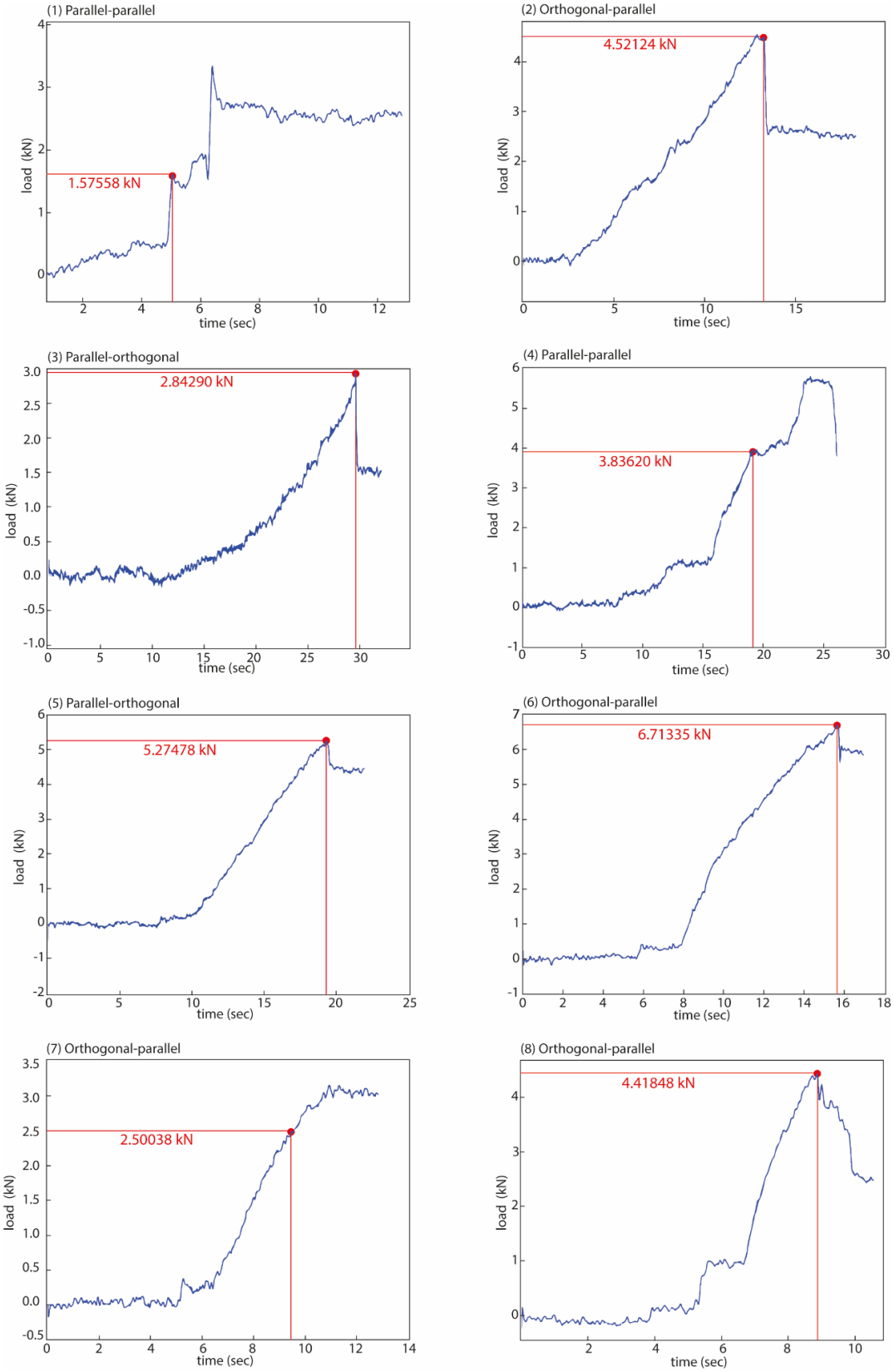

Figure 3.4.2.8. *Stress drop curves for each test. Red dots indicate failure of the specimen. Both parallel-parallel specimens showed relatively minor stress drops at failure. The parallel-orthogonal specimens showed more obvious stress drops, whilst the orthogonal-parallel specimens were much more variable in their behaviour.*

Specimen	Stress	//	T	-	T and -
P1	3.21566	✓			
O1	6.89284			✓	✓
P2	6.60751		✓		✓
P4	6.42148	✓			
P3	9.58781		✓		✓
O2	14.81216			✓	✓
O4	5.13719			✓	✓
O3	10.70663			✓	✓
Mean σ (Mpa)		4.8186	8.0977	9.3872	8.9574
Standard deviation		2.26685	2.10739	4.29944	3.52460
Mean tensile strength (MPa)		5 ± 2	8 ± 2	9 ± 4	9 ± 3

Table 3.4.2.3. *Mean tensile strength calculations.*

3.4.3. Calculation results

Using the Brazil test to find the tensile strength of the gneiss, accounts for just one parameter required to ultimately calculate the fall height of the block. In addition, the shear modulus (μ), the first Lame parameter (λ), and the P wave velocity (V_P) of the gneiss must be known, along with the acoustic wave velocity (V_w) and the bulk modulus (K) of the liquid substrate, here assumed to have the properties of water. The acoustic wave velocity of water is well known, at 1500 m/s. A value of 2200 MPa for the bulk modulus of water was also easily obtained (Engineering ToolBox 2004).

Ascertaining the Lame parameters of the gneiss proved much more challenging, typically only being reported for rocks at depth. Ji, Sun, Wang, *et al.* (2010) report a λ value for felsic-intermediate gneiss of 25 – 50 GPa at pressures of 600 MPa (20-25 km depth). This value decreases to 11 – 12 GPa at surface pressures (Figure 1c, Ji, Sun, Wang, *et al.* 2010). μ is also reported for rocks at depth, and no sources were found that allowed a value to be extrapolated to surface pressures. Ji, Sun, Wang, *et al.* (2010) give a μ/λ ratio of 1.057 for felsic rocks, or $\mu \approx \lambda$, supported by the trend of a μ- λ plots in their figures 8 and 9. It was therefore decided to let $\mu = \lambda$.

This just leaves the P-wave velocity of the gneiss remaining. Again, this value is reported in the literature for rocks at depth. Hall & Al-Haddad (1976) give a V_P value of 5.28 ± 0.23 km/s for the Lewisian gneiss in their 'Boundary region', taken as their closest location to the Clachtoll megablock. They also report a velocity gradient of ~0.1 km/s/km in the

uppermost crust. Levander et al. (1994) report a V_P of 6.10 – 6.24 km/s corrected to 250 MPa and 140 °C, i.e. a depth of ~10 km. Using the velocity gradient of Hall and Al-Haddad (1976), this extrapolates to 5.10 – 5.24 km/s at the surface, though it may not be reasonable to assume that this gradient is linear. Christensen (1965) gives average velocities of 5.1 and 4.8 for their gneiss samples 3 and 4 respectively – those which most closely resemble the Lewisian gneiss at Clachtoll in mineralogy and grainsize. They also report no clear relationship between P-wave velocity and P-wave direction relative to foliation orientation, effectively allowing us to assume the gneiss is seismically isotropic. Averaging the values obtained from these sources gives a P-wave velocity of 5.1 km/s.

Another approach to obtain a P-wave velocity of the gneiss is to substitute the λ and μ values into the equation,

$$V_P = \sqrt{\frac{\lambda + 2\mu}{\rho}}$$

using a ρ value of 2700 kg/m^3.

$$\Rightarrow V_P = \sqrt{\frac{12\ GPa + 2 \times 12\ GPa}{2700}} = 3650\ m/s$$

Whilst significantly lower than the values in the literature, this does not seem unreasonable for a P-wave velocity at the surface when compared to the λ-V_P plots in Ji et al.'s (2010) figure 6.

It was ultimately decided to perform the calculation twice, using both V_P values of both 5100 m/s and 3650 m/s.

Once values are known for σ (the tensile strength of the gneiss), λ, μ, K, V_P and V_w, these can be used to find Z_w and Z_r, where,

$$Z_w = \frac{K}{V_w}$$

and,

$$Z_r = \frac{\lambda + 2\mu}{V_P}$$

These values can be substituted into,

$$\overline{Z} = \frac{1}{2}\left(\frac{1}{Z_r} + \frac{1}{Z_w}\right)^{-1}$$

to find $\overline{Z}$, which can be substituted into,

$$v_i = \frac{\sigma_c}{2\overline{Z}\left(1 - \frac{\lambda}{\lambda + 2\mu}\right)}$$

Once v_i, the impact velocity of the block, is known, the freefall equation can be used to find the minimum height from which the block must have fallen. The results of this process are shown in Table 3.4.3.1.

For a tensile strength of the gneiss of 9 MPa, and a V_P value of 3650 m/s, the minimum fall height is for 5.7 m, or 6.3 m with a V_P of 5100 m/s. Ultimately, 6 m is a good estimate for the height from which the block must fall to generate sufficient overpressure to fracture the gneiss. Given the dimensions of the block, it also seems feasible that the block wouldn't significantly disaggregate over such a distance.

σ (MPa)	λ (MPa)	μ (MPa)	K (MPa)	V_P (m/s)	V_W (m/s)	Z_r	Z_w	Z	v_i (m/s)	h (m)
6	12000	12000	2200	3650	1500	9.8630	1.4667	0.6384	7.0	2.5
7	12000	12000	2200	3650	1500	9.8630	1.4667	0.6384	8.2	3.5
8	12000	12000	2200	3650	1500	9.8630	1.4667	0.6384	9.4	4.5
9	12000	12000	2200	3650	1500	9.8630	1.4667	0.6384	10.6	5.7
10	12000	12000	2200	3650	1500	9.8630	1.4667	0.6384	11.7	7.0
11	12000	12000	2200	3650	1500	9.8630	1.4667	0.6384	12.9	8.5
12	12000	12000	2200	3650	1500	9.8630	1.4667	0.6384	14.1	10.1
6	12000	12000	2200	5100	1500	7.0588	1.4667	0.6072	7.4	2.8
7	12000	12000	2200	5100	1500	7.0588	1.4667	0.6072	8.6	3.8
8	12000	12000	2200	5100	1500	7.0588	1.4667	0.6072	9.9	5.0
9	12000	12000	2200	5100	1500	7.0588	1.4667	0.6072	11.1	6.3
10	12000	12000	2200	5100	1500	7.0588	1.4667	0.6072	12.4	7.8
11	12000	12000	2200	5100	1500	7.0588	1.4667	0.6072	13.6	9.4
12	12000	12000	2200	5100	1500	7.0588	1.4667	0.6072	14.8	11.2

Table 3.4.3.1. *Values of parameters (left side of table) required to calculate the impact velocity and fall height of the Clachtoll megablock (right side of table).*

3.5. Limitations, problems and possible models for detachment and emplacement of the Clachtoll Megablock

The difficulty with modelling such an ancient event is that so many parameters are unknown. The mathematics involved in modelling or predicting the complex movements of a block in motion are also beyond the scope of this study. As mentioned in section 3.4, this movement has had to be significantly simplified. These simplifications include assuming simple vertical freefall, a mechanically isotropic block with a cuboid shape, and the flat impact of the basal surface of the block. To overcome the assumption that the block is mechanically isotropic, the tensile strength values obtained from samples that were oriented in the apparatus with their foliation vertical, were used. The calculations give the minimum height from which the block had to fall to overcome the tensile strength of the gneiss. It is therefore reasonable to simplify the impact to one involving the flat impact of the base of the block because this also represents the least possible impact force generated. If the tensile strength of the gneiss can be overcome in this scenario, then a scenario in which the block impacts in any other orientation will definitely overcome the tensile strength of the gneiss, as an impact of to same volume of rock involving a smaller contact surface area would produce even higher impact forces.

There are still several problems that solutions must be found for, however:

- Extensional and compressional features at the back and front of the block respectively.
- Dominant trend of sediment filled fractures being perpendicular to the orientation of the foliation.
- The misorientation of the foliation in the Clachtoll Megablock with respect to the surrounding gneiss.

In section 3.1. and 3.3, downslope sliding of a block was discussed as a mechanism for inducing extensional features in the back of the block, and compressional features in the front. This is the simplest explanation for such features. The orientation of the Clachtoll Megablock with its long axis oriented NNE-SSW and extensional features (WNW-ESE trending tensile fractures) observed in the north side and compressional features in the south side, indicates an emplacement direction from the NNE towards the SSW. To explain these

features in the simplest way possible, any final model for the emplacement of the Clachtoll Megablock should contain an element of downslope sliding in a south-south-westerly direction.

The orientation of many of the sediment filled fractures lying perpendicular to foliation is more of a conundrum. Fluid overpressure creates a (supra)hydrostatic stress state, i.e. $\sigma_1 = \sigma_1 = \sigma_3$. In a homogeneous and mechanically isotropic material with fluid injection from below, this produces vertical fractures with randomly oriented strikes, as in figure 3.5.1a. Note that figure 3.5.1. shows a stress state where $\sigma_1 > \sigma_1 = \sigma_3$, rather than a truly hydrostatic stress state, but this is because the figure is drawn to show a vertical σ_1 resulting from vertical compression upon impact of a block with a horizontal surface. In a mechanically isotropic material, fractures with a preferred orientation would suggest a deviatoric stress state, i.e. $\sigma_1 > \sigma_1 > \sigma_3$. In a mechanically anisotropic material, such as a gneiss with pervasive foliation, it may be expected that such a fracture pattern would develop even in a hydrostatic stress state, because the foliation forms parallel planes of weakness. The foliation essentially has the effect of locally setting up a deviatoric stress state, as seen in figure 3.5.1b. Despite the mechanical anisotropy imposed by the foliation, much of the Clachtoll Megablock does display the randomly oriented fractures indicative of a hydrostatic stress state. There are particular regions, however – notably locality 38 at the back of the block – where a definite preferred orientation is observed which is perpendicular to the foliation. The simplest way to reconcile this is to infer a deviatoric state of stress within the back of the block. In the context of a landslide, such a state could result from the tractional processes occurring within downslope sliding (fig. 3.5.1c). Given that an element of sliding has already been inferred to account for the presence of extensional and compressional features within the Clachtoll Megablock, it follows that this process could also account for the orientation of fractures within the back of the block.

Another problem to be resolved is the misorientation of the foliation in the Clachtoll Megablock. Simple toppling or sliding alone, from either the NNE or ESE does not result in a subvertical megablock foliation trending NNE-SSW (Fig. 3.5.2). Emplacement directions from the NNE or ESE are chosen because this is where the basement gneiss is found relative to the block. To account for this 90 degree misoriented foliation, an element of rotation during the emplacement history of the block must be invoked. Rotation may have occurred

during sliding or falling. Initial thoughts were that the sliding of tabular block on a slope would cause rotation of the block about an axis perpendicular to the slope, such that the long axis of the block becomes aligned parallel with the gradient of the slope (Fig. 3.5.3). This was quickly tested in a very simple experiment by dropping a tabular MDF block onto a plywood slope. All slope

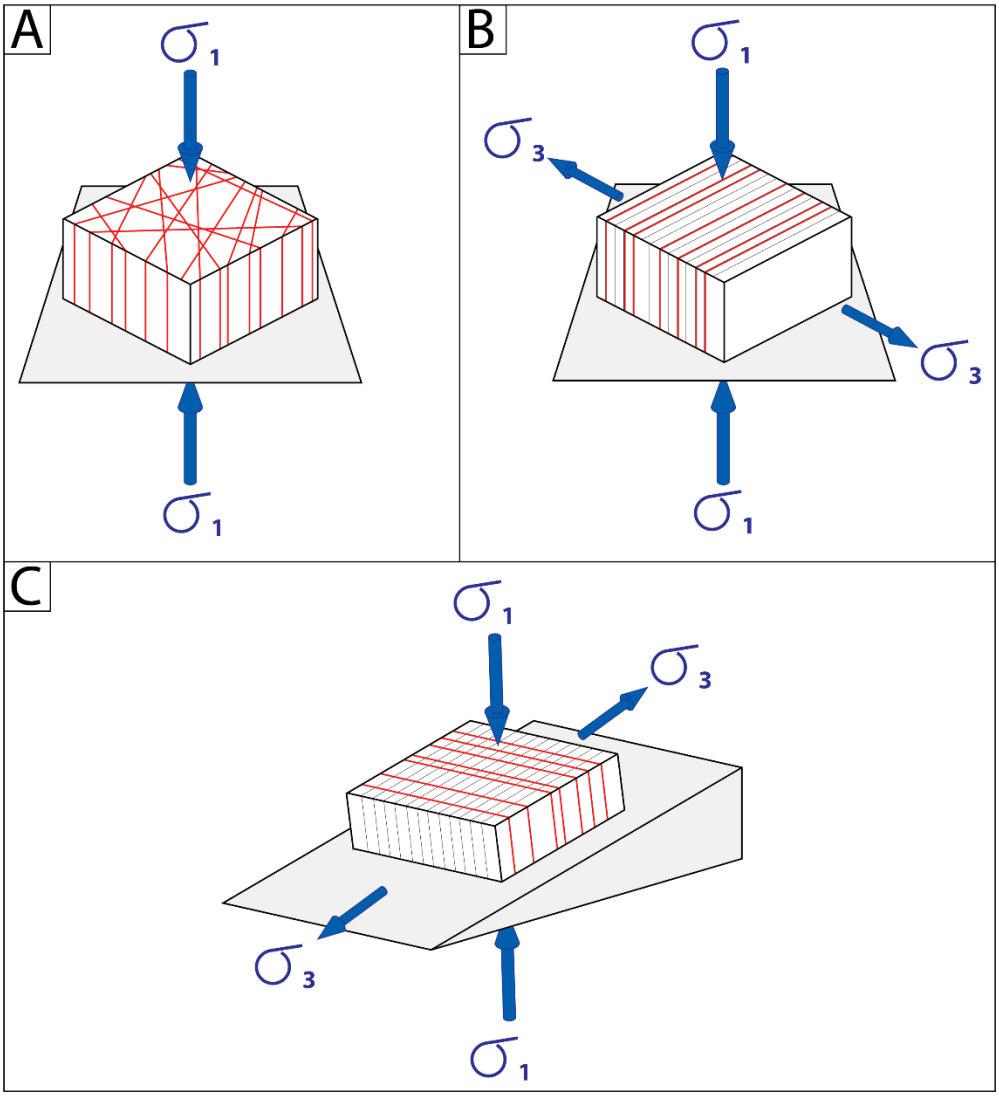

Figure 3.5.1. *(A) Vertical fractures with randomly oriented strikes resulting from tensile extension in all horizontal directions due to vertical compression. (B) Foliation acts to impose a preferred orientation of σ_3, resulting in alignment of fractures with foliation. (C) Downslope sliding as a mechanism for inducing a deviatoric stress state in which σ_3 runs parallel to foliation rather than being perpendicular.*

angles sufficient to overcome the frictional forces between the block and the slope and induce sliding, also resulted in rotation of the block. This mini experiment is by no means

robust, nor does it come close to accurately simulate the many parameters involved in the sliding of a large gneiss block. The rotational mechanics of a block sliding down a slope are well beyond the scope of this study, but the experiment does however, go to show that the idea is at least plausible. Given that the final model of emplacement is already expected to involve an element of downslope sliding; it is consistent that rotation of the block may also result from this type of motion.

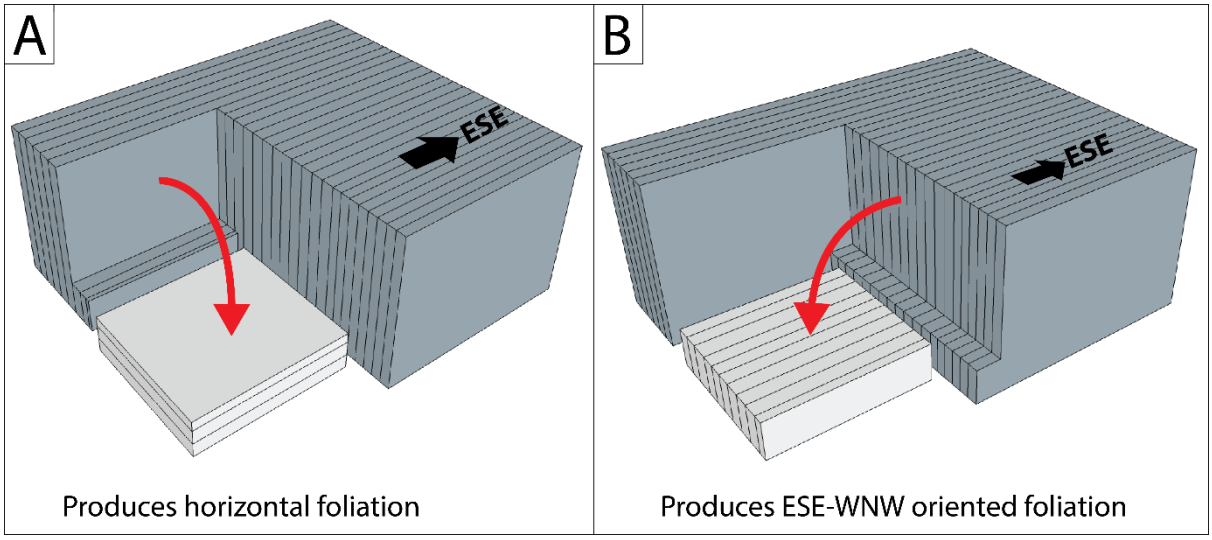

Figure 3.5.2. *Toppling from the NNE would produce a sub-horizontally oriented foliation in the Clachtoll Megablock, as shown in (A). Toppling from the ESE gives sub-vertical ESE-WNW oriented foliation – the same as the surrounding basement – as seen in (B). Not shown here, simple sliding from either direction would produce a sub-vertical, ESE-WNW oriented foliation.*

Assuming that block emplacement included sliding, there is also the question of whether the Clachtoll Megablock toppled before it slid, or whether simple detachment along a basal rupture surface and subsequent sliding (as in the first image of Fig. 3.1.2.) could explain all of the observed features. Both scenarios have their merits and problems. The advantage of a model that first involves toppling is that a larger area of the basal surface of the block could have instantaneously impacted the surface below, explaining the widespread nature of the injected fractural fills across all of the lower portion of the block. It could also be proposed (albeit very speculatively) that toppling may account for the greater degree of fragmentation observed on the west side of the Clachtoll Megablock – a crush zone about a pivot axis has been identified as a characteristic feature of toppling blocks. A remaining problem when it

comes to the toppling model, however, is the unknown degree to which the block might completely disaggregate before even impacting the surface below.

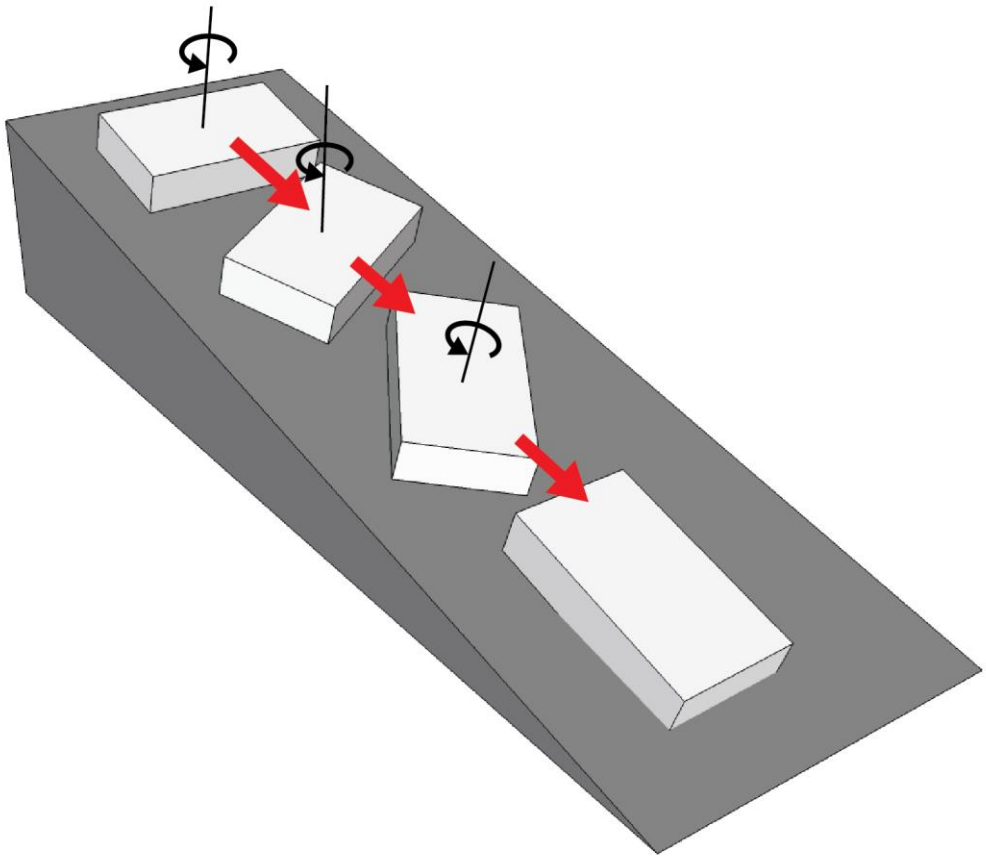

Figure 3.5.3. *Preliminary idea whereby a block sliding down a slope undergoes rotation so that its long axis is aligned parallel with the gradient of the slope.*

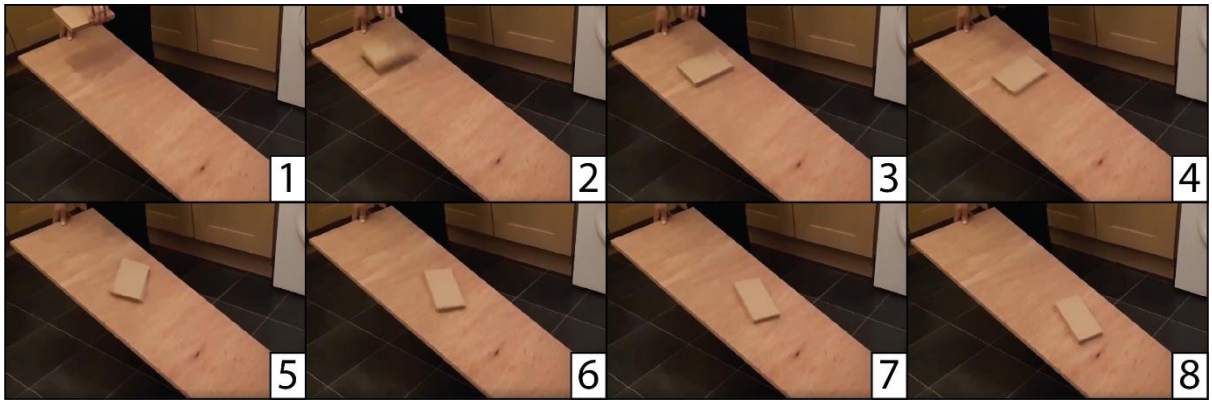

Figure 3.5.4. *Example of a very simple experiment involving dropping a tabular block (MDF) onto a slope (plywood). The block undergoes rotation about an axis perpendicular to the slope as it slides, until its long axis is parallel to the slope.*

It should also be noted that it is not known if there was other material involved in the landslide event that travelled further and has since been completely buried by the sedimentary units of the Stoer Group, if not also downfaulted away from the present level of the Clachtoll Megablock. The depth of the Stoer Group sediments into which the block was emplaced is also unknown.

Ultimately, there are simply too many unknown parameters to conclude a specific or detailed emplacement history.

3.6. Possible causes of rockfall

The likelihood of a rock fall occurring is determined by a complex relationship between geology, geomorphology, weathering and trigger mechanisms. Dorren (2003) notes that the slope morphology of and surrounding the potential falling rocks, is the most important factor in determining whether a rock could fall. Weathering is also significant. It may cause additional fracturing, as in the case of freeze-thaw, or generally widen and weaken pre-existing fractures and joints (Dorren 2003). Joints preferentially control the occurrence of rock falls and topples in less weathered rocks, whilst in heavily weathered terranes, failure is controlled by the interactions between constituent clasts (Calcaterra & Parise 2010). Highland and Bobrowsky (2008) define three groups of landslide causes: geological, morphological and human (Table 3.6.1.). Given the Proterozoic age of the event at Clachtoll, human causes can immediately be dismissed.

Highland and Bobrowsky (2008) then go on to state that the three main causes of landslides are water, volcanic activity and seismic activity. Here, these three causes are discussed in the context of the geology and environment at Clachtoll ca. 1.2 Ga.

With regards to water, Highland and Bobrowsky (2008) cite slope saturation by water as the primary cause of landslides. Given the semi-arid palaeo-environment of the Stoer Group inferred by Stewart (1990), van de Kamp and Leake (1997) and Young (1999), saturation by water is less important than the weathering processes facilitated by water. Also of note is the significant diurnal temperature change frequently observed today in arid environments with

a latitude equivalent to that of Clachtoll during Stoer Group deposition. Infiltration of water into pre-existing fractures in the gneiss may have resulted in freeze-thaw weathering if night-time temperatures dropped sufficiently. As previously discussed in section 3.2.2. Schumm & Chorley (1964) identified freeze-thaw as one of the primary mechanisms causing tilting and then toppling of a block in the arid environment of New Mexico. Salt weathering, where high evaporation rates facilitate the precipitation and growth of salt within cracks, is also an important process in arid environments (Cooke 1981).

Geological causes	Morphological causes	Human causes
Weak or sensitive materials. Weathered materials. Sheared, jointed, or fissured materials. Adversely oriented discontinuities. Contrasts in material permeability and/or stiffness.	Tectonic or volcanic uplift. Glacial rebound. Fluvial, wave, or glacial erosion of slope toe or lateral margins. Subterranean erosion. Deposition loading slope or its crest. Vegetation removal (drought, fire). Thawing Freeze-and-thaw weathering. Shrink-and-swell weathering.	Excavation of slope or its toe. Loading of slope or its crest. Drawdown (of reservoirs). Deforestation. Irrigation. Mining. Artificial vibration. Water leakage from utilities.

Table 3.6.1. *Causes of landslides, produced by Highland and Bobrowsky* (2008).

When discussing volcanic activity, Highland and Bobrowsky (2008) refer to the melting of ice as a mechanism for causing lahars, but the eruption itself also frequently triggers or is triggered by, the collapse of the volcanic edifice; the most famous example being Mount St. Helen's in 1980 (Dzurisin 2018). Landslides are also induced by tremors resulting from the subsurface movement of magma or emplacement of lava domes (e.g. Calder, Luckett, Sparks, *et al.* 2002). For a volcanic trigger mechanism causing rock fall to be inferred at Clachtoll, there must be evidence of volcanism occurring in the vicinity at this time. Stewart (1990) noted that the Clachtoll formation has an anomalous geochemistry, given its derivation from the local gneiss, that can be accounted for if it contains a "now petrographically indistinguishable tuffaceous component". Kinnaird et al. (2007) however, state that with the exception of the Stac Fada Member in the Stoer Group, no volcaniclastic detritus, or evidence for rift related volcanism is found anywhere within the Torridonian. Even the Stac Fada Member, first described as a volcanic unit by Lawson (1973) is now

thought by many to be the ejecta deposit of a bolide impact (Amor, Hesselbo, Porcelli, *et al.* 2008; Parnell, Mark, Fallick, *et al.* 2011; Simms 2015; Reddy, Johnson, Fischer, *et al.* 2015). Should Stewart (Stewart 1990) be correct in assuming a tuffaceous component to the Stoer Group, he does state that this would be very fine grained, thus implying distance from the inferred volcano. Given that rockfalls triggered by volcanoes tend to occur on the flanks of the volcanoes themselves, a volcanic trigger for the rockfall at Clachtoll seems highly unlikely.

The causative relationship between seismic activity and rock falls is well known (Keefer 1984; Vidrih, Ribičič & Suhadolc 2001; Havenith, Torgoev, Braun, *et al.* 2016). Keefer (1984) noted a positive correlation between earthquake magnitude and landslide volume. They also observed that the triggering of rock falls and rock slides requires relatively weak shaking, when compared to lateral spreads and flows, or highly disruptive rock avalanches, which require much stronger shaking. Vidrih, Ribičič & Suhadolc (2001) explain that because earthquakes are dynamic processes, comprised of successive oscillations, they can rapidly trigger rock falls that would otherwise require weakening of the rock over a much longer period of time. Early oscillations in the potentially unstable volume of rock overcome the cohesive strength of cracks, and subsequent oscillations allow the volume to "jump" over asperities on this surface of discontinuity. This process may also break off asperities, smoothing the sliding plane.

Evidence of seismicity in the vicinity of Clachtoll is present in the gneiss in the form of pseudotachylytes (NC 0421 2658), but clearly these significantly predate the deposition of the Stoer Group. Seismicity during Stoer Group deposition seems likely however, given that sedimentation was occurring in an evolving rift basin (Stewart 1990; van de Kamp & Leake 1997). Pre-lithification extensional faults with displacements up to 30 cm are regularly found in the Clachtoll Formation (Stewart 2002), and palaeocurrent reversals are most easily justified by a rift setting with intermittently active marginal faults (Stewart 1982). At the Bay of Clachtoll, palaeocurrent directions are particularly unusual, and the stratigraphy changes significantly across the bay. Stewart's (2002) favoured explanation for this is that a block to the south of the Bay of Clachtoll was moving upwards during sedimentation. It's possible that this movement could have caused seismicity, which may further be evidenced by slump structures observed here (Stewart 2002).

It should also be pointed out that the Stac Fada impact event occurs several hundred metres higher in the stratigraphy than the Clachtoll Megablock (Stewart 2002), and therefore post-dates its emplacement. Whilst such an impact could certainly (and very conveniently) trigger a variety of landslide phenomena, it cannot have caused the event observed at Clachtoll.

Ultimately, and whilst still speculative, it seems the most likely cause of the rock fall producing the Clachtoll megablock, was seismically induced shaking acting upon an already unstable substrate, where weathering processes had exploited joints, fractures and foliation planes within the rock. Previous earthquakes may have aided this destabilisation process prior to the main failure event.

3.7. Final 3D model/sequence of events

Two possible models of emplacement are presented here in Figs. 3.7.1 and 3.7.2. Each model occurs in a block of Lewisian gneiss that is susceptible to landslide as a result of weakening along joints due to weathering processes and seismic shaking. The landslide event itself is likely triggered by an earthquake.

Figure 3.7.1.

1. The Clachtoll Megablock detaches along a basal discontinuity surface.
2. Downslope sliding directed towards the SSW begins.
3. The block starts to undergo rotation about an axis oriented perpendicular to the slope.
4. Frictional drag on the block allows ~WNW-ESE oriented tensile fractures to open, whilst the block simultaneously impacts the wet sediments of the Stoer Group, overpressuring them and inducing hydrofracturing of the block and the injection of fluidised sediment.
5. Rotation continues to bring the long axis of the block into alignment with the gradient of the slope.
6. The block decelerates and stops in the sediments of the Stoer Group, inducing thrusting and brittle folding of the front of the block.

Figure 3.7.2.

1. The Clachtoll Megablock topples from a position to the ESE of its present position. Crushing of the block about a pivot axis occurs during this process.
2. The block impacts the wet sediments of the Stoer Group, overpressuring them and inducing hydrofracturing of the block and the injection of fluidised sediment. Simultaneously, the block starts to undergo rotation about an axis oriented perpendicular to the slope. This initial impact my account for some of the compressional features observed in the front of the block.
3. Further rotation occurs as the block starts sliding down the slope.
4. Frictional drag on the block allows ~WNW-ESE oriented tensile fractures to open.
5. Rotation continues to bring the long axis of the block into alignment with the gradient of the slope.
6. The block decelerates and stops in the sediments of the Stoer Group, inducing further thrusting and brittle folding of the front of the block.

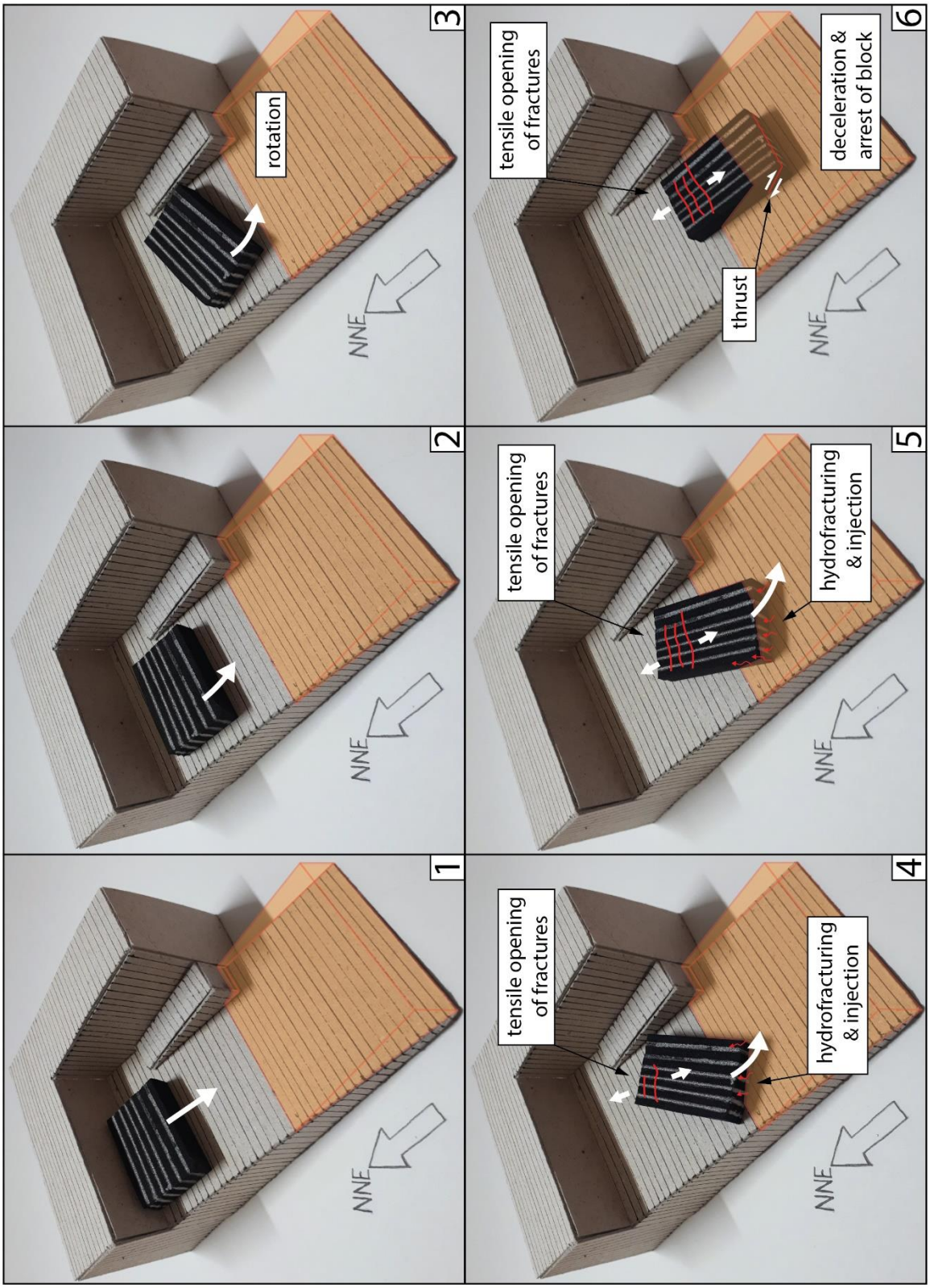

Figure 3.7.1. *Sliding model.*

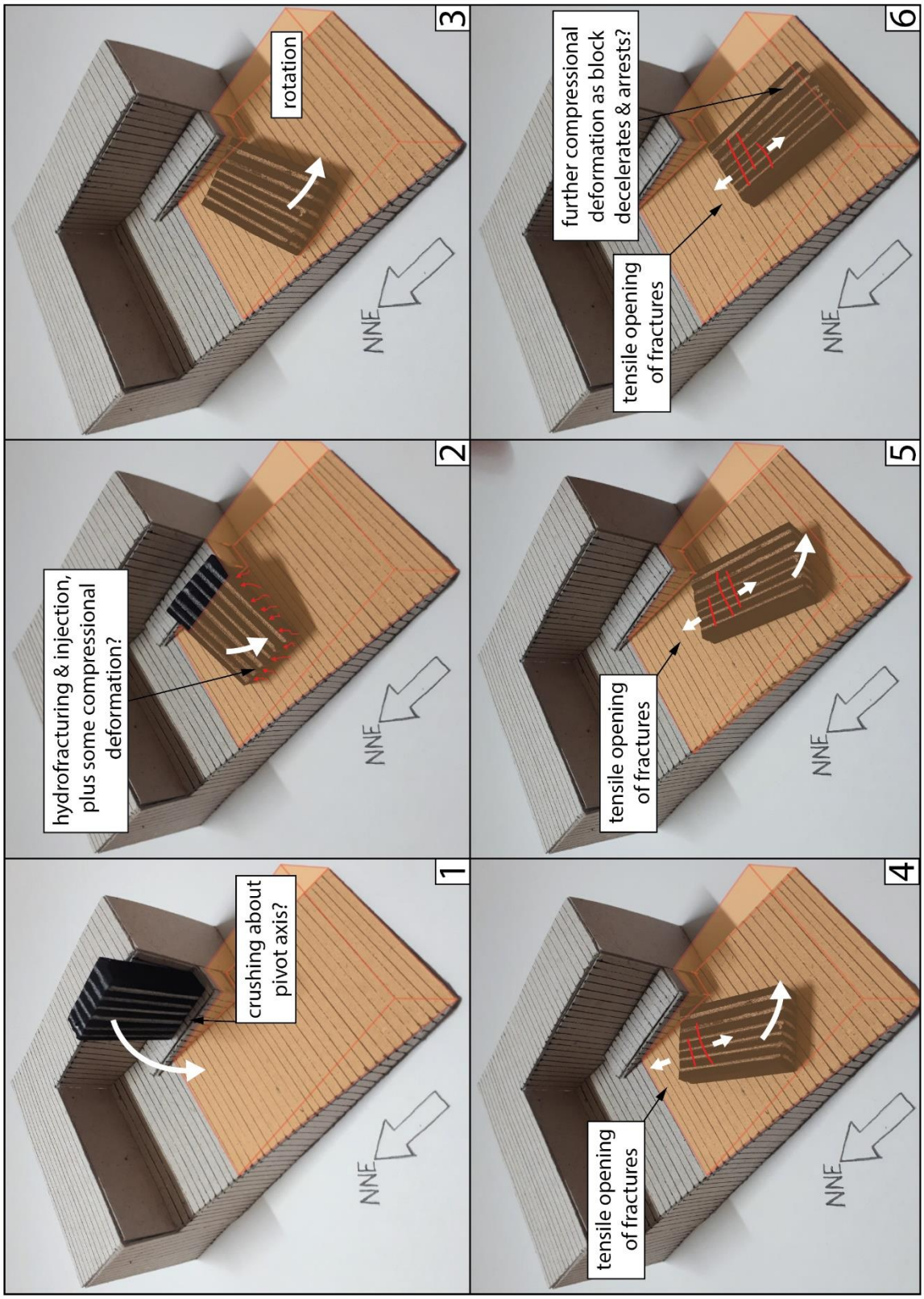

Figure 3.7.2. *Toppling model*

CHAPTER 4
Conclusion

A previously unrecognised, fallen megablock is found on the regional scale nonconformity between the Lewisian gneiss and the Stoer Group at Clachtoll in northwest Scotland. The foliation in the megablock is misoriented by 90 degrees compared to the surrounding basement, and the megablock itself is cut by networks of open, passively infilled fractures and injected, sediment filled fractures.

The kinematics, geometric relationships and distributions of these fractures were studied in the field, and evidence of compressional features at the front of the block were also observed. Other possible causes for the field relationships observed at Clachtoll – including folding, glacial processes and the development of fractures around a localised fault zone – were also considered, but the evidence available favours a catastrophic landslide event rather than any of these processes.

Simple numerical modelling was performed to calculate the minimum height a block of gneiss would have to fall to sufficiently overpressure the underlying unconsolidated sediment to overcome the tensile strength of the gneiss. This height was found to be approximately 6 metres. Given the scale of the Clachtoll Megablock, this seems reasonable to produce the observed features without completely disaggregating the block.

Several models of emplacement were considered in an attempt to reconcile all of the features observed in the block. Features, including WNW-ESE oriented tensile fractures in the back of the block, and a small thrust associated with brittle folding in the front of the block, indicate an incomplete syn-emplacement disaggregation of the Clachtoll Megablock, consistent with gravity-driven transport from the NNE. An emplacement mechanism involving sliding is invoked to explain this. Sliding could also account for the opening of tensile fractures perpendicular to the foliation in the block by setting up a deviatoric stress state. The event also had to involve an element of rotation to explain the misorientation of the foliation in the block compared to the surrounding gneiss.
The most likely cause of the event was an earthquake.

References

Amor, K., Hesselbo, S.P., Porcelli, D., Thackrey, S., et al. (2008) A Precambrian proximal ejecta blanket from Scotland. *Geology*. [Online] 36 (4), 303. Available at: doi:10.1130/G24454A.1.

Anon (2019) Chaco Culture National Historical Park *Wikipedia*. [Online]. Available at: https://en.wikipedia.org/w/index.php?title=Chaco_Culture_National_Historical_Park&oldid=900181446 (Accessed: 8 June 2019).

Attfield, P. (1987) The structural history of the Canisp Shear Zone. *Geological Society, London, Special Publications*. [Online] 27 (1), 165–173. Available at: doi:10.1144/GSL.SP.1987.027.01.14.

Barber, A.J., Beach, A., Park, R.G., Tarney, J., et al. (1978) *The Lewisian and Torridonian rocks of north-west Scotland.* Geologists' Association Guide.

Beacom, L.E., Anderson, T.B. and Holdsworth, R.E. (1999) Using basement-hosted clastic dykes as syn-rifting palaeostress indicators: an example from the basal Stoer Group, northwest Scotland. *Geological Magazine*. [Online] 136 (3), 301–310. Available at: doi:10.1017/S0016756899002605.

Benn, D.I. and Evans, D.J.A. (2013) *Glaciers & glaciation*. 2. ed. London, Routledge.

BGS (n.d.) *What is a landslide? | Landslides at BGS | Shallow geohazards & risks | Engineering geology | Our research | British Geological Survey (BGS)*. [Online]. Available at: https://www.bgs.ac.uk/landslides/how_does_bgs_classify_landslides.html (Accessed: 3 June 2019).

Bieniawski, Z.T. and Hawkes, I. (1978) Suggested methods for determining tensile strength of rock materials. *Int. J. Rock Mech. Min. Sci. & Geomech. Abstr.* 15 (3), 99–103.

Boulton, G.S. (1978) Boulder shapes and grain-size distributions of debris as indicators of transport paths through a glacier and till genesis. *Sedimentology*. [Online] 25 (6), 773–799. Available at: doi:10.1111/j.1365-3091.1978.tb00329.x.

Branney, M. and Acocella, V. (2015) Calderas. In: Haraldur Sigurdsson Dr, Bruce Houghton, Steve McNutt, Hazel Rymer, et al. (eds.). *The Encyclopedia of Volcanoes*. 2 edition. Amsterdam ; Boston, Academic Press. pp. 299–320.

Calcaterra, D. and Parise, M. (2010) Weathering as a predisposing factor to slope movements: an introduction. *Geological Society, London, Engineering Geology Special Publications*. [Online] 23 (1), 1–4. Available at: doi:10.1144/EGSP23.1.

Calder, E.S., Luckett, R., Sparks, R.S.J. and Voight, B. (2002) Mechanisms of lava dome instability and generation of rockfalls and pyroclastic flows at Soufrière Hills Volcano, Montserrat. *Geological Society, London, Memoirs*. [Online] 21 (1), 173–190. Available at: doi:10.1144/GSL.MEM.2002.021.01.08.

Christensen, N.I. (1965) Compressional wave velocities in metamorphic rocks at pressures to 10 kilobars. *Journal of Geophysical Research (1896-1977)*. [Online] 70 (24), 6147–6164. Available at: doi:10.1029/JZ070i024p06147.

Clayton, A., Stead, D., Kinakin, D. and Wolter, A. (2017) Engineering geomorphological interpretation of the Mitchell Creek Landslide, British Columbia, Canada. *Landslides*. [Online] 14 (5), 1655–1675. Available at: doi:10.1007/s10346-017-0811-1.

Cooke, R.U. (1981) Salt weathering in deserts. *Proceedings of the Geologists' Association*. [Online] 92 (1), 1–16. Available at: doi:10.1016/S0016-7878(81)80015-6.

Cruden, D.M. and Varnes, D.J. (1996) Landslide Types and Processes. In: *Special report 247: Landslides: Investigation and Mitigation*. Transportation Research Board, Washington D.C. p.

Davison, S. and Hambrey, M.J. (1996) Indications of glaciation at the base of the Proterozoic Stoer Group (Torridonian), NW Scotland. *Journal of the Geological Society*. [Online] 153 (1), 139–149. Available at: doi:10.1144/gsjgs.153.1.0139.

Diller, J.S. (1889) Sandstone Dykes. *Bulletin of the Geological Society of America*. 1411–442.

Dorren, L.K.A. (2003) A review of rockfall mechanics and modelling approaches. *Progress in Physical Geography: Earth and Environment*. [Online] 27 (1), 69–87. Available at: doi:10.1191/0309133303pp359ra.

Dott, R.H. (1966) Cohesion and flow phenomena in clastic intrusions. *AAPG Bulletin*. 50 (3), 610–611.

Dulin, S., Elmore, R.D., Engel, M.H., Parnell, J., et al. (2005) Palaeomagnetic dating of clastic dykes in Proterozoic basement, NW Scotland: evidence for syndepositional faulting during deposition of the Torridonian. *Scottish Journal of Geology*. [Online] 41 (2), 149–157. Available at: doi:10.1144/sjg41020149.

Dzurisin, D. (2018) Mount St. Helens Retrospective: Lessons Learned Since 1980 and Remaining Challenges. *Frontiers in Earth Science*. [Online] 6. Available at: doi:10.3389/feart.2018.00142 (Accessed: 4 June 2019).

Editions Le Nouvelliste (2015) *Evolène: un pan du Rocher du Mel de la Niva s'est détaché* [Online]. Available at: https://www.youtube.com/watch?v=mSLVhNl4YxY (Accessed: 3 June 2019).

Engineering ToolBox (2004) *Bulk Modulus and Fluid Elasticity*. [Online]. 2004. Available at: https://www.engineeringtoolbox.com/bulk-modulus-elasticity-d_585.html (Accessed: 8 June 2019).

euronews (in English) (2014) *Caught on tape: Huge rocks collapse, fall on highway in China* [Online]. Available at: https://www.youtube.com/watch?v=qcrRf8wY8YE (Accessed: 9 June 2019).

Friese, N., Vollbrecht, A., Leiss, B. and Jacke, O. (2011) Cambrian sedimentary dykes in the Proterozoic basement of the Västervik area (southeast Sweden): episodic formation

inferred from macro- and microfabrics. *International Journal of Earth Sciences*. [Online] 100 (4), 741–752. Available at: doi:10.1007/s00531-009-0508-3.

Gent, H., Abe, S., Urai, J. and Holland, M. (2010) The formation of open fractures in cohesive materials, results of scaled analogue and numerical modelling on fault zone porosity development. *http://dx.doi.org/10.1051/epjconf/20100622016*. [Online] 6. Available at: doi:10.1051/epjconf/20100622016.

Giacomini, A., Buzzi, O., Renard, B. and Giani, G.P. (2009) Experimental studies on fragmentation of rock falls on impact with rock surfaces. *International Journal of Rock Mechanics and Mining Sciences*. [Online] 46 (4), 708–715. Available at: doi:10.1016/j.ijrmms.2008.09.007.

Hall, J. and Al-Haddad, F.M. (1976) Seismic velocities in the Lewisian metamorphic complex, northwest Britain—'in situ' measurements. *Scottish Journal of Geology*. [Online] 12 (4), 305–314. Available at: doi:10.1144/sjg12040305.

Hardman, K. (2019) Cracking Canisp: Deep void evolution during ancient earthquakes *Geoscientist*. 29 (1) pp.10–15.

Harms, J.C. (1965) Sandstone Dikes in Relation to Laramide Faults and Stress Distribution in the Southern Front Range, Colorado. *GSA Bulletin*. [Online] 76 (9), 981–1002. Available at: doi:10.1130/0016-7606(1965)76[981:SDIRTL]2.0.CO;2.

Havenith, H.-B., Torgoev, A., Braun, A., Schlögel, R., et al. (2016) A new classification of earthquake-induced landslide event sizes based on seismotectonic, topographic, climatic and geologic factors. *Geoenvironmental Disasters*. [Online] 3 (1). Available at: doi:10.1186/s40677-016-0041-1 (Accessed: 4 June 2019).

Highland, L.M. and Bobrowsky, P. (2008) *The Landslide Handbook - A Guide to Understanding Landslides*. Reston, Virginia, U.S. Geological Survey Circular 1325.

Holland, M., van Gent, H., Bazalgette, L., Yassir, N., et al. (2011) Evolution of dilatant fracture networks in a normal fault — Evidence from 4D model experiments. *Earth and Planetary Science Letters*. [Online] 304 (3–4), 399–406. Available at: doi:10.1016/j.epsl.2011.02.017.

Hungr, O., Leroueil, S. and Picarelli, L. (2014) The Varnes classification of landslide types, an update. *Landslides*. [Online] 11 (2), 167–194. Available at: doi:10.1007/s10346-013-0436-y.

Hurst, A., Scott, A. and Vigorito, M. (2011) Physical characteristics of sand injectites. *Earth-Science Reviews*. [Online] 106 (3), 215–246. Available at: doi:10.1016/j.earscirev.2011.02.004.

Ji, S., Sun, S., Wang, Q. and Marcotte, D. (2010) Lamé parameters of common rocks in the Earth's crust and upper mantle. *Journal of Geophysical Research: Solid Earth*. [Online] 115 (B6). Available at: doi:10.1029/2009JB007134 (Accessed: 7 June 2019).

Johnson, H.D. and Baldwin, C.T. (2002) Shallow clastic seas. In: H. G. Reading (ed.). *Sedimentary environments: processes, facies, and stratigraphy*. 3rd ed. Oxford ; Cambridge, Mass, Blackwell Science. pp. 232–280.

Jolly, R.J.H. and Lonergan, L. (2002) Mechanisms and controls on the formation of sand intrusions. *Journal of the Geological Society*. [Online] 159 (5), 605–617. Available at: doi:10.1144/0016-764902-025.

Jonk, R., Kelly, J. and Parnell, J. (2004) The origin and tectonic significance of Lewisian- and Torridonian-hosted clastic dykes near Gairloch, NW Scotland. *Scottish Journal of Geology*. [Online] 40 (2), 123–130. Available at: doi:10.1144/sjg40020123.

van de Kamp, P.C. and Leake, B.E. (1997) Mineralogy, geochemistry, provenance and sodium metasomatism of Torridonian rift basin clastic rocks, NW Scotland. *Scottish Journal of Geology*. [Online] 33 (2), 105–124. Available at: doi:10.1144/sjg33020105.

Keefer, D.K. (1984) Landslides caused by earthquakes. *Geological Society of America Bulletin*. 95 (4), 406–421.

Kinnaird, T.C., Prave, A.R., Kirkland, C.L., Horstwood, M., et al. (2007) The late Mesoproterozoic–early Neoproterozoic tectonostratigraphic evolution of NW Scotland: the Torridonian revisited. *Journal of the Geological Society*. [Online] 164 (3), 541–551. Available at: doi:10.1144/0016-76492005-096.

Lawson, D.E. (1973) Torridonian volcanic sediments. *Scottish Journal of Geology*. [Online] 8 (4), 345–362. Available at: doi:10.1144/sjg08040345.

Le Heron, D.P. and Etienne, J.L. (2005) A complex subglacial clastic dyke swarm, Sólheimajökull, southern Iceland. *Sedimentary Geology*. [Online] 181 (1), 25–37. Available at: doi:10.1016/j.sedgeo.2005.06.012.

Levander, A., Hobbs, R.W., Smith, S.K., England, R.W., et al. (1994) The crust as a heterogeneous "optical" medium, or "crocodiles in the mist". *Tectonophysics*. [Online] 232 (1), 281–297. Available at: doi:10.1016/0040-1951(94)90090-6.

Montenat, C., Barrier, P. and d'Estevou, P.O. (1991) Some aspects of the recent tectonics in the Strait of Messina, Italy. *Tectonophysics*. [Online] 194 (3), 203–215. Available at: doi:10.1016/0040-1951(91)90261-P.

Montenat, C., Barrier, P., Ott d′Estevou, P. and Hibsch, C. (2007) Seismites: An attempt at critical analysis and classification. *Sedimentary Geology*. [Online] 196 (1), 5–30. Available at: doi:10.1016/j.sedgeo.2006.08.004.

Montenat, C., Ott d'Estevou, P., Leyrit, H. and Barrier, P. (2000) *The 'Brèche Rouge of Carboneras'. An example of Late Miocene volcanic megabreccia deposited in a deep-marine basin controlled by wrench tectonics (Eastern*. In: pp. 193–215.

Parnell, J., Mark, D., Fallick, A.E., Boyce, A., et al. (2011) The age of the Mesoproterozoic Stoer Group sedimentary and impact deposits, NW Scotland. *Journal of the Geological Society*. [Online] 168 (2), 349–358. Available at: doi:10.1144/0016-76492010-099.

Peach, B.N., Horne, J., Gunn, W., Clough, C.T., et al. (1907) *The geological structure of the north-west Highlands of Scotland*. Memoirs of the Geological Survey of Great Britain.

Peterson, G.L. (1968) Flow structures in sandstone dikes. *Sedimentary Geology*. [Online] 2 (3), 177–190. Available at: doi:10.1016/0037-0738(68)90024-9.

Phillips, C.A. and Alsop, G.I. (2000) Post-tectonic clastic dykes in the Dalradian of Scotland and Ireland: implications for delayed lithification and deformation of sediments. *Geological Journal*. 3599–110.

Pickering, K.T. (1984) The Upper Jurassic 'Boulder Beds' and related deposits: a fault-controlled submarine slope, NE Scotland. *Journal of the Geological Society*. [Online] 141 (2), 357–374. Available at: doi:10.1144/gsjgs.141.2.0357.

Reddy, S.M., Johnson, T.E., Fischer, S., Rickard, W.D.A., et al. (2015) Precambrian reidite discovered in shocked zircon from the Stac Fada impactite, Scotland. *Geology*. [Online] 43 (10), 899–902. Available at: doi:10.1130/G37066.1.

Richter, D. (1966) On the New Red Sandstone Neptunian dykes of the Tor Bay area (Devonshire). *Proceedings of the Geologists' Association*. [Online] 77 (2), 173-IN3. Available at: doi:10.1016/S0016-7878(66)80068-8.

Schumm, S.A. and Chorley, R.J. (1964) The fall of Threatening Rock. *American Journal of Science*. [Online] 262 (9), 1041–1054. Available at: doi:10.2475/ajs.262.9.1041.

Simms, M.J. (2015) The Stac Fada impact ejecta deposit and the Lairg Gravity Low: evidence for a buried Precambrian impact crater in Scotland? *Proceedings of the Geologists' Association*. [Online] 126 (6), 742–761. Available at: doi:10.1016/j.pgeola.2015.08.010.

Stalker, A.M. (1956) *THE ERRATICS TRAIN FOOTHILLS OF ALBERTA: Geological Survey of Canada, Bulletin 37*. Department of Mines & Technical Surveys.

Stewart, A.D. (1997) Discussion on indications of glaciation at the base of the Proterozoic Stoer Group (Torridonian), NW Scotland. *Journal of the Geological Society of London*. 154375–376.

Stewart, A.D. (1990) Geochemistry, provenance and climate of the Upper Proterozoic Stoer Group in Scotland. *Scottish Journal of Geology*. [Online] 26 (2), 89–97. Available at: doi:10.1144/sjg26020089.

Stewart, A.D. (1993) Late Proterozoic and Late Palaeozoic movement on the Coigach fault in NW Scotland. *Scottish Journal of Geology*. [Online] 29 (1), 21–28. Available at: doi:10.1144/sjg29010021.

Stewart, A.D. (1982) Late Proterozoic rifting in NW Scotland: the genesis of the 'Torridonian'. *Journal of the Geological Society*. [Online] 139 (4), 413–420. Available at: doi:10.1144/gsjgs.139.4.0413.

Stewart, A.D. (2002) *The later Proterozoic Torridonian rocks of Scotland: their sedimentology, geochemistry, and origin*. Geological Society memoir no. 24. London, Geological Society.

Stewart, A.D. and Irving, E. (1974) Palaeomagnetism of Precambrian sedimentary rocks from NW Scotland and the apparent polar wandering path of Laurentia. *Geophysical Journal of the Royal Astronomical Society*. 3751–72.

Storyful Rights Management (2017) *Major Rock Fall Occurs Next to a Climber in Chulilla, Spain* [Online]. Available at: https://www.youtube.com/watch?v=fi2dMUT8WAo (Accessed: 9 June 2019).

Strachan, R.A., Holdsworth, R.E. and Prave, A.R. (2012) 4: Proterozoic Sedimentation, Orogenesis and Magmatism on the Laurentian Craton (2500 - 750 Ma). In: *Geological history of Britain and Ireland*. 2nd ed. Chichester, West Sussex ; Hoboken, NJ, Wiley-Blackwell. p.

Strachan, R.A., Storey, C.D. and Prave, A.R. (2012) 3: Early Earth History an Development of the Archaean Crust. In: *Geological history of Britain and Ireland*. 2nd ed. Chichester, West Sussex ; Hoboken, NJ, Wiley-Blackwell. p.

Terzaghi, K. (1950) Mechanism of Landslides. In: Sidney Paige (ed.). *Application of Geology to Engineering Practice*. [Online]. New York, N. Y., Geological Society of America. pp. 83–123. Available at: doi:10.1130/Berkey.1950.83 (Accessed: 3 June 2019).

Troll, V.R., Emeleus, C.H. and Donaldson, C.H. (2000) Caldera formation in the Rum Central Igneous Complex, Scotland. *Bulletin of Volcanology*. [Online] 62 (4), 301–317. Available at: doi:10.1007/s004450000099.

Varnes, D.J. (1978) Slope movement types and processes. In: R. L. Schuster and R. J. Krizek (eds.). *Special report 176: Landslides-Analysis and control*. Transportation Research Board, Washington D.C. pp. 11–33.

Vidrih, R., Ribičič, M. and Suhadolc, P. (2001) Seismogeological effects on rocks during the 12 April 1998 upper Soča Territory earthquake (NW Slovenia). *Tectonophysics*. [Online] 330 (3), 153–175. Available at: doi:10.1016/S0040-1951(00)00219-5.

Walker, R.J., Holdsworth, R.E., Imber, J. and Ellis, D. (2011) The development of cavities and clastic infills along fault-related fractures in Tertiary basalts on the NE Atlantic margin. *Journal of Structural Geology*. [Online] 33 (2), 92–106. Available at: doi:10.1016/j.jsg.2010.12.001.

Waters, D.J. (2003) *Rocks of NW Scotland - Rock Sample Images*. [Online]. May 2003. Available at: https://www.earth.ox.ac.uk/~oesis/nws/nws-a98-st6.html#field (Accessed: 21 May 2019).

Wilson, R., Holdsworth, R.E. and Wightman, R. (2011) A Transect through the Canisp Shear Zone, Achmelvich. In: Kathryn Goodenough, Maarten Krabbendam, and Edinburgh Geological Society (eds.). *A geological excursion guide to the North-West Highlands of Scotland*. Edinburgh, Edinburgh Geological Society. pp. 53–61.

Winslow, M.A. (1983) Clastic dike swarms and the structural evolution of the foreland fold and thrust belt of the southern Andes. *GSA Bulletin*. [Online] 94 (9), 1073–1080. Available at: doi:10.1130/0016-7606(1983)94<1073:CDSATS>2.0.CO;2.

Winterer, E.L., Metzler, C.V. and Sart, M. (1991) Neptunian dykes and associated breccias (Southern Alps, Italy and Switzerland): role of gravity sliding in open and closed systems. *Sedimentology*. [Online] 38 (3), 381–404. Available at: doi:10.1111/j.1365-3091.1991.tb00358.x.

Woodcock, N.H. and Mort, K. (2008) Classification of fault breccias and related fault rocks. *Geological Magazine*. [Online] 145 (3), 435–440. Available at: doi:10.1017/S0016756808004883.

yosemitenationalpark (2010) *Yosemite Nature Notes - 10 - Rock Fall* [Online]. Available at: https://www.youtube.com/watch?time_continue=195&v=H0YhlqP1BgE (Accessed: 9 June 2019).

Young, G.M. (1999) Some aspects of the geochemistry, provenance and palaeoclimatology of the Torridonian of NW Scotland. *Journal of the Geological Society*. [Online] 156 (6), 1097–1111. Available at: doi:10.1144/gsjgs.156.6.1097.

Appendices

Appendix A.

Maps showing fieldwork locality numbers and sample collection locations.

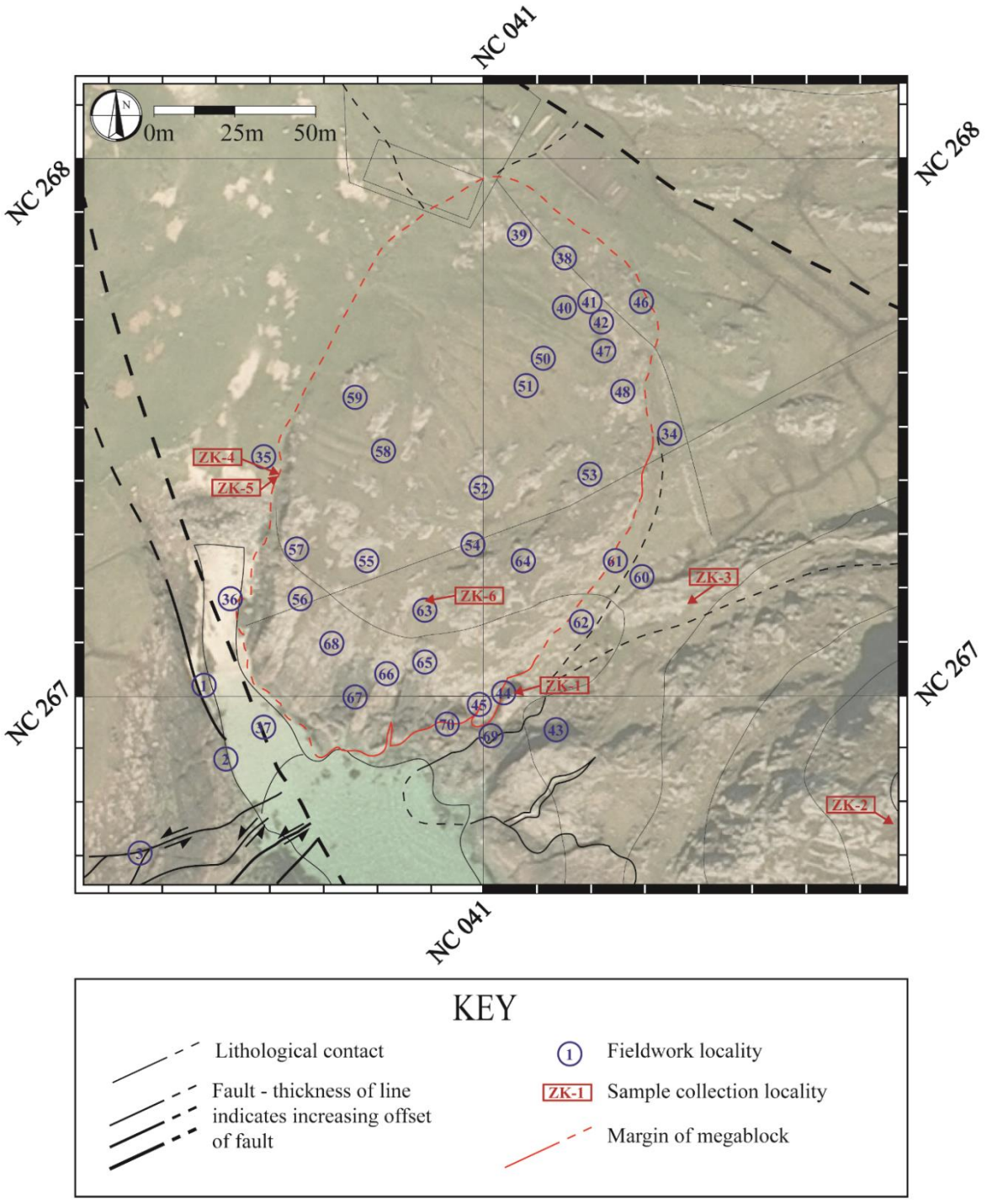

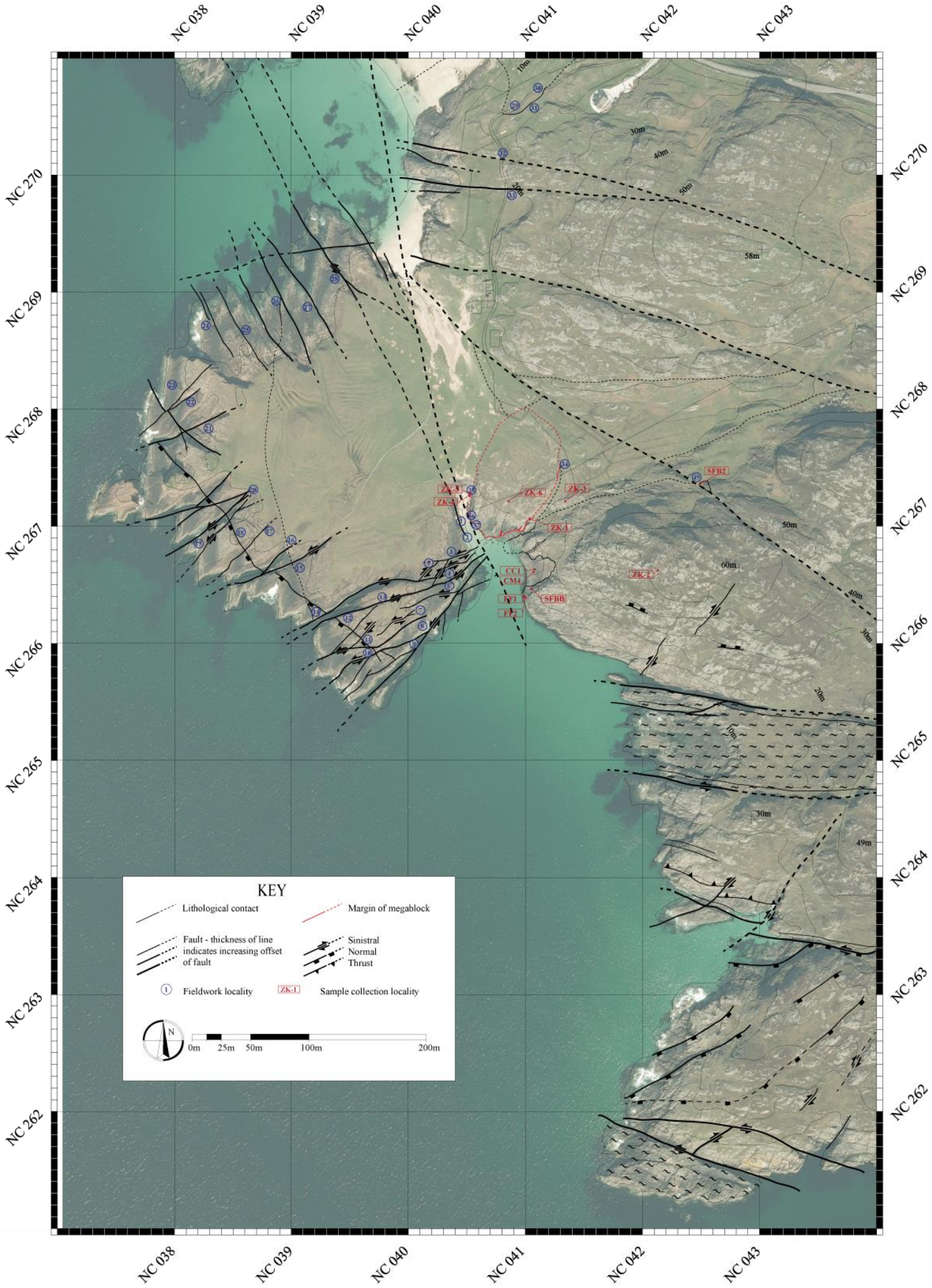
NC 038
NC 039
NC 040
NC 041
NC 042
NC 043
NC 270
NC 269
NC 268
NC 267
NC 266
NC 265
NC 264
NC 263
NC 262
10m
20m
30m
40m
50m
58m
60m
49m
ZK-1
ZK-2
ZK-3
ZK-4
ZK-5
ZK-6
CC1
CM4
FF1
FF2
SFBB
SFB2
KEY
Lithological contact
Margin of megablock
Fault - thickness of line indicates increasing offset of fault
Sinistral
Normal
Thrust
Fieldwork locality
Sample collection locality
N
0m
25m
50m
100m
200m

Appendix B.

Table of quantitative data collected

Locality Code:

SG	Stoer Group
G	Surrounding Gneiss
MC	Mega-clast

Structure Code:

Bed	Bedding
MF	Main Fault
SF	Secondary Fractures
Fol	Foliation
CM	Chatter marks
SFF	Sediment filled fractures (MC)
N-SFF	Non-sediment filled fractures (MC)
SL	Slickenlines
Lam	Laminations in sed. fractures

Locality Code	Locality #	Structure Code	Structure #	Strike	Dip	Dip Direction	Plunge	Azimuth	Pitch	Pitch Direction	Comment
SG	1	Bed	-	171	28	W	-	-	-	-	-
		Bed	-	174	25	W	-	-	-	-	-
		Bed	-	165	26	W	-	-	-	-	-
		Bed	-	176	24	W	-	-	-	-	-
		SF	-	014	70	W	-	-	-	-	-
		SF	-	018	72	W	-	-	-	-	-
		SF	-	026	60	W	-	-	-	-	-
		SF	-	027	58	W	-	-	-	-	-
SG	2	Bed	-	170	22	W	-	-	-	-	-
		Bed	-	165	23	W	-	-	-	-	-
		SF	-	025	69	W	-	-	-	-	-
		SF	-	015	76	W	-	-	-	-	-
		SF	-	028	84	W	-	-	-	-	-
		SF	-	010	80	W	-	-	-	-	-
		SF	-	016	86	W	-	-	-	-	-
SG	3	MF	MF1	093	87	N	-	-	-	-	Sinistral
		MF	MF1	085	78	N	-	-	-	-	Sinistral
		SF	MF1	036	85	NW	-	-	-	-	-
		SF	MF1	052	88	S	-	-	-	-	-
		SF	MF1	073	85	S	-	-	-	-	-
		SF	MF1	027	58	S	-	-	-	-	-
		SF	MF1	040	80	SE	-	-	-	-	-
		MF	MF2	039	78	E	-	-	-	-	Dextral
		SF	MF2	080	80	S	-	-	-	-	-
		SF	MF2	086	82	S	-	-	-	-	-
		SF	MF2	077	85	N	-	-	-	-	-
		MF	MF3	078	86	S	-	-	-	-	Sinistral
		SF	MF3	047	76	SE	-	-	-	-	-

		SF	MF3	035	72	SE	-	-	-	-	-
SG	4	MF	MF4	072	88	S	-	-	-	-	Sinistral
		MF	MF4	078	75	N	-	-	-	-	Sinistral

Locality Code	Locality #	Structure Code	Structure #	Strike	Dip	Dip Direction	Plunge	Azimuth	Pitch	Pitch Direction	Comment
		MF	MF4	074	84	S	-	-	-	-	Sinistral
		MF	MF4	076	88	S	-	-	-	-	Sinistral
		SF	MF4 - P?	082	82	S	-	-	-	-	-
		SF	MF4 - P?	083	90	-	-	-	-	-	-
		SF	MF4 - 2nd	042	80	SE	-	-	-	-	-
		SF	MF4 - 2nd	029	79	SE	-	-	-	-	-
		SF	MF4 - 2nd	032	64	SE	-	-	-	-	-
		SF	MF4 - 2nd	031	72	SE	-	-	-	-	-
		SF	MF4 - 2nd	027	67	SE	-	-	-	-	-
		SF	MF4 - 2nd	032	72	SE	-	-	-	-	-
		Bed	-	176	22	W	-	-	-	-	-
		Bed	-	003	21	W	-	-	-	-	-
		MF	MF5	085	76	S	-	-	-	-	Sinistral
		MF	MF5	076	87	S	-	-	-	-	Sinistral
		SF	MF5	018	59	E	-	-	-	-	-
		SF	MF5	040	80	SE	-	-	-	-	-
		SF	MF5	043	83	SE	-	-	-	-	-
		SF	MF5	033	74	SE	-	-	-	-	-
		Bed	-	006	28	W	-	-	-	-	-
		Bed	-	170	19	W	-	-	-	-	-
SG	5	MF	MF6	050	87	NW	-	-	-	-	Dextral
		SF	MF6	044	81	NW	-	-	-	-	-
		SF	MF6	048	88	NW	-	-	-	-	-
		SF	other	146	64	SW	-	-	-	-	-
		SF	other	147	66	SW	-	-	-	-	-
		SF	other	140	56	SW	-	-	-	-	-
		SF	other	153	62	SW	-	-	-	-	-
SG	6	MF	MF8	148	46	SW	-	-	-	-	Normal
		MF	MF8	155	43	SW	-	-	-	-	Normal
		MF	MF8	158	38	W	-	-	-	-	Normal
		SL	MF8	-	-	-	30	265	-	-	-
		SF	MF8	166	46	W	-	-	-	-	-
		SF	MF8	160	49	W	-	-	-	-	-
		SF	MF8	150	48	W	-	-	-	-	-
		SF	other	078	85	S	-	-	-	-	-
		SF	other	073	80	S	-	-	-	-	-
		SF	other	087	82	S	-	-	-	-	-
		SF	other	087	84	S	-	-	-	-	-

		SF	other	075	90	-	-	-	-	-	-
		SF	other	076	85	S	-	-	-	-	-
		SF	other	077	84	S	-	-	-	-	-
		MF	MF7-A	083	90	-	-	-	-	-	Sinistral

Locality Code	Locality #	Structure Code	Structure #	Strike	Dip	Dip Direction	Plunge	Azimuth	Pitch	Pitch Direction	Comment
		MF	MF7-A	078	83	S	-	-	-	-	Sinistral
		MF	MF7-B	060	85	SE	-	-	-	-	Sinistral
		MF	MF7-B	060	83	SE	-	-	-	-	Sinistral
		MF	MF7-C	040	86	SE	-	-	-	-	Sinistral
		MF	MF7-C	038	83	SE	-	-	-	-	Sinistral
		SF	MF7-SET 1	040	76	SE	-	-	-	-	-
		SF	MF7-SET 1	030	82	SE	-	-	-	-	-
		SF	MF7-SET 1	055	76	SE	-	-	-	-	-
		SF	MF7-SET 1	043	80	SE	-	-	-	-	-
		SF	MF7-SET 1	026	80	SE	-	-	-	-	-
		SF	MF7-SET 1	034	84	SE	-	-	-	-	-
		SF	MF7-SET 1	029	80	SE	-	-	-	-	-
		SF	MF7-SET 2	171	78	E	-	-	-	-	-
		SF	MF7-SET 2	170	81	E	-	-	-	-	-
		SF	MF7-SET 2	172	71	E	-	-	-	-	-
		SF	MF7-SET 2	169	82	E	-	-	-	-	-
		SF	MF7-SET 2	168	78	E	-	-	-	-	-
		SF	MF7-SET 3	105	65	N	-	-	-	-	-
		SF	MF7-SET 3	117	72	N	-	-	-	-	-
		SF	MF7-SET 3	114	69	N	-	-	-	-	-
		SF	MF7-SET 4	074	85	S	-	-	-	-	-
		CM	MF7-A	033	83	SE	-	-	-	-	-
		Bed	-	171	19	W	-	-	-	-	-
		Bed	-	008	24	W	-	-	-	-	-
		Bed	-	001	24	W	-	-	-	-	-
SG	7	SF	-	157	54	W	-	-	-	-	-
		SF	-	148	48	W	-	-	-	-	-
		SF	-	153	42	W	-	-	-	-	-
		SF	-	144	40	W	-	-	-	-	-
		SF	-	140	51	W	-	-	-	-	-
		SF	-	151	47	W	-	-	-	-	-
		Bed	-	018	28	W	-	-	-	-	-
		MF	MF10a	036	80	NW	-	-	-	-	Sinistral
		SF	MF10a	159	72	E	-	-	-	-	-
		SF	MF10a	167	80	E	-	-	-	-	-

		SF	MF10a	168	80	E	-	-	-	-	-
		SF	MF10a	165	60	E	-	-	-	-	-
		SF	MF10a	160	70	E	-	-	-	-	-
		SF	MF10a	165	84	E	-	-	-	-	-
Locality Code	**Locality #**	**Structure Code**	**Structure #**	**Strike**	**Dip**	**Dip Direction**	**Plunge**	**Azimuth**	**Pitch**	**Pitch Direction**	**Comment**
		SF	MF10a	154	65	E	-	-	-	-	-
		MF	MF10b	056	80	NW	-	-	-	-	Sinistral
		MF	MF10b	061	78	E	-	-	-	-	Sinistral
		SF	MF10b	012	70	E	-	-	-	-	-
		SF	MF10b	025	75	E	-	-	-	-	-
		SF	MF10b	016	78	E	-	-	-	-	-
SG	8	SF	MF11-SET 1	172	56	E	-	-	-	-	-
		SF	MF11-SET 1	166	58	E	-	-	-	-	-
		SF	MF11-SET 1	173	57	E	-	-	-	-	-
		SF	MF11-SET 1	174	55	E	-	-	-	-	-
		SF	MF11-SET 1	003	70	E	-	-	-	-	-
		SF	MF11-SET 1	180	56	E	-	-	-	-	-
		SF	MF11-SET 1	007	68	E	-	-	-	-	-
		SF	MF11-SET 1	010	75	E	-	-	-	-	-
		SF	MF11-SET 1	177	60	E	-	-	-	-	-
		SF	MF11-SET 1	175	59	E	-	-	-	-	-
		SF	MF11-SET 2	030	85	SE	-	-	-	-	-
		SF	MF11-SET 2	027	84	SE	-	-	-	-	-
		SF	MF11-SET 2	020	82	SE	-	-	-	-	-
		SF	MF11-SET 2	017	79	SE	-	-	-	-	-
		SF	MF11-SET 2	019	80	SE	-	-	-	-	-
		SF	MF11-SET 2	032	80	SE	-	-	-	-	-
		SF	MF11-SET 2	036	82	SE	-	-	-	-	-
SG	9	MF	MF12	073	76	S	-	-	-	-	Sinistral
		MF	MF12	076	80	N	-	-	-	-	Sinistral
		SF	MF12-R'	028	82	SE	-	-	-	-	-
		SF	MF12-R'	038	72	SE	-	-	-	-	-
		SF	MF12-R'	037	90	-	-	-	-	-	-
		SF	MF12-R'	027	78	SE	-	-	-	-	-
		SF	MF12-P	083	83	S	-	-	-	-	-
		SF	MF12-P	080	89	S	-	-	-	-	-
		SF	MF12-P	075	87	S	-	-	-	-	-
		SF	MF12-P	073	90	-	-	-	-	-	-
SG	10	SF	R'	028	80	SE	-	-	-	-	-

		SF	R'	038	88	NW	-	-	-	-	-
		SF	R'	027	66	SE	-	-	-	-	-
		SF	R'	034	81	SE	-	-	-	-	-
		SF	R'	038	86	SE	-	-	-	-	-

Locality Code	Locality #	Structure Code	Structure #	Strike	Dip	Dip Direction	Plunge	Azimuth	Pitch	Pitch Direction	Comment
SG	11	MF	MF14	079	86	N	-	-	-	-	Sinistral
		SF	MF14	048	87	SE	-	-	-	-	-
		SF	MF14	055	90	-	-	-	-	-	-
		SF	MF14	043	72	SE	-	-	-	-	-
		Bed	-	180	20	W	-	-	-	-	-
		Bed	-	176	22	W	-	-	-	-	-
		MF	MF15	054	80	SE	-	-	-	-	Dextral
		SF	MF15	055	90	-	-	-	-	-	-
		SF	MF15	063	87	NW	-	-	-	-	-
		SF	MF15	066	83	SE	-	-	-	-	-
		SF	MF15	070	90	-	-	-	-	-	-
		SF	MF15	071	83	SE	-	-	-	-	-
		MF	MF16	035	74	SE	-	-	-	-	-
		SL	MF16	-	-	-	-	-	18	SW	-
SG	12	Bed	-	033	23	NW	-	-	-	-	-
SG	13	MF	MF4	070	89	S	-	-	-	-	Sinistral
		MF	MF4	073	88	S	-	-	-	-	Sinistral
		SF	MF4-SET 1	144	54	SW	-	-	-	-	-
		SF	MF4-SET 1	147	54	SW	-	-	-	-	-
		SF	MF4-SET 1	154	55	SW	-	-	-	-	-
		SF	MF4-SET 1	151	56	SW	-	-	-	-	-
		SF	MF4-SET 1	153	53	SW	-	-	-	-	-
		SF	MF4-SET 1	149	57	SW	-	-	-	-	-
		SF	MF4-SET 2	074	90	-	-	-	-	-	-
		SF	MF4-SET 2	073	89	S	-	-	-	-	-
		SF	MF4-SET 2	073	88	N	-	-	-	-	-
		SF	MF4-SET 2	082	86	N	-	-	-	-	-
		SF	MF4-SET 3	075	16	N	-	-	-	-	-
		SF	MF4-SET 3	075	18	N	-	-	-	-	-
		SF	MF4-SET 3	083	19	N	-	-	-	-	-
		SF	MF4-SET 3	077	18	N	-	-	-	-	-
		SF	MF4-SET 4	019	22	W	-	-	-	-	-
		SF	MF4-SET 4	020	20	W	-	-	-	-	-
		SF	MF4-SET 4	018	19	W	-	-	-	-	-

SG	14	Bed	-	170	23	W	-	-	-	-	-
		Bed	-	177	24	W	-	-	-	-	-
		MF	-	142	84	SW	-	-	-	-	Sinistral
		MF	-	097	69	S	-	-	-	-	Sinistral

Locality Code	Locality #	Structure Code	Structure #	Strike	Dip	Dip Direction	Plunge	Azimuth	Pitch	Pitch Direction	Comment
SG	15	MF	MF15(2)	050	67	SE	-	-	-	-	Sinistral
		MF	MF15(2)	072	60	SE	-	-	-	-	Sinistral
		MF	MF15(2)	058	54	SE	-	-	-	-	Sinistral
		SF	MF15(2)-SET 1	162	76	E	-	-	-	-	-
		SF	MF15(2)-SET1	163	72	E	-	-	-	-	-
		SF	MF15(2)-SET 1	159	73	E	-	-	-	-	-
		SF	MF15(2)-SET 1	156	71	E	-	-	-	-	-
		SF	MF15(2)-SET 1	168	83	E	-	-	-	-	-
		SF	MF15(2)-SET 1	160	66	E	-	-	-	-	-
		SF	MF15(2)-SET 2	050	88	SE	-	-	-	-	-
		SF	MF15(2)-SET 2	053	78	SE	-	-	-	-	-
		SF	MF15(2)-SET 2	049	80	SE	-	-	-	-	-
		SF	MF15(2)-SET 2	056	60	SE	-	-	-	-	-
		SF	MF15(2)-SET 3	067	90	-	-	-	-	-	-
		SF	MF15(2)-SET 3	066	68	NW	-	-	-	-	-
		SF	MF15(2)-SET 3	078	64	N	-	-	-	-	-
		SF	MF15(2)-SET 3	063	74	N	-	-	-	-	-
		SF	MF15(2)-SET 3	074	65	N	-	-	-	-	-
		SF	MF15(2)-SET 3	071	79	N	-	-	-	-	-
		MF	int. MF15(2)	057	75	NW	-	-	-	-	Sinistral
		SL	int. MF15(2)	-	-	-	-	-	60	NE	-
SG	16	MF	MF16(2)	037	79	SE	-	-	-	-	Sinistral
SG	17	MF	MF17	053	79	SE	-	-	-	-	-
		MF	MF17	052	88	NW	-	-	-	-	-
		SF	MF17-SET 1	148	86	SW	-	-	-	-	-
		SF	MF17-SET 1	152	82	NE	-	-	-	-	-
		SF	MF17-SET 1	145	82	NE	-	-	-	-	-
		SF	MF17-SET 1	153	85	SW	-	-	-	-	-
		SF	MF17-SET 2	007	86	W	-	-	-	-	-
		SF	MF17-SET 2	179	89	W	-	-	-	-	-
		SF	MF17-SET 2	008	90	-	-	-	-	-	-

		SF	MF17-SET 2	176	88	E	-	-	-	-	-
		Bed	-	009	21	W	-	-	-	-	-
		Bed	-	175	24	W	-	-	-	-	-
		Bed	-	179	25	W	-	-	-	-	-

Locality Code	Locality #	Structure Code	Structure #	Strike	Dip	Dip Direction	Plunge	Azimuth	Pitch	Pitch Direction	Comment
		MF	MF18	160	82	NE	-	-	-	-	Normal
		MF	MF18	137	81	SW	-	-	-	-	Normal
SG	18	MF	MF18	156	80	SW	-	-	-	-	Normal
		MF	MF18	155	78	SW	-	-	-	-	Normal
		MF	MF18	157	83	SW	-	-	-	-	Normal
		MF	MF18	155	86	SW	-	-	-	-	Normal
		SL	MF18	-	-	-	77	254	-	-	-
		SL	MF18	-	-	-	78	244	-	-	-
		SL	MF18	-	-	-	-	-	76	SE	-
		Bed	-	010	21	W	-	-	-	-	-
		Bed	-	007	18	W	-	-	-	-	-
		SF	MF18-SET 2	169	81	E	-	-	-	-	-
		SF	MF18-SET 2	180	79	E	-	-	-	-	-
		SF	MF18-SET 2	003	83	E	-	-	-	-	-
		SF	MF18-SET 2	005	83	E	-	-	-	-	-
		SF	MF18-SET 2	171	78	E	-	-	-	-	-
		SF	MF18-SET 3	056	76	NW	-	-	-	-	-
		SF	MF18-SET 3	049	86	NW	-	-	-	-	-
		SF	MF18-SET 3	040	85	SE	-	-	-	-	-
		SF	MF18-SET 3	055	86	NW	-	-	-	-	-
		SF	MF18-SET 3	039	80	SE	-	-	-	-	-
SG	19	MF	MF19	045	77	SE	-	-	-	-	Sinistral
		SF	MF19-SET 1	032	69	SE	-	-	-	-	-
		SF	MF19-SET 1	046	63	SE	-	-	-	-	-
		SF	MF19-SET 2	005	88	W	-	-	-	-	-
		SF	MF19-SET 2	179	89	W	-	-	-	-	-
SG	20	SF	MF20-SET 1	037	84	SE	-	-	-	-	Sinistral
		SF	MF20-SET 1	048	79	SE	-	-	-	-	-
		SF	MF20-SET 1	041	71	SE	-	-	-	-	-
		SF	MF20-SET 2	174	82	E	-	-	-	-	-
		SF	MF20-SET 2	173	87	E	-	-	-	-	-
		SF	MF20-SET 2	178	90	-	-	-	-	-	-
		SF	MF20-SET 2	171	85	W	-	-	-	-	-

Locality Code	Locality #	Structure Code	Structure #	Strike	Dip	Dip Direction	Plunge	Azimuth	Pitch	Pitch Direction	Comment
SG	21	MF	MF22	080	79	S	-	-	-	-	-
		SF	MF22-SET 1	107	47	N	-	-	-	-	-
		SF	MF22-SET 1	101	43	N	-	-	-	-	-
		SF	MF22-SET 1	102	35	N	-	-	-	-	-
		SF	MF22-SET 1	109	38	N	-	-	-	-	-
		SF	MF22-SET 1	107	48	N	-	-	-	-	-
		SF	MF22-SET 2	084	84	S	-	-	-	-	-
		SF	MF22-SET 2	083	82	S	-	-	-	-	-
		SF	MF22-SET 2	075	82	S	-	-	-	-	-
		SF	MF22-SET 2	080	84	S	-	-	-	-	-
		SF	MF22-SET 2	084	83	S	-	-	-	-	-
		SF	MF22-SET 3	007	79	E	-	-	-	-	-
		SF	MF22-SET 3	026	74	E	-	-	-	-	-
		SF	MF22-SET 3	009	72	E	-	-	-	-	-
		SF	MF22-SET 3	016	71	E	-	-	-	-	-
		Bed	-	017	25	W	-	-	-	-	-
		Bed	-	016	29	W	-	-	-	-	-
SG	22	MF	MF23	055	80	SE	-	-	-	-	-
		SF	MF23-SET 1	039	70	SE	-	-	-	-	-
		SF	MF23-SET 1	035	70	SE	-	-	-	-	-
		SF	MF23-SET 2	119	72	N	-	-	-	-	-
		SF	MF23-SET 2	115	75	N	-	-	-	-	-
		Bed	A	038	48	NW	-	-	-	-	-
		Bed	A	035	43	NW	-	-	-	-	-
		Bed	B	005	30	W	-	-	-	-	-
		Bed	B	020	31	W	-	-	-	-	-
		Bed	C	008	22	W	-	-	-	-	-
		Bed	C	015	27	W	-	-	-	-	-
SG	23	MF	MF24	146	84	SW	-	-	-	-	-
		Bed	-	013	22	W	-	-	-	-	-
SG	24	Bed	-	010	24	W	-	-	-	-	-
		SF	SET 1	153	70	NE	-	-	-	-	-
		SF	SET 1	144	68	NE	-	-	-	-	-
		SF	SET 1	158	75	NE	-	-	-	-	-
		SF	SET 1	158	66	NE	-	-	-	-	-
		SF	SET 2	042	82	SE	-	-	-	-	-
		SF	SET 2	040	80	SE	-	-	-	-	-
		SF	SET 2	050	82	SE	-	-	-	-	-

		SF	SET 2	036	76	SE	-	-	-	-	-
		SF	SET 3	085	73	S	-	-	-	-	-
		SF	SET 3	073	82	S	-	-	-	-	-

Locality Code	Locality #	Structure Code	Structure #	Strike	Dip	Dip Direction	Plunge	Azimuth	Pitch	Pitch Direction	Comment
		SF	SET 3	070	74	S	-	-	-	-	-
		SF	SET 3	080	74	S	-	-	-	-	-
SG	25	MF	MF25	154	83	NW	-	-	-	-	-
		SF	MF25-SET 1	040	75	SE	-	-	-	-	-
		SF	MF25-SET 1	043	80	SE	-	-	-	-	-
		SF	MF25-SET 1	034	65	SE	-	-	-	-	-
		SF	MF25-SET 1	037	68	SE	-	-	-	-	-
		SF	MF25-SET 2	080	85	S	-	-	-	-	-
		SF	MF25-SET 2	088	88	S	-	-	-	-	-
		SF	MF25-SET 2	093	83	S	-	-	-	-	-
		SF	MF25-SET 3	179	84	W	-	-	-	-	-
		SF	MF25-SET 3	001	78	W	-	-	-	-	-
		SF	MF25-SET 3	003	77	W	-	-	-	-	-
		MF	MF26	140	76	NE	-	-	-	-	-
SG	26	MF	MF27	165	90	-	-	-	-	-	-
		SF	MF27-SET 1	044	58	SE	-	-	-	-	-
		SF	MF27-SET 1	036	76	SE	-	-	-	-	-
		SF	MF27-SET 1	032	79	SE	-	-	-	-	-
		SF	MF27-SET 1	043	64	SE	-	-	-	-	-
		SF	MF27-SET 1	040	71	SE	-	-	-	-	-
		SF	MF27-SET 2	087	75	S	-	-	-	-	-
		SF	MF27-SET 2	083	74	S	-	-	-	-	-
		SF	MF27-SET 2	091	80	S	-	-	-	-	-
		SF	MF27-SET 2	084	70	S	-	-	-	-	-
		SF	MF27-SET 2	090	70	S	-	-	-	-	-
		SF	MF27-SET 3	140	74	NE	-	-	-	-	-
		SF	MF27-SET 3	145	78	NE	-	-	-	-	-
		SF	MF27-SET 3	144	79	NE	-	-	-	-	-
		SF	MF27-SET 3	140	88	NE	-	-	-	-	-
		SF	MF27-SET 3	144	88	SW	-	-	-	-	-
SG	27	MF	MF28	150	78	NE	-	-	-	-	-
		SF	MF28-SET 1	050	70	SE	-	-	-	-	-

		SF	MF28-SET 1	036	70	SE	-	-	-	-	-
		SF	MF28-SET 1	048	64	SE	-	-	-	-	-
Locality Code	**Locality #**	**Structure Code**	**Structure #**	**Strike**	**Dip**	**Dip Direction**	**Plunge**	**Azimuth**	**Pitch**	**Pitch Direction**	**Comment**
		SF	MF28-SET 1	044	60	SE	-	-	-	-	-
		SF	MF28-SET 2	093	75	S	-	-	-	-	-
		SF	MF28-SET 2	083	76	S	-	-	-	-	-
		SF	MF28-SET 2	089	74	S	-	-	-	-	-
		SF	MF28-SET 2	087	76	S	-	-	-	-	-
		SF	MF28-SET 3	153	86	NE	-	-	-	-	-
		SF	MF28-SET 3	147	85	NE	-	-	-	-	-
SG	28	MF	MF29	140	80	NE	-	-	-	-	Sinistral
		MF	MF29	146	77	NE	-	-	-	-	Sinistral
		SF	MF29-SET R'	074	76	S	-	-	-	-	-
		SF	MF29-SET R'	064	72	S	-	-	-	-	-
		SF	MF29-SET R'	076	78	S	-	-	-	-	-
		SF	MF29-SET R'	062	72	S	-	-	-	-	-
		SF	MF29-SET R'	084	80	S	-	-	-	-	-
		SF	MF29-SET R'	081	78	S	-	-	-	-	-
		SF	MF29-SET R	118	69	N	-	-	-	-	-
		SF	MF29-SET R	118	68	N	-	-	-	-	-
		SF	MF29-SET R	127	70	N	-	-	-	-	-
		SF	MF29-SET R	125	69	N	-	-	-	-	-
		Bed	-	021	27	W	-	-	-	-	-
		MF	MF30	088	78	S	-	-	-	-	-
SG	29	Bed	-	027	18	W	-	-	-	-	-
G	30	Fol	-	107	70	S	-	-	-	-	-
G	31	Fol	-	086	75	S	-	-	-	-	-
		Fol	-	100	80	S	-	-	-	-	-
		Fol	-	103	74	S	-	-	-	-	-
		Fol	-	098	72	S	-	-	-	-	-
		Fol	-	101	73	S	-	-	-	-	-
G	32	Fol	-	104	73	S	-	-	-	-	-
G	33	MF	MF31 int.	097	54	S	-	-	-	-	-
		MF	MF31 int.	134	80	NE	-	-	-	-	-
		SL	MF31	-	-	-	-	-	52	NW	-
		SF	MF31	057	12	NW	-	-	-	-	-
		SF	MF31	050	18	NW	-	-	-	-	-

		Fol	-	091	45	S	-	-	-	-	-
		Fol	-	102	59	S	-	-	-	-	-
		Fol	-	90	50	S	-	-	-	-	-

Locality Code	Locality #	Structure Code	Structure #	Strike	Dip	Dip Direction	Plunge	Azimuth	Pitch	Pitch Direction	Comment
		Fol	-	83	52	S	-	-	-	-	-
		Fol	-	102	45	S	-	-	-	-	-
		Fol	-	103	48	S	-	-	-	-	-
MC	34	Fol	-	032	75	NW	-	-	-	-	-
		Fol	-	088	46	N	-	-	-	-	-
		Fol	-	016	76	E	-	-	-	-	-
		Fol	-	080	60	N	-	-	-	-	-
		Fol	-	075	82	N	-	-	-	-	-
		Fol	-	149	78	NE	-	-	-	-	-
		Fol	-	023	76	W	-	-	-	-	-
		Fol	-	002	78	W	-	-	-	-	-
		Fol	-	010	75	W	-	-	-	-	-
		Fol	-	146	69	E	-	-	-	-	-
		Fol	-	167	66	E	-	-	-	-	-
MC	35	SFF	-	156	87	NE	-	-	-	-	3.5cm
		SFF	-	140	89	NE	-	-	-	-	0.7cm
		SFF	-	130	49	NE	-	-	-	-	0.3cm
		SFF	-	102	82	S	-	-	-	-	0.5cm
		SFF	-	024	72	NW	-	-	-	-	3.0cm
		SFF	-	051	87	SE	-	-	-	-	1.0cm
		SFF	-	160	72	E	-	-	-	-	4.5cm
		SFF	-	045	68	SE	-	-	-	-	1.5cm
		SFF	-	046	68	SE	-	-	-	-	0.2cm
		SFF	-	067	83	S	-	-	-	-	4.5cm
		SFF	-	105	80	S	-	-	-	-	0.5cm
		SFF	-	010	31	E	-	-	-	-	1.0cm
		SFF	-	136	83	NE	-	-	-	-	0.8cm
		SFF	-	126	52	NE	-	-	-	-	0.7cm
		SFF	-	065	62	SE	-	-	-	-	0.3cm
		SFF	-	033	48	SE	-	-	-	-	0.8cm
		SFF	-	095	38	S	-	-	-	-	18.0cm
		SFF	-	085	82	S	-	-	-	-	6.0cm
		SFF	-	130	83	NE	-	-	-	-	0.5cm
		SFF	-	136	66	NE	-	-	-	-	0.5cm
		SFF	-	122	70	NE	-	-	-	-	-
		SFF	-	027	26	SE	-	-	-	-	-
		SFF	-	138	82	NE	-	-	-	-	9.0cm
		SFF	-	111	47	S	-	-	-	-	2.0cm
		SFF	-	033	85	SE	-	-	-	-	>25.0cm
		SFF	-	121	84	NE	-	-	-	-	0.8cm

		SFF	-	067	60	SE	-	-	-	-	1.0cm
		SFF	-	091	50	E	-	-	-	-	0.5cm
		SFF	-	015	36	E	-	-	-	-	2.5cm

Locality Code	Locality #	Structure Code	Structure #	Strike	Dip	Dip Direction	Plunge	Azimuth	Pitch	Pitch Direction	Comment
		SFF	-	026	46	SE	-	-	-	-	3.0cm
		SFF	-	109	76	N	-	-	-	-	2.5cm
		SFF	-	123	67	SW	-	-	-	-	0.5cm
		SFF	-	097	89	N	-	-	-	-	-
		SFF	-	140	70	NE	-	-	-	-	3.0cm
		SFF	-	129	47	NE	-	-	-	-	2.0cm
		SFF	-	035	58	SE	-	-	-	-	1.5cm
		SFF	-	073	44	S	-	-	-	-	0.5cm
		SFF	-	116	69	NE	-	-	-	-	1.5cm
		SFF	-	113	51	SW	-	-	-	-	-
		SFF	-	122	53	SW	-	-	-	-	-
		SFF	-	068	86	S	-	-	-	-	6.0cm
		SFF	-	143	67	NE	-	-	-	-	3.5cm
		SFF	-	060	53	SE	-	-	-	-	15.0cm
		SFF	-	124	81	SW	-	-	-	-	2.0cm
		SFF	-	105	64	SW	-	-	-	-	3.5cm
		SFF	-	55	74	SE	-	-	-	-	1.5cm
		SFF	-	106	72	S	-	-	-	-	1.0cm
		SFF	-	014	71	W	-	-	-	-	4.0cm
		Fol	-	040	59	NW	-	-	-	-	-
		Fol	-	031	57	NW	-	-	-	-	-
		Lam	-	124	22	SW	-	-	-	-	-
		Lam	-	084	20	S	-	-	-	-	-
		SF	SET 1	100	60	S	-	-	-	-	-
		SF	SET 1	089	62	S	-	-	-	-	-
		SF	SET 1	082	64	S	-	-	-	-	-
		SF	SET 1	090	59	S	-	-	-	-	-
		SF	SET 1	073	60	S	-	-	-	-	-
		SF	SET 2	087	60	N	-	-	-	-	-
		SF	SET 2	068	40	N	-	-	-	-	-
		SF	SET 2	072	42	N	-	-	-	-	-
		SF	SET 2	065	43	N	-	-	-	-	-
		SF	SET 2	066	42	N	-	-	-	-	-
MC	36	SF	SET 1	087	40	N	-	-	-	-	-
		SF	SET 1	095	60	N	-	-	-	-	-
		SFF	SET 1	091	52	N	-	-	-	-	3.0cm
		SF	SET 1	079	42	N	-	-	-	-	-
		SFF	SET 2	087	56	S	-	-	-	-	10.0cm
		SFF	SET 2	083	50	S	-	-	-	-	40.0cm
		SF	SET 2	045	40	SE	-	-	-	-	-
		SFF	-	064	22	NW	-	-	-	-	2.0cm

		SFF	-	030	62	SE	-	-	-	-	2.0cm
MC	37	SFF	-	155	35	NE	-	-	-	-	4.0cm
Locality Code	**Locality #**	**Structure Code**	**Structure #**	**Strike**	**Dip**	**Dip Direction**	**Plunge**	**Azimuth**	**Pitch**	**Pitch Direction**	**Comment**
		SFF	-	135	58	SW	-	-	-	-	12.0cm
		SFF	-	134	55	SW	-	-	-	-	16.0cm
		Fol	-	027	74	NW	-	-	-	-	-
		Fol	-	033	70	NW	-	-	-	-	-
MC	38	SFF	-	170	75	W	-	-	-	-	0.5cm
		SFF	-	135	82	SW	-	-	-	-	3.0cm
		SFF	-	134	85	SW	-	-	-	-	2.0cm
		SFF	-	033	77	SE	-	-	-	-	-
		SFF	-	133	82	NE	-	-	-	-	-
		SFF	-	129	74	SW	-	-	-	-	1.0cm
		SFF	-	133	89	NE	-	-	-	-	3.6cm
		SFF	-	021	77	W	-	-	-	-	1.0cm
		SFF	-	026	70	W	-	-	-	-	2.0cm
		SFF	-	134	77	NE	-	-	-	-	0.8cm
		SFF	-	140	72	NE	-	-	-	-	3.0cm
		SFF	-	147	68	NE	-	-	-	-	2.2cm
		SFF	-	126	83	NE	-	-	-	-	4.0cm
		SFF	-	086	72	N	-	-	-	-	2.8cm
		SFF	-	123	89	NE	-	-	-	-	1.2cm
		SFF	-	125	87	NE	-	-	-	-	4.6cm
		SFF	-	137	90	-	-	-	-	-	2.0cm
		SFF	-	133	85	SW	-	-	-	-	3.2cm
		Fol	-	033	81	NW	-	-	-	-	-
		Fol	-	022	76	NW	-	-	-	-	-
		Fol	-	018	70	NW	-	-	-	-	-
		Fol	-	024	72	NW	-	-	-	-	-
		Fol	-	016	80	W	-	-	-	-	-
MC	39	SFF	-	092	57	N	-	-	-	-	1cm
		SFF	-	098	48	N	-	-	-	-	-
		SFF	-	100	70	N	-	-	-	-	-
		SFF	-	075	58	N	-	-	-	-	-
		SFF	-	80	48	N	-	-	-	-	-
		SFF	-	125	84	NE	-	-	-	-	-
		SFF	-	130	70	SW	-	-	-	-	-
		SFF	-	090	85	S	-	-	-	-	1.0cm
		SFF	-	094	84	S	-	-	-	-	1.5cm
		SFF	-	137	70	SW	-	-	-	-	2.0cm
		SFF	-	126	83	NE	-	-	-	-	3.5cm
		SFF	-	091	79	S	-	-	-	-	0.8cm
		SFF	-	146	81	NE	-	-	-	-	2.0cm
		SFF	-	071	72	W	-	-	-	-	14.0cm

		SFF	-	012	40	W	-	-	-	-	16.0cm
		SFF	-	110	60	N	-	-	-	-	13.0cm
Locality Code	**Locality #**	**Structure Code**	**Structure #**	**Strike**	**Dip**	**Dip Direction**	**Plunge**	**Azimuth**	**Pitch**	**Pitch Direction**	**Comment**
		SFF	-	120	84	SW	-	-	-	-	12.0cm
		SFF	-	030	79	NW	-	-	-	-	0.3cm
		Lam	-	080	65	N	-	-	-	-	-
		Lam	-	084	50	N	-	-	-	-	-
		Lam	-	045	28	NW	-	-	-	-	-
		Lam	-	160	25	W	-	-	-	-	-
		Lam	-	010	29	W	-	-	-	-	-
		Lam	-	172	26	W	-	-	-	-	-
		Lam	-	110	35	N	-	-	-	-	-
		Fol	-	008	76	E	-	-	-	-	-
		Fol	-	038	77	NW	-	-	-	-	-
		Fol	-	000	75	W	-	-	-	-	-
		Fol	-	043	89	NW	-	-	-	-	-
MC	40	SFF	-	107	82	S	-	-	-	-	2.0cm
		SFF	-	106	74	S	-	-	-	-	3.0cm
		SFF	-	135	78	SW	-	-	-	-	1.0cm
		SFF	-	024	77	SE	-	-	-	-	2.0cm
MC	41	SFF	-	117	80	N	-	-	-	-	<1.0cm
		SFF	-	060	74	NW	-	-	-	-	<1.0cm
		SFF	SET 1	114	82	SSW	-	-	-	-	<1.0cm
		SFF	SET 1	100	80	SSW	-	-	-	-	<1.0cm
		SFF	SET 1	090	85	N	-	-	-	-	<1.0cm
		SFF	SET 1	101	80	N	-	-	-	-	<1.0cm
		SFF	SET 2	056	28	SE	-	-	-	-	<1.0cm
		SFF	SET 2	054	30	SE	-	-	-	-	<1.0cm
		SFF	SET 2	050	36	SE	-	-	-	-	<1.0cm
		Fol	-	020	80	W	-	-	-	-	-
		Fol	-	007	83	W	-	-	-	-	-
MC	42	SFF	-	130	80	SW	-	-	-	-	2.0cm
		SFF	-	147	90	-	-	-	-	-	2.0cm
		SFF	-	065	74	S	-	-	-	-	4.0cm
		SFF	-	070	80	S	-	-	-	-	26.0cm
		SFF	-	104	75	S	-	-	-	-	5.0cm
		Lam	-	086	35	N	-	-	-	-	-
MC	43	Planar surface	-	040	78	NW	-	-	-	-	-
		SL	Planar surface	-	-	-	-	-	38	SW	-
	NOT IN SITU!!	SFF	-	116	72	N	-	-	-	-	-
		SFF	-	033	68	SE	-	-	-	-	-
		SFF	-	020	62	SE	-	-	-	-	-
		MF	-	028	20	NW	-	-	-	-	-

		Fol	-	168	40	W	-	-	-	-	-
MC	44	SFF	-	063	21	NW	-	-	-	-	1.0cm
Locality Code	**Locality #**	**Structure Code**	**Structure #**	**Strike**	**Dip**	**Dip Direction**	**Plunge**	**Azimuth**	**Pitch**	**Pitch Direction**	**Comment**
		SFF	-	059	26	NW	-	-	-	-	0.5cm
		SFF	-	099	27	NW	-	-	-	-	0.7cm
		SFF	-	108	31	N	-	-	-	-	0.8cm
		SFF	-	063	80	SE	-	-	-	-	-
		Lam	-	045	17	NW	-	-	-	-	-
		Fol	-	025	79	SE	-	-	-	-	-
		Fol	-	178	76	E	-	-	-	-	-
		Fol	-	018	31	N	-	-	-	-	-
		SL	-	-	-	-	20	218	-	-	-
MC	45	SFF	-	049	74	SE	-	-	-	-	-
		SFF	-	130	74	SW	-	-	-	-	-
		SFF	-	052	80	NW	-	-	-	-	-
		SFF	-	003	87	E	-	-	-	-	-
		Fol	-	179	72	W	-	-	-	-	-
		Lam	-	093	28	N	-	-	-	-	-
MC	46	SFF	-	017	85	W	-	-	-	-	-
		SFF	-	084	83	N	-	-	-	-	-
		Fol	-	016	72	W	-	-	-	-	-
		Fol	-	018	83	W	-	-	-	-	-
MC	47	SFF	-	050	82	NW	-	-	-	-	15-20cm
		SFF	-	083	82	N	-	-	-	-	15-20cm
		SFF	-	084	76	N	-	-	-	-	15-20cm
		SFF	-	111	75	N	-	-	-	-	15-20cm
		SFF	-	167	71	W	-	-	-	-	15-20cm
		Fol	-	017	70	E	-	-	-	-	-
		Fol	-	179	58	W	-	-	-	-	-
		Lam	-	046	20	NW	-	-	-	-	-
MC	48	SFF	-	105	87	S	-	-	-	-	-
		SFF	-	144	89	SW	-	-	-	-	-
		SFF	-	080	56	N	-	-	-	-	-
		SFF	-	140	77	NE	-	-	-	-	-
		SFF	-	060	85	SE	-	-	-	-	-
		SFF	-	050	83	NE	-	-	-	-	-
		SFF	-	160	76	W	-	-	-	-	-
		SFF	-	092	42	N	-	-	-	-	-
		SFF	-	115	63	SW	-	-	-	-	-
		SFF	-	075	63	N	-	-	-	-	-
		SFF	-	084	71	N	-	-	-	-	-
		SFF	-	109	60	S	-	-	-	-	-

		SFF	-	137	70	S	-	-	-	-	-
		Fol	-	137	83	NE	-	-	-	-	-
		Fol	-	163	80	W	-	-	-	-	-

Locality Code	Locality #	Structure Code	Structure #	Strike	Dip	Dip Direction	Plunge	Azimuth	Pitch	Pitch Direction	Comment
		Fol	-	145	78	W	-	-	-	-	-
		Fol	-	001	75	W	-	-	-	-	-
		Fol	-	050	82	SE	-	-	-	-	-
		Fol	-	064	83	SE	-	-	-	-	-
		Fol	-	017	82	E	-	-	-	-	-
		Fol	-	002	78	W	-	-	-	-	-
		Fol	-	170	73	W	-	-	-	-	-
		Fol	-	148	72	SW	-	-	-	-	-
		Fol	-	102	65	NE	-	-	-	-	-
		Fol	-	026	75	W	-	-	-	-	-
G	49	Fol	-	113	76	S	-	-	-	-	-
		Fol	-	115	82	S	-	-	-	-	-
		Fol	-	119	88	S	-	-	-	-	-
MC	50	Fol	-	046	89	SE	-	-	-	-	-
		SFF	-	157	90	-	-	-	-	-	0.5-10.0cm ?
		SFF	-	130	45	SW	-	-	-	-	0.5-10.0cm ?
		SFF	-	150	52	SW	-	-	-	-	0.5-10.0cm ?
		SFF	-	042	80	NW	-	-	-	-	0.5-10.0cm ?
		SFF	-	103	40	N	-	-	-	-	0.5-10.0cm ?
MC	51	Fol	-	004	28	W	-	-	-	-	-
		SFF	-	120	62	NE	-	-	-	-	1.0cm
		SFF	-	158	88	SW	-	-	-	-	1.0cm
MC	52	Fol	-	047	78	NW	-	-	-	-	-
		Fol	-	032	78	NE	-	-	-	-	-
		Fol	-	100	57	N	-	-	-	-	-
		Fol	-	030	65	NW	-	-	-	-	-
		SFF	-	028	55	NW	-	-	-	-	6.0cm
		SFF	-	122	82	NE	-	-	-	-	-
		SFF	-	055	40	SE	-	-	-	-	-
		SFF	-	116	78	SW	-	-	-	-	-
		SFF	-	035	79	NW	-	-	-	-	-
		SFF	-	057	90		-	-	-	-	-
		SFF	-	130	88	SW	-	-	-	-	-
		SFF	-	125	70	SW	-	-	-	-	8.0cm
		Lam	-	028	26	NW	-	-	-	-	-

		Lam	-	025	24	NW	-	-	-	-	-
		Lam	-	093	78	N	-	-	-	-	-
MC	53	Lam	-	004	28	W	-	-	-	-	-
Locality Code	**Locality #**	**Structure Code**	**Structure #**	**Strike**	**Dip**	**Dip Direction**	**Plunge**	**Azimuth**	**Pitch**	**Pitch Direction**	**Comment**
MC	54	SFF	-	083	62	S	-	-	-	-	-
		SFF	-	147	80	NE	-	-	-	-	-
		Fol	-	016	90	-	-	-	-	-	-
MC	55	Fol	-	024	73	NW	-	-	-	-	-
		SFF	-	131	74	NE	-	-	-	-	-
		SFF	-	140	72	NE	-	-	-	-	-
		Lam	-	064	24	NW	-	-	-	-	-
MC	56	Fol	-	006	75	W	-	-	-	-	-
		SFF	-	129	88	NW	-	-	-	-	3.0cm
		SFF	-	175	68	W	-	-	-	-	3.0cm
MC	57	No structural data					-	-	-	-	-
MC	58	Fol	-	019	70	W	-	-	-	-	-
		SFF	-	099	67	S	-	-	-	-	-
		SFF	-	067	45	SE	-	-	-	-	-
MC	59	Fol	-	013	60	W	-	-	-	-	-
		SFF	-	034	82	SE	-	-	-	-	-
		SFF	-	039	80	SE	-	-	-	-	-
MC	60	Fol	-	111	75	N	-	-	-	-	-
		Fol	-	170	55	E	-	-	-	-	-
		Fol	-	177	74	E	-	-	-	-	-
		Fol	-	139	58	NE	-	-	-	-	-
		Fol	-	142	34	NE	-	-	-	-	-
		SFF	-	176	80	E	-	-	-	-	4.0cm
		SFF	-	145	34	NE	-	-	-	-	0.6cm
MC	61	Fol	-	036	53	NW	-	-	-	-	-
		Fol	-	018	56	NW	-	-	-	-	-
		SFF	-	165	42	W	-	-	-	-	6.0cm
		SFF	-	100	85	N	-	-	-	-	-
		SFF	-	167	63	E	-	-	-	-	-
		SFF	-	010	40	E	-	-	-	-	-
		Lam	-	170	22	W	-	-	-	-	-
MC	62	Fol	-	012	65	W	-	-	-	-	-
		Fol	-	013	68	W	-	-	-	-	-
		SFF	-	101	73	N	-	-	-	-	-
		SFF	-	105	83	N	-	-	-	-	-
		SFF	-	120	78	S	-	-	-	-	-
		SFF	-	018	84	E	-	-	-	-	-

Locality Code	Locality #	Structure Code	Structure #	Strike	Dip	Dip Direction	Plunge	Azimuth	Pitch	Pitch Direction	Comment
MC	63	Fol	-	006	90	-	-	-	-	-	-
		SFF	-	025	52	NW	-	-	-	-	3.0-5.0cm
		Lam	-	020	38	NW	-	-	-	-	-
MC	64	SFF	-	025	40	E	-	-	-	-	-
		SFF	-	149	82	NE	-	-	-	-	-
		SFF	-	150	71	SW	-	-	-	-	-
MC	65	Fol	-	018	82	W	-	-	-	-	-
MC	66	SFF	-	143	78	NE	-	-	-	-	-
		SFF	-	020	80	W	-	-	-	-	-
		SFF	-	134	60	NE	-	-	-	-	-
		SFF	-	133	62	NE	-	-	-	-	-
		Fol	-	024	70	W	-	-	-	-	-
MC	67	Fol	-	177	73	W	-	-	-	-	-
		Fol	-	173	78	W	-	-	-	-	-
		N-SFF	-	108	76	S	-	-	-	-	-
		N-SFF	-	130	77	S	-	-	-	-	-
		N-SFF	-	127	68	S	-	-	-	-	-
		N-SFF	-	121	65	S	-	-	-	-	-
MC	68	SFF	-	157	88	SW	-	-	-	-	4.0cm
		SFF	-	156	70	SW	-	-	-	-	3.0cm
		SFF	-	027	63	W	-	-	-	-	1.0cm
		Lam	-	140	24	SW	-	-	-	-	-
MC	69	SFF	-	040	02	NW	-	-	-	-	0.8cm
		SFF	-	125	72	SW	-	-	-	-	2.0cm
MC	70	SFF	-	053	10	NW	-	-	-	-	1.0cm
		SFF	-	015	10	E	-	-	-	-	2.0cm
		SFF	-	005	16	E	-	-	-	-	1.0cm
		Fol	-	017	63	W	-	-	-	-	-
		Fol	-	020	60	W	-	-	-	-	-
		MF	THRUST	024	25	NW	-	-	-	-	-
G	SE conglom.	Fol	-	104	80	S	-	-	-	-	-
		Fol	-	100	85	S	-	-	-	-	-
		Fol	-	101	86	S	-	-	-	-	-
		Fol	-	103	84	S	-	-	-	-	-
		Fol	-	101	80	S	-	-	-	-	-